

Nucleotide metabolism and the control of mitochondrial gene expression



Inaugural – Dissertation

zur Erlangung des Doktorgrades
der Mathematisch-Naturwissenschaftlichen Fakultät
der Universität zu Köln

vorgelegt von

Nils Grotehans
aus Hagen-Hohenlimburg

Köln, 2023

Berichtersteller:

Prof. Dr. Thomas Langer

Prof. Dr. Jan Riemer

Tag der mündlichen Prüfung:

19.10.2023

Abstract

Nucleotides are the building blocks of life, that make up the DNA and RNA in all living beings. Cellular nucleotide metabolism, a fundamental biological process, regulates the uptake, synthesis, distribution and recycling of nucleotides. The sufficient supply of nucleotides ensures the functional expression of genes, which not only takes place in the cytosol but also occurs in mitochondria, which contain their own genome. Mitochondria rely on the expression of their few but essential genes to fulfil their pleiotropic cellular functions such as ATP production, iron-sulfur cluster biogenesis and innate immune signaling. Here we studied the impact of perturbed nucleotide homeostasis on mitochondrial gene expression and cellular function. We identified the mitochondrial nucleoside diphosphate kinase 6 (NME6) as a novel regulator of mitochondrial gene expression. NME6 provides ribonucleotides for mitochondrial transcription and deoxyribonucleotides for mitochondrial DNA replication. NME6 becomes essential for the maintenance of the mitochondrial DNA if the mitochondrial nucleotide uptake from the cytosol is impaired. Moreover, reduced mitochondrial cytidine triphosphate levels become rate-limiting for mitochondrial transcription in the absence of NME6 and lead to a respiratory deficiency. Pyrimidine nucleoside supplementation suffices to fully restore mitochondrial transcript levels and respiratory capacity upon loss of NME6. Thus, we describe NME6 as the first mitochondrial enzyme that regulates mitochondrial gene expression by the supply of ribonucleotides. Our work advances the current understanding of mitochondrial nucleotide metabolism and its contribution to mitochondrial function in health and disease.

Table of Contents

Abstract.....	II
Table of Contents.....	III
List of Figures.....	V
Expanded view.....	VI
1. Introduction.....	1
1.1. The mitochondrial gene expression machinery.....	2
1.1.1. The mitochondrial genome and its organization.....	2
1.1.2. The mechanism of mitochondrial DNA replication.....	4
1.1.3. The mechanism of mitochondrial transcription.....	6
1.1.4. The mechanism of mitochondrial translation.....	9
1.1.5. The coordination of the nuclear and mitochondrial gene expression machinery.....	10
1.2. Nucleotide metabolism fuels mitochondrial gene expression.....	13
1.2.1. The cellular genomes and nucleotide pools.....	13
1.2.2. The nucleotide <i>de novo</i> synthesis pathway.....	16
1.2.2.1. The purine synthesis pathway.....	16
1.2.2.2. The pyrimidine synthesis pathway.....	18
1.2.2.3. The deoxyribonucleotide synthesis pathway.....	19
1.2.3. The coordination of the mitochondrial and cytosolic nucleotide pools.....	20
1.2.4. The mitochondrial deoxyribonucleotide salvage pathway.....	23
1.3. Mitochondrial gene expression and disease.....	26
1.4. Aims of the thesis.....	29
2. Results.....	30
2.1. Loss of SLC25A33 and SLC25A36 causes mitochondrial nucleotide depletion.....	30
2.2. <i>SLC25A33/SLC25A36</i> DKO cells sustain mitochondrial gene expression.....	34
2.3. Mitochondrial proteome profiling of <i>SLC25A33/SLC25A36</i> DKO cells...	36
2.4. Loss of DGUOK is not rate-limiting for mitochondrial gene expression..	39
2.5. Mitochondrial nucleotide import and salvage synergize to maintain mtDNA levels.....	42
2.6. Ribonucleotide synthesis by NME6 fuels mitochondrial gene expression.....	44
2.6.1. The maintenance of mtDNA depends on NME6 when pyrimidine nucleotide import is blocked.....	47

2.6.2. NME6 supports cell proliferation independent of mtDNA synthesis	48
2.6.3. Mitochondrial respiration and OXPHOS subunit homeostasis depend on NME6	48
2.6.4. Mitochondrial gene expression depends on NME6	49
2.6.5. NME6 supplies rNTPs for mitochondrial transcription	51
2.7. Adenosine feeding exacerbates the nucleotide imbalance in <i>NME6</i> KO cells	75
3. Discussion	79
3.1. The role of SLC25A33 and SLC25A36 in nucleotide metabolism and mitochondrial gene expression	80
3.2. The role of NME6 in nucleotide metabolism and mitochondrial gene expression	84
3.3. Nucleotide depletion vs nucleotide imbalance	87
3.4. NME6 beyond nucleotide metabolism	89
3.5. The physiologic role of NME6	90
4. Appendix	92
5. Material and Methods	94
5.1. Materials	94
5.2. Methods	95
6. List of abbreviations	97
7. References	101
8. Summary	117
9. Acknowledgements	119
10. Eidesstattliche Erklärung	120
11. Curriculum Vitae	121

List of Figures

Figure 1.1 Human mitochondria	1
Figure 1.2 Organization of the mitochondrial genome	4
Figure 1.3 The mitochondrial gene expression machinery	8
Figure 1.4 The nucleotide amounts of a HeLa cell at scale	15
Figure 1.5 The <i>de novo</i> nucleotide synthesis pathway	17
Figure 1.6 The deoxyribonucleotide synthesis pathway	19
Figure 1.7 The nucleotide carriers of the inner mitochondrial membrane	21
Figure 1.8 The mitochondrial deoxyribonucleotide salvage pathway	23
Figure 2.1 Loss of SLC25A33 and SLC25A36 causes mitochondrial nucleotide depletion	33
Figure 2.2 <i>SLC25A33/SLC25A36</i> DKO cells sustain mitochondrial gene expression	35
Figure 2.3 Mitochondrial proteome profiling of <i>SLC25A33/SLC25A36</i> DKO cells	38
Figure 2.4 Loss of DGUOK is not rate-limiting for mitochondrial gene expression	41
Figure 2.5 Mitochondrial nucleotide import and salvage synergize to maintain mtDNA levels	43
Figure 2.6 NME6 is required for the maintenance of mtDNA when mitochondrial pyrimidine import is blocked	46
Figure 2.7 NME6 supports cell proliferation independent of mtDNA synthesis	49
Figure 2.8 Mitochondrial respiration and OXPHOS depend on NME6	50
Figure 2.9 NME6 regulates mitochondrial gene expression	52
Figure 2.10 NME6 maintains pyrimidine ribonucleoside triphosphates for mitochondrial transcription	54
Figure 2.11 Mitochondria pyrimidine nucleotide synthesis is required for mitochondrial gene expression	55
Figure 2.12 Adenosine feeding exacerbates the nucleotide imbalance in <i>NME6</i> KO cells	77
Figure 8.1 Nucleotide metabolism and the control of mitochondrial gene expression	118

Expanded view

EV 1 CRISPR-SpCas9 screen analysis and validation by RNA interference ...	65
EV 2 Glucose is limiting for growth in HPLM	66
EV 3 Alterations to the proteome upon NME6 depletion and further characterization of NME6 in liver cancer.....	67
EV 4 Proteomic analysis of immunoprecipitates shows interaction between NME6 and RCC1L	69
EV 5 NME6 supplies pyrimidines for mitochondrial transcription and OXPHOS	71
EV 6 Pyrimidine nucleoside supplementation improves nucleotide scarcity in <i>NME6</i> KO HeLa cells	73
EV 7 Loss of SLC25A33 and SLC25A36 causes mitochondrial nucleotide depletion	93
EV 8 Loss of DGUOK is not rate-limiting for mitochondrial gene expression ...	93
EV 9 Schematic representation of the cytosolic adenosine salvage pathway ..	93

1. Introduction

Adenosine triphosphate (ATP) is the universal energy currency used by all living cells. In the cellular environment, the hydrolysis of the terminal phosphoanhydride bond of ATP leads to a reduction of the Gibbs free energy that is harnessed to drive numerous metabolic reactions^{1,2}. Thus, ATP is essential to sustain life. The consumption of ATP by endergonic metabolic reactions is opposed by ATP-generating reactions that are required to maintain ATP concentrations¹. ATP is most efficiently synthesized by the process of oxidative phosphorylation (OXPHOS), that occurs within the mitochondria of almost all eukaryotic cells^{3,4}. Mitochondria are essential organelles that are thought to have originated from the engulfment of an α -proteobacterium by a proto-eukaryotic cell some 2 billion years ago (**Figure 1.1**)⁵. Mitochondria contain their own genome

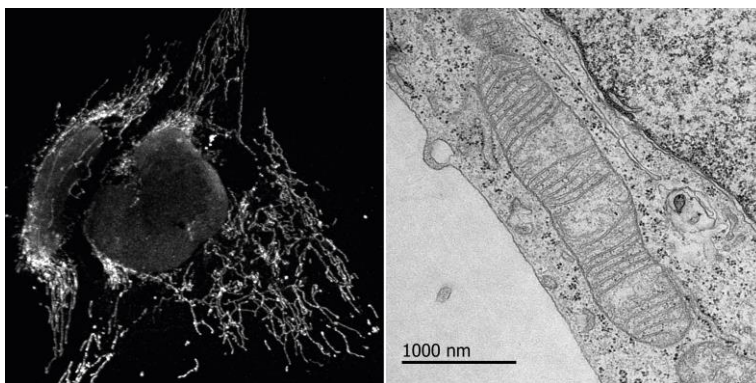


Figure 1.1 Human mitochondria

The mitochondrial network of cervical cancer cells (HeLa) seen through a light microscope (left).

The mitochondrial ultrastructure of human embryonic kidney cells (HEK) seen through an electron microscope (right).

and have evolved an intricate machinery of dual genetic origin termed the electron transport chain (ETC) which facilitates OXPHOS and thereby ATP production^{6–8}. The oxidation of sugars, lipids and amino acids and the subsequent transfer of electrons to molecular oxygen is coupled to the pumping of protons across the inner of the two mitochondrial membranes by the ETC⁴. The energy that is contained in the resulting chemiosmotic gradient is ultimately sequestered by a proton-flow through the mitochondrial protein ATP synthase, which generates ATP from adenosine diphosphate (ADP) and inorganic phosphate (P_i). The idea that ATP can be synthesized without the long sought “high energy” intermediates was initially proposed as the “chemiosmotic” theory in a seminal paper by Peter Mitchell in the 1960s and became widely accepted in the following decade^{9,10}.

Today, however, it has become clear that the chemiosmotic gradient and the resulting mitochondrial membrane potential, established by the ETC, is not only used for ATP synthesis but is an essential prerequisite for mitochondrial function in general ¹¹. The mitochondrial membrane potential determines mitochondrial shape and ultrastructure; it drives the import of numerous mitochondrial proteins as well as cations such as Fe²⁺ and Ca²⁺ and affects other mitochondrial functions such as antiviral signaling ¹²⁻¹⁵. Hence mitochondrial function goes beyond the production of ATP and is intimately coupled to the membrane potential and consequently to the ETC. The ETC is unique among all mitochondrial protein complexes as it is comprised of nuclear- as well as mitochondrial-encoded proteins ⁸. The mitochondrial-encoded subunits are an integral part of the ETC and therefore essential for the various functions of mitochondria in general. Mutations in mitochondrial- and nuclear-encoded genes, that affect mitochondrial gene expression, can induce neuropathies, myopathies, metabolic diseases and are associated with oncogenesis and tumor progression ^{16,17}. Thus, a comprehensive insight into the factors that control mitochondrial gene expression is essential to understand mitochondrial function in health and disease.

The following paragraphs will outline the current understanding of mitochondrial gene expression. This includes the description of the mitochondrial genome, the machinery which maintains and expresses these genes, the metabolic pathways that provide the building blocks of the mitochondrial genome, as well as the coordination and regulation of these biological processes.

1.1. The mitochondrial gene expression machinery

1.1.1. The mitochondrial genome and its organization

Besides the nucleus, the mitochondrion is the only genome-containing organelle in mammalian cells. The mitochondrial genome differs in multiple ways from its nuclear counterpart, it has its unique genetic code, it is circular in shape, made up of ~16.550 base pairs (bp) and present in almost every cell type in multiple copies (10^2 - 10^4) ^{7,18,19}. It encodes for 37 genes that include two ribosomal RNAs (rRNA), 11 protein coding messenger RNAs (mRNA) (giving rise to 13 proteins) and 22 transfer RNAs (tRNA), thereby the mitochondrial genome encodes only for less than 0.1% of the proteins that can be synthesized in a human cell

(Figure 1.2) ^{7,20,21}.

Yet, the mitochondrial genes are essential for mitochondrial function and therefore essential for cellular and organismal health. Mutations in the mitochondrial DNA (mtDNA) can lead to devastating diseases that affect multiple tissues and organs (see **1.3**)¹⁷. The mitochondrial genome is distributed within the mitochondrial network and is organized in so called nucleoids which reside in the mitochondrial matrix. These nucleoids (~100 nm in diameter) are generally comprised of a single mtDNA molecule associated with proteins such as the mitochondrial transcription factor A (TFAM)^{22–25}. TFAM is an important regulator of mitochondrial gene expression. TFAM binds directly to mtDNA, increased binding leads to compaction of the mtDNA, which renders it inaccessible for replication and transcription^{25,26}. Therefore, TFAM has been proposed to fulfill histone-like function for the mitochondrial genome. At the same time TFAM is also an essential component to initiate replication and transcription, giving TFAM a dual role in mitochondrial gene expression^{18,27}. How the switch from compact and inactive nucleoids to replication- and transcription-active nucleoids is regulated is not clear however. The TFAM to mtDNA ratio has been recently proposed to be a determining factor of such a regulation (**Figure 1.2**)²⁵.

In case a nucleoid is in its replication/ transcription-active state, mitochondrial gene expression is initiated from a single non-coding region (NCR) that contains regulatory elements on the two DNA strands^{18,27,28}. The two DNA strands of the mitochondrial genome are differentiated based on their nucleobase content and denoted as the H- (heavy; high Guanosine (G)/Thymidine (T)) and the L-(light; low G/T) strand^{29,30}. The NCR is roughly 1100 bps in length and is confined at its ends by the H-strand promotor (HSP) and the termination associated sequence (TAS) on the L-strand. The L-strand's first feature within the NCR is the L-strand promotor 1 (LSP) which serves as a major initiation site for transcription of nine mitochondrial transcripts but is also the starting point for RNA-primer formation which are required to initiate mtDNA replication³¹. Downstream of the LSP1 within 200 bps, three conserved sequence blocks (CSB1-3) are located that represent important regulatory DNA segments for the switching between mitochondrial replication and transcription³². Following the CSBs, the mtDNA obtains a triple strand conformation that is termed displacement loop (D-loop) region. The D-loop region owes its name to a short DNA fragment (7S DNA; ~500-600 bps) that stably hybridizes to the L-strand,

thereby displacing the H-strand in this region³³. The 7S DNA covers the origin of replication for the heavy strand (O_H) and stretches to the TAS that marks the other end of the NCR. It should be noted that a second LSP (LSP2) has been recently identified that lies in-between the TAS and the first L-strand transcript $tRNA^{Pro}$ ³⁴. However, its physiological role and its contribution to L-strand transcript abundance is not yet clear.

How mitochondrial gene expression is regulated from the NCR will be described in the following paragraph.

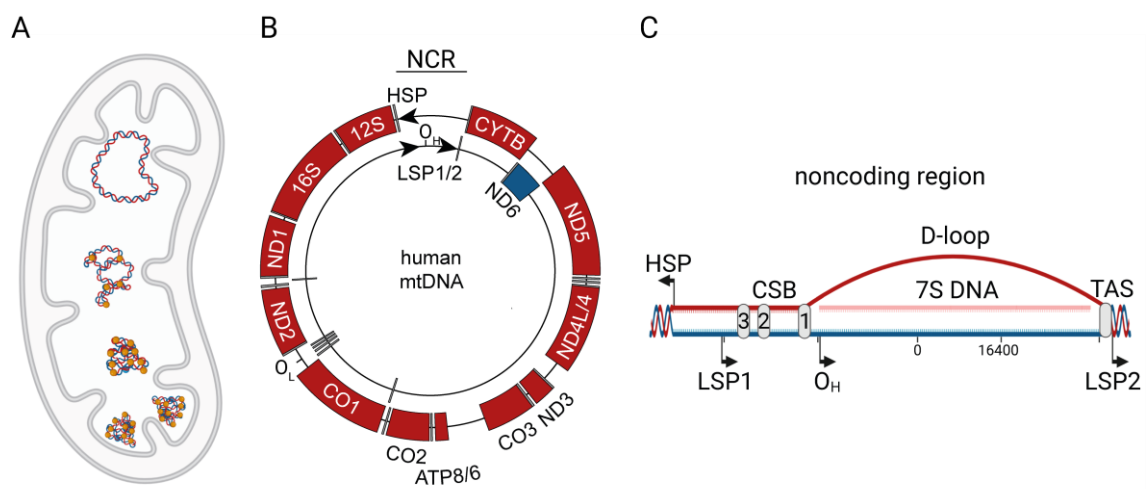


Figure 1.2 Organization of the mitochondrial genome

(A) Mitochondrial DNA (mtDNA) in different compaction-stages. Bottom: fully compacted mtDNA nucleoid with a high content of TFAM (yellow); Middle: intermediate state of mtDNA nucleoid partially bound to TFAM; Top: fully accessible mtDNA molecule.

(B) Schematic of the structure of human mtDNA, with the noncoding region (NCR) at the top, heavy-strand transcripts in red, light-strand transcripts in blue, tRNAs in grey and heavy/light strand promoter (HSP, LSP1/2) indicated as arrows. O_L : origin of replication for the light strand. O_H : origin of replication for the heavy strand.

(C) Magnification of the NCR indicated in B. Heavy strand in red, light strand in blue. Conserved sequence blocks 1-3 in grey, as well as the termination-associated sequence. 7S DNA fragment in pink.

1.1.2. The mechanism of mitochondrial DNA replication

Mitochondrial DNA replication is a cell cycle-independent process which regulates mtDNA copy number and thus is a precondition for mitochondrial gene expression. According to the strand-displacement model, mtDNA replication is initiated in the NCR from the LSP1³⁵. The core machinery to initiate replication and also transcription includes TFAM, the mitochondrial DNA-directed RNA polymerase (POLRMT) and the mitochondrial dimethyl adenosine transferase 2 (TFB2M)^{36–39}. Even though the exact order of events is still debated, replication

is likely initiated by TFAM-binding to the LSP1, which causes a U-shaped bend in the mtDNA that allows POLRMT- and subsequent TFB2M recruitment which is necessary for promotor melting^{23,38}. Transcription from the LSP1 can lead to a near genome-length polycistronic transcript but can also produce a short (~200 bp) 7S RNA primer that is essential for DNA replication. How the switch between mtDNA replication and transcription from one regulatory element is induced is not fully understood. Likely, the transcription of the guanine-rich CBS2 favors G-quadruplex formation of the nascent RNA that interacts with the mtDNA forming an R-loop structure that causes POLRMT stalling and leads eventually to its dissociation from the L-strand^{32,40,41}.

POLRMT progression beyond the CBS2 *in vitro* is supported by the mitochondrial transcription elongation factor (TEFM), however the notion that TEFM is a pro-transcription factor is questioned by recent *in vivo* data^{42,43}. In the case of premature transcription termination from LSP1 at CBS2, the resulting 3'-end of the 7S RNA primer is recognized by the mitochondrial DNA polymerase gamma (POLG). POLG together with the mtDNA helicase TWINKLE and mitochondrial single strand binding protein (mtSSBP1), constitute the minimal mitochondrial replication machinery⁴⁴⁻⁴⁷. However, POLG-binding of the 7S RNA primer does not necessary lead to the replication of the H-strand. The majority of replication events are terminated by the TAS at the end of the NCR. This leads to the formation of the 7S DNA fragment and the formation of the D-loop region⁴⁸. Replication termination at the TAS is another important regulatory step in mitochondrial gene expression, which is not well understood. Factors that might associate to the TAS have not yet been identified and the regulatory role of the 7S DNA remains unclear as well.

If the TAS is successfully passed by POLG, the mitochondrial helicase TWINKLE unwinds the double stranded mtDNA in front of POLG, which allows the continuation of H-strand replication beyond the NCR⁴⁷. The nascent DNA strand replaces the original H-strand which is covered by mtSSBP1, preventing its degradation by nucleases. Replication proceeds along the L-strand, which eventually uncovers the origin of replication of the L-strand (OL) that locates ~11000 bps downstream of the O_H. After strand separation by the replisome, the replaced H-strand forms a hairpin-like stem loop structure that prevents the binding of mtSSBP1⁴⁹. The free stem loop is recognized by POLRMT and RNA-

primer synthesis is initiated ⁵⁰. POLG-binding to the newly synthesized primer then facilitates replication of the L-strand in the opposite direction to the H-strand replication. Once both replisomes reach their start-sites, they encounter the 5'-ends of their respective primers, which need to be removed from the template strand to allow ligation. Primer removal and end processing likely involves the ribonuclease H1 (RNase H1) and the mitochondrial genome maintenance exonuclease 1 (MGME1) ⁵¹⁻⁵⁴. Ligation of the newly synthesized strands is then performed by DNA-ligase III ⁵⁵. To successfully complete mtDNA replication, the two daughter molecules that are still physically intertwined with one another must be separated. The mitochondrial isoform of topoisomerase 3 α is required for the removal of the mtDNA catenates, although other proteins are likely to be involved in this process as well ⁵⁶. Separation of the two DNA molecules marks the final step of mtDNA replication.

1.1.3. The mechanism of mitochondrial transcription

Mitochondrial transcription represents the first step of mitochondrial gene expression which leads to the synthesis of two polycistronic transcripts that contain all mtDNA-encoded genes. Similar to mtDNA replication, transcription is also initiated and regulated from the NCR. As outlined in the previous chapter, TFAM, POLRMT and TFB2M comprise the minimal machinery to initiate transcription. It was recently shown that mitochondrial transcription can be regulated by a short non-coding RNA transcript termed 7S RNA ⁵⁷. The 7S RNA is different from the RNA primer, as it does not hybridize with mtDNA, has a distinct sequence and becomes polyadenylated. The 7S RNA was shown to bind to POLRMT and to facilitate its dimerization, thereby preventing POLRMT-mtDNA interaction and mitochondrial transcription ⁵⁷. If POLRMT-binding is not inhibited by the 7S RNA and the replisome is successfully recruited to any of the described promoters, TEFM-binding to POLRMT replaces TFB2M and increases processivity of POLRMT ^{58,59}. TEFM is required to sustain and prolong transcription that can produce the almost genome-length transcripts of the H- and L-strand.

Due to historical reasons, the H-strand is often referred to as the main coding strand for 28 out of the 37 transcripts. However, it should be noted that according to the contemporary definition of "coding strand", the L-strand is the actual coding

strand for the transcripts that are initiated from the HSP. The non-canonical annotation of the coding- and template-strand of the mitochondrial genome has led to continued confusion in the literature and should be standardized in the future ^{7,21,60}.

HSP-originating transcripts are synthesized in a long polycistronic transcript that extends full circle up to the TAS region of the NCR ⁶¹. It is not clear however, how mitochondrial transcription is terminated in this region. Proteins that facilitate transcription termination events are largely missing. So far, the mitochondrial transcription termination factor 1 (MTFER1) is the only mitochondrial protein that has been shown to end transcription. Initially thought to stop H-strand transcription, MTERF1 stops L-strand transcription by binding to a sequence motif located between the coding sequence of 16S and ND1 causing conformational changes to the mtDNA ⁶². The synthesis of polycistronic transcripts leads to equal amounts of transcripts that are encoded on the same strand. However, RNA-sequencing data have shown that mitochondrial transcripts are not in equilibrium with each other, specifically the mitochondrial rRNAs can occur in 100-fold excess to other mitochondrial transcripts ⁶³. It is now recognized that this is due to differences in RNA-processing and modification that change the stability of specific transcripts.

RNA-processing and posttranscriptional modification occurs in mitochondrial RNA granules (MRGs) (**Figure 1.3**) ^{64–66}. These membrane-less compartments (100-150 nm in size) form in very close proximity (within 200 nm) to mitochondrial nucleoids by lipid-lipid phase separation, are composed RNAs and proteins and control mitochondrial gene expression on the posttranscriptional level. Specifically, MRG proteins are required to liberate the individual mitochondrial transcripts from the polycistronic strand. The RNase P complex (composed of MRPP1-3) and the RNase Z recognize the 5'- and 3'-ends of mt-tRNAs and induce cleavage at these sites ^{67–69}. This so called tRNA-punctuation model accounts for the majority of mitochondrial transcript separation events, yet not all transcripts are interspaced with tRNAs (such as *ND5-CYTB* and *ATP8/6-COX3*) and alternative processing mechanisms must exist. It was recently shown that MRG protein FASTKD5 is required for successful processing of several non-canonical processing sites. Loss of FASTKD5 leads to increased transcript intermediates of *ND5-CYTB* and *ATP8/6-COX3* ⁷⁰. Successfully excised

transcripts undergo further processing in the MRG environment. Poly-adenylation by mitochondrial polyA-polymerase changes transcript stability but is also required for stop-codon completion of several transcripts. Other processing events within the MRGs include CCA-tail addition to tRNAs and pseudouridylation of m-, t- and rRNAs ⁷¹. A protein complex of MRG proteins has been identified as a mitochondrial pseudouridylation module that is essential for mitochondrial-ribosome assembly, translation and OXPHOS function ⁷². This multi-protein complex includes RCC1L, RPUSD3/4, FASTKD2, and TRUB2 amongst other proteins and was shown to specifically pseudouridylate a single residue of the 16S rRNA, which determines rRNA stability and ribosome assembly ^{71–73}.

This exemplifies that MRGs are not only required for RNA-processing and maturation but are hubs for mitochondrial ribosome formation ⁷⁰. Additionally, the association of more than 50 proteins with MRGs suggests that further, yet unknown, processing- and regulating-events take place in these compartments that influence mitochondrial gene expression ⁶⁴.

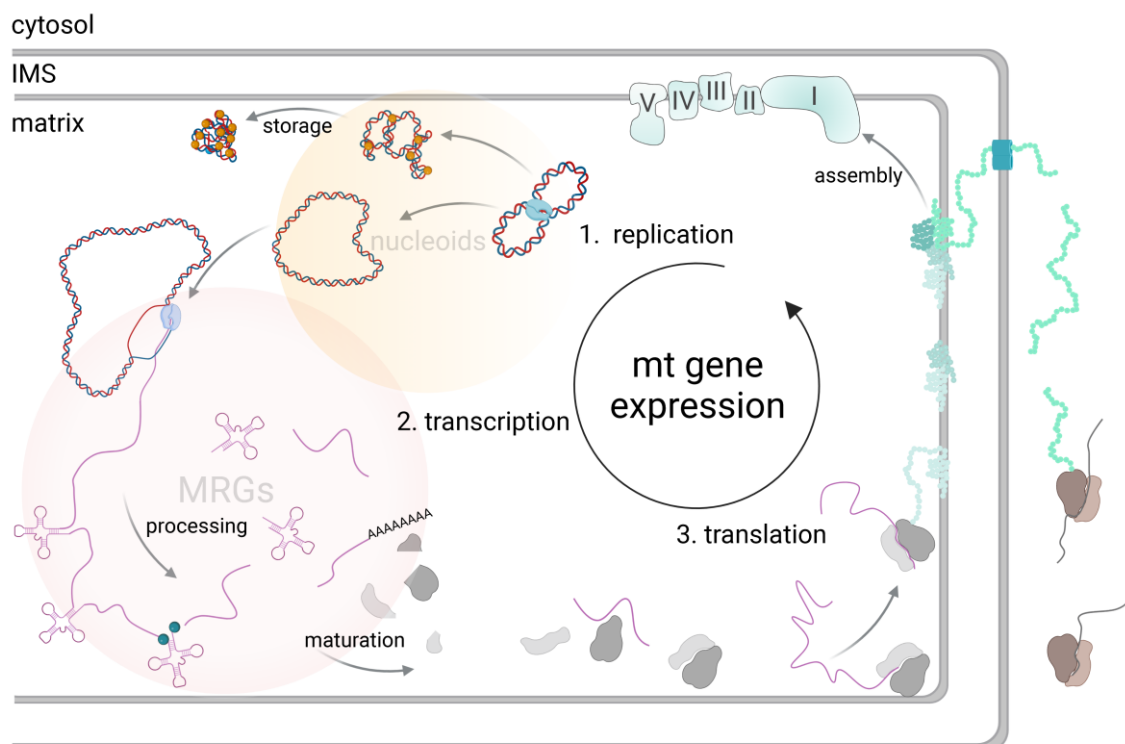


Figure 1.3 The mitochondrial gene expression machinery

Schematic depiction of the different steps of mitochondrial gene expression. From mtDNA replication (1), to mitochondrial transcription, RNA processing in the mitochondrial RNA granules (MRGs) (2), to mitochondrial ribosome maturation and assembly, to mitochondrial translation (3) and subsequently OXPHOS complex assembly with nuclear-encoded genes.

1.1.4. The mechanism of mitochondrial translation

The process of mitochondrial gene expression is completed by the translation of the 11 mRNAs that give rise to the 13 ETC-subunits that are encoded by the mitochondrial genome. Mitochondrial protein translation is initiated by the assembly of the mitochondrial ribosome within the MRGs ⁷⁰. The mitochondrial ribosome has diverged substantially from its bacterial origin and differs from its cytosolic counterpart in several ways. The human mitochondrial ribosome forms a 2.7 MDa complex that is rich in protein content compared to cytosolic ribosomes. It consists of two mitochondrial encoded rRNAs, 12S and 16S and 82 nuclear encoded proteins ⁷⁴. Mitochondrial ribosome assembly is a complex multi-step process that was reported to take 2-3 h and is not fully understood ⁷⁵. The assembly involves the maturation of the small ribosomal subunit 28S (mtSSU) and the large ribosomal subunit 39S (mtLSU) that takes place co-transcriptionally in the MRGs (**Figure 1.3**). Maturation steps involve the modification of RNA-components and the assembly of multi-protein modules that are inserted into the nascent ribosome subunit by ribosome assembly factors ⁷⁵⁻⁷⁷. The successfully assembled ribosome is then ready to enter the translation cycle that involves three steps: initiation, elongation and termination. Translation initiation starts with the binding of a mature mRNA to the mtSSU and assembly with the mtLSU, forming the 55S monosome. The start codon is directed to the ribosomal P-site by mitochondrial translation initiation factor 2 (mtIF2) which efficiently blocks the A-site, a mechanism unique to mitochondrial ribosomes. A formylated Methionine loaded tRNA is required to engage in translation ^{78,79}. Next, several mitochondrial elongation factors, such as mtEFTu, mtEFG1, mediate the delivery of loaded tRNAs to the ribosome, their binding, release and subsequent reloading, as well as the forward movement of the ribosome along the mRNA ^{80,81}. The emerging polypeptide chain is then co-translationally inserted into the inner mitochondrial membrane (IMM) by the protein translocase OXA1 ^{82,83}. Translation termination is induced upon the occurrence of a stop codon in the A-site of the ribosome. Mitochondrial release factors catalyze the hydrolysis of the polypeptide-chain from the last tRNA located at the ribosomal P-site and induce their release from the ribosome complex ^{84,85}. Translation termination and the subsequent ribosome recycling marks the final step in mitochondrial gene expression.

1.1.5. The coordination of the nuclear and mitochondrial gene expression machinery

According to the classical view of the central dogma of molecular biology, in which genetic information flows from DNA to RNA to protein, mitochondrial gene expression can be regarded as successfully completed with the synthesis of mitochondrial-encoded proteins and their incorporation into OXPHOS complexes⁸⁶. However, in the special case of mitochondrial OXPHOS complexes that originate from two distinct genetic systems, mitochondrial gene expression cannot be fully understood as a stand-alone process but needs to be studied in the context of nuclear gene expression. Mitochondrial gene expression fails to produce functional OXPHOS complexes if the coordination with the nuclear gene expression machinery is impaired and *vice versa*⁸⁷. Mitochondrial- and nuclear encoded OXPHOS component synthesis needs to be regulated such that assembly of the five OXPHOS complexes occurs at a sufficient rate to meet the metabolic demands of the cell. This coordination is regulated at numerous steps out of which a few are described in the following.

Regulating the accessibility of genetic information and thereby regulating gene expression is achieved by DNA-packaging proteins such as histones in the nucleus. A similar process can be envisioned for mitochondria that lack histones. The mtDNA-binding protein TFAM has been shown to readily compact mtDNA into nucleoids *in vitro* and *in vivo*²⁶. The mtDNA to TFAM ratio, which binds unspecifically and covers 16-17 bps of DNA, is a determining factor of mtDNA compaction. This is in line with distinct nucleoid populations observed in cells that, depending on their TFAM content, were in a replication- and transcription-active or inactive state^{25,26}. TFAM levels generally correlate with mtDNA levels and since TFAM is also required for transcription and replication, controlling TFAM expression influences mitochondrial gene expression on multiple levels. TFAM and other proteins such as POLRMT and MTERF1 have been reported to be under the control of nuclear transcription factors such as NRF1 and NRF2 respectively^{88,89}. These in turn are regulated by peroxisome proliferator-activated receptor gamma coactivator 1 α (PGC1 α), the first identified *bona fide* mitochondrial biogenesis factor⁹⁰⁻⁹². Hence, mitochondrial gene expression can be regulated in part by nuclear transcription programs. Mitochondrial transcript stability is another important regulatory factor that influences mitochondrial gene

expression. Polyadenylation of mRNAs, generally thought to increase transcript stability, has opposing effects on certain mitochondrial transcripts, stabilizing some complex IV subunits whilst destabilizing certain subunits of complex I. The leucine-rich pentatricopeptide repeat containing (LRPPRC) protein has been shown affect mitochondrial polyadenylation. Loss of LRPPRC leads to an aberrant mitochondrial transcription pattern, showing reduced levels of all mRNAs except for *ND6* and increased rRNA levels^{93,94}.

Coordination of nuclear and mitochondrial gene expression on the transcriptional level was recently shown to be only modestly synchronized in mammalian cells⁹⁵. Refinement of the mitochondria- nuclear coordination was suggested to significantly occur on the translational level. The average translation rates of the different OXPHOS complexes correlated significantly more with their final abundance than their average transcript levels⁹⁵. Yet, it should be noted that no such correlation was observed when the translation rates of individual subunits were analyzed. Why mitochondrial- and nuclear-encoded OXPHOS subunits are not synthesized according to their stoichiometric levels is unclear at this point. So far very few mitochondrial translation factors have been identified that could explain why certain OXPHOS subunits are produced in excess and others in seemingly rate-limiting quantities.

The mitochondrial translation activator of COX1 (TACO1) was the first translation activator that was shown to associate with the mitochondrial ribosome and to specifically bind the cytochrome c oxidase subunit 1 (*COX1*) mRNA. Loss of TACO1 leads to complex IV deficiency^{96,97}. Also, in the case of *COX1* translation, coordination between the cytosolic- and mitochondrial- gene expression has been reported. *COX1* translation was stalled upon the depletion of nuclear-encoded cytochrome c oxidase subunit 4 (*COX4*), indicating that mitochondrial translation can adapt dynamically to the availability of nuclear-encoded OXPHOS subunits⁹⁸. However, to this end it is not clear whether the observed translational plasticity is a general feature of the mitochondrial gene expression system or a unique phenomenon of complex IV assembly.

Another study suggests less coordination between mitochondrial and nuclear gene expression on shorter time scales and a unidirectional coordination of the transcriptomes that is dictated by the cytosol⁹⁵. Impaired mitochondrial gene expression by loss of LRPPRC did not lead to significant adaptations in nuclear

encoded OXPHOS proteins but instead induced a proteostatic stress response, likely targeted to degrade excessively produced nuclear-encoded OXPHOS subunits.

In summary, mitochondrial gene expression is a multi-step process. Maintenance and replication of the mitochondrial genome is essential to facilitate the expression of its few, but essential genes. Mitochondrial transcription produces polycistronic transcripts that are processed in membrane-less dynamic compartments called MRGs. Mitochondrial protein translation occurs on an organelle-specific set of ribosomes that synergizes with the cytosolic translation machinery to produce functional OXPHOS complexes. Regulation of the mitochondrial gene expression machinery occurs on multiple levels and needs to be coordinated with nuclear gene expression at all times to ensure cellular and organismal homeostasis.

1.2. Nucleotide metabolism fuels mitochondrial gene expression

Mitochondrial gene expression is a complex multi-step process that not only requires a functional protein machinery but also critically depends on the sufficient supply of nucleotides that make up the mitochondrial DNA and RNA. Nucleotide metabolism, that coordinates the uptake, synthesis, distribution and degradation of nucleotides, is therefore an integral part of mitochondrial gene expression. Impaired nucleotide homeostasis can lead to defective mitochondrial gene expression despite the presence of a functional synthesis machinery and mutations in nucleotide metabolizing enzymes as well as therapeutic interventions that target nucleotide synthesis have been long known to affect mitochondrial gene expression and cause mitochondrial toxicity^{17,99}.

The following paragraphs describe the molecular underpinnings of the cellular nucleotide metabolism and its relevance for mitochondrial gene expression.

1.2.1. The cellular genomes and nucleotide pools

Nucleotides are a main constituent of every cell, accounting for 15-20% of the biomass, which makes nucleotides the second most abundant molecule class in cells after proteins (50-60%) and before lipids (15%) and carbohydrates (5%)⁹⁹. Thus, to replicate the nuclear- and mitochondrial genome, cells must synthesize deoxyribonucleotides in vast quantities for a sustained period of time. However, “vast quantities” is not a defined term to describe nucleotide levels or synthesis rates and should rather be replaced by precise values. Yet, absolute values and concentrations of nucleotide pools are rarely reported in the literature, which limits our understanding of cellular nucleotide homeostasis. Efforts have been made to convert reported values (usually nucleotides/ 10^6 cells; or nucleotides/mg protein) into comparable units such as concentrations^{100,101}. Although these studies point out the error that is introduced by such conversions and the high variation between different studies, these calculations are still valuable as they allow at least for a rough estimation of nucleotide pool sizes. Some important conclusions from these studies are summarized in the following.

Proliferating- and tumor cells have five- to ten-fold higher deoxyribonucleoside triphosphates (dNTP) levels and two- to five-fold higher ribonucleoside triphosphate (rNTP) levels compared to non-proliferating cells and essentially represent different models to study nucleotide metabolism.

Further, rNTPs (present at ~100-1000 μM) are ten- to hundred-fold more abundant than dNTPs (present at ~10-100 μM) in tumor cells^{99–101}. This statement does not apply to ATP and dATP, since ATP due to its special role as the energy currency of the cell, is by far the most abundant nucleotide in any cell and is present at concentrations between ~2-5 mM, making it ten-fold more abundant than any other ribonucleotide.

The cell contains compartmentalized nucleotide pools, that is the cytosolic- and nuclear pool which are in equilibrium with each other and the mitochondrial pool that is isolated by the IMM^{102–104}. The mitochondrial dNTP pool is less than 10% of the size of the cytosolic dNTP pool¹⁰⁰. This leads to the conclusion that changes in the cytosolic pool might have a great effect on the mitochondrial pool but not *vice versa*. Yet, despite the small size of the mitochondrial nucleotide pool, recent work has shown that affecting mitochondrial nucleotide homeostasis can have severe consequences for cellular and organismal health^{105,106}. Defective mitochondrial replication has been shown to induce increased mitochondrial nucleotide uptake, which ultimately led to overall cellular nucleotide depletion, reducing nuclear DNA damage repair fidelity and replication speed¹⁰⁵. Further, impaired nucleotide synthesis and altered mitochondrial nucleotide uptake, caused by the loss the mitochondrial protease yeast mitochondrial DNA escape 1 like (YME1L), leads to mtDNA release and an innate immune response¹⁰⁶.

Estimations of the absolute nucleotide levels of the different cellular compartments also bears the advantage that these values can be put into perspective to the mitochondrial- and nuclear genome size. A diploid human cell stores $1.2 \cdot 10^{10}$ deoxyribonucleotides in its genome²⁰. Even in highly proliferative cancer cells, that are known to have increased nucleotide levels, the free cytosolic deoxyribonucleotide pools account for only ~1-2% of the nucleotides required for a complete genome replication (calculated for HeLa cells based on previous studies^{20,100}) (**Figure 1.4**). Calculating a similar ratio for the mtDNA and the mitochondrial dNTP pool is more challenging since the mtDNA copy number is not a fixed value and varies across tissues and cell types by several orders of magnitude^{19,107–109}. HeLa cells, that have been reported to contain on average 550 nucleoids per cell²⁵.

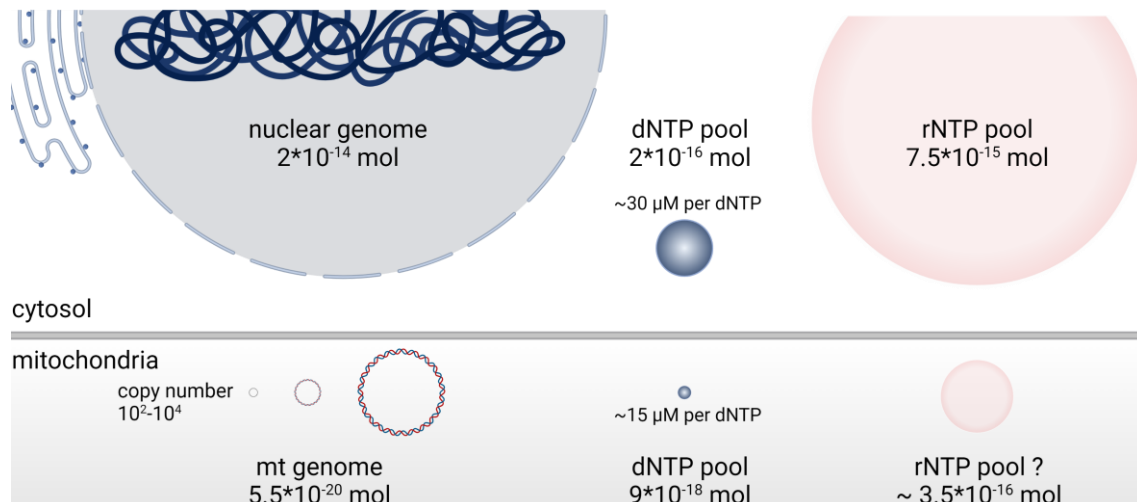


Figure 1.4 The nucleotide amounts of a HeLa cell at scale

Schematic representation of nucleotide abundances in the nuclear- and mitochondrial-genome, as well as the free dNTP and rNTP pools in the cytosol and mitochondria. Nucleotide abundance depicted by surface area of the respective circle. (Nucleus size represents, nucleotide amount stored in DNA; mtDNA circle size represents nucleotide amount stored in mtDNA present at different copy numbers). Calculated for HeLa cells, based on previously reported values ^{7,19,20,99–101,109}. Note that the mitochondrial rNTP pool size was estimated based on the ratio between cytosolic dNTP and rNTP pools

Considering the mitochondrial genome size and the reported mitochondrial dNTPs pools, the free mitochondrial dNTPs account for ~30% of the nucleotides required for a complete mitochondrial genome replication ^{7,100}. Interestingly, even though mitochondria contain more dNTPs in regards to their genome size compared to the cytosol, the mitochondrial dNTP concentration (15 μM per nucleotide) was only half of the cytosolic dNTP concentration (30 μM) in HeLa cells ¹⁰⁰. Maintaining a dNTP concentration gradient between the cytosol and the mitochondria might determine the direction of nucleotide exchange and could ensure sufficient mitochondrial dNTP supply.

Similar calculation for ribonucleotide pools compared to RNA abundance in a cell are even more challenging to make, since the transcriptome does not have a defined size, is dynamically regulated and more difficult to access experimentally ⁹⁹. Further, absolute values for rNTP pool sizes of the mitochondria are missing so far, making organelle specific statements currently impossible ¹⁰⁰. Nonetheless, the size of the transcriptome is generally reported to exceed the genome size by several fold, hence similar to free dNTPs that make up only a fraction of the deoxyribonucleotides contained in the genome, the free rNTPs must be significantly less than the ribonucleotides contained in the transcriptome.

In summary, absolute quantification of nucleotides enables direct comparisons between pool sizes of different compartments and between pool sizes and genome sizes. These comparisons reveal notable differences between the genome size and the steady state levels of available nucleotides for the mitochondria as well as for the nucleus. Further, the mitochondrial genome as well as its nucleotide content make up only a fraction of the total nucleotide amounts of the cell. In light of that fact, it is not surprising that mitochondrial gene expression relies on the supply of nucleotides from the cytosol. The following paragraph will cover how nucleotides are synthesized, how mitochondria obtain nucleotides from the cytosol and which alternative routes of nucleotide supply exists that fuel mitochondrial gene expression.

1.2.2. The nucleotide *de novo* synthesis pathway

Ribonucleotides and deoxyribonucleotides are synthesized through the *de novo* synthesis pathway. The term “*de novo*” synthesis describes the anabolic process of nucleotide synthesis, that derives nitrogen and carbon atoms from amino acids, and various other carbon sources to assemble the nucleobase rings that are connected to the activate pentose-sugar phosphoribosyl pyrophosphate (PRPP)^{110–112}. The synthesis occurs almost exclusively in the cytosol and follows two largely independent routes that produce the purine ribonucleotides ATP and guanosine triphosphate (GTP) as well as the pyrimidine ribonucleotides uridine triphosphate (UTP) and cytidine triphosphate (CTP) (**Figure 1.5**). All nucleotides are initially synthesized as ribonucleotides and subsequently reduced to deoxyribonucleotides. Mitochondria do not possess *de novo* synthesis capacity, and rely on the import of cytosolic nucleotides¹⁰⁴. Thus, mitochondrial gene expression depends on cytosolic nucleotide *de novo* synthesis.

1.2.2.1. The purine synthesis pathway

Purine synthesis is a ten-step reaction that consumes 4 moles ATP, 2 moles glutamine and formyl-groups delivered by N¹⁰-tetrahydrofolate, as well as 1 mole glycine, aspartate and CO₂ to produce 1 mole of the purine precursor inosine monophosphate (IMP)⁹⁹. These reactions are carried out by a set of six multifunctional enzymes that are capable of forming an active metabolon called the purinosome^{113,114}.

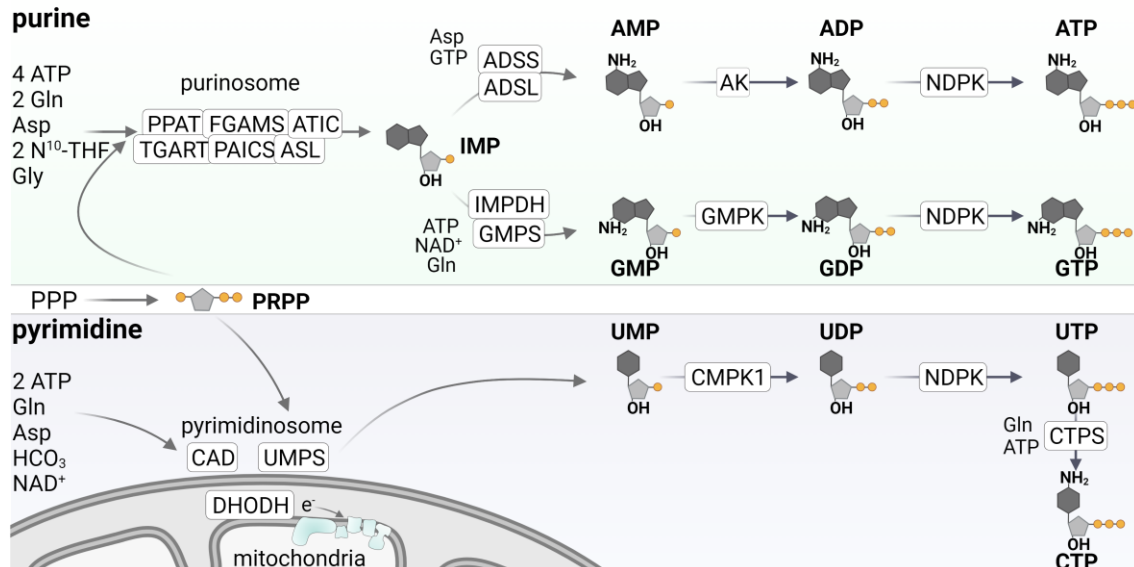


Figure 1.5 The *de novo* nucleotide synthesis pathway

Top: The purine ribonucleotide synthesis pathway from left to right.

Bottom The pyrimidine ribonucleotide synthesis pathway from left to right.

Note: Enzyme names indicated in white boxes, purine and pyrimidines indicated by their distinct ring structure and their defining chemical group; PPP: pentose phosphate pathway.

Purinosome formation has been shown to occur in purine-scarce conditions and was proposed to increase substrate channeling in HeLa cells^{113,115}. The final product of the purinosome activity, IMP, is then further converted into either adenosine monophosphate (AMP) or guanosine monophosphate (GMP). AMP synthesis is GTP driven and requires an additional aspartate, whereas GMP synthesis is ATP driven and requires an additional glutamine^{116–120}. Thus, ATP and GTP synthesis rates are coupled to the availability of the respective purine counterpart, which is an important self-regulatory mechanism to maintain purine nucleotide balance.

Even though purine *de novo* synthesis is mainly required to produce sufficient dNTPs for DNA replication and repair, AMP synthesis can also provide substrates for other metabolic pathways. The recycling of AMP via AMP deaminase (ADA), and its subsequent re-amination via adenylosuccinate synthetase (ADSS) and adenylosuccinate lyase (ADSL) leads to the release of ammonia and fumarate and is known as the purine nucleotide cycle. This pathway operates mainly in the muscle to provide the anapleurotic tricarboxylic acid (TCA) cycle intermediate fumarate¹²¹.

AMP and GMP undergo additional phosphorylation steps either via adenylate kinases (AK1-9), in the case of AMP or via guanosine monophosphate kinase (GMPK) to form adenosine diphosphate (ADP) and guanosine diphosphate

(GDP) respectively ¹²²⁻¹²⁶. The synthesis of the activated ribonucleoside triphosphates ATP and GTP denotes the endpoint of purine nucleotide *de novo* synthesis and is performed by cytosolic nucleoside diphosphate kinases (NDPK) ¹²⁷.

1.2.2.2. The pyrimidine synthesis pathway

Similar to purine synthesis, pyrimidine synthesis is also an ATP-consuming multistep-reaction that leads to the production of UTP and CTP. However, the pyrimidine base moiety is less complex than the purine moiety, and therefore requires fewer catalyzing steps and less precursors. The pyrimidine ring structure is assembled independently before it is attached to PRPP and requires 2 moles of ATP, one mole of glutamine, aspartate and bicarbonate ^{99,128}. The synthesis is initiated by the cytosolic trifunctional enzyme carbamoyl-phosphate synthetase 2 - aspartate transcarbamylase - dihydroorotase (CAD), forming carbamoyl phosphate (CP) which consumes glutamine-derived nitrogen, bicarbonate and two molecules of ATP. CP reacts with Aspartate in a second reaction step producing carbamoyl aspartate, which subsequently condenses in a third reaction into the cyclic intermediate dihydroorotate ^{99,129,130}. Dihydroorotate is oxidized by the mitochondrial intermembrane space (IMS) protein dihydroorotate dehydrogenase (DHODH), making it the only synthesis step in the nucleotide *de novo* synthesis pathway that does not occur in the cytosol. The electrons derived from DHO oxidation are deposited into the ETC via ubiquinone, consequently coupling cellular respiration to pyrimidine synthesis (**Figure 1.5**) ⁹⁹. Pyrimidine synthesis is completed via the bi-functional enzyme uridine monophosphate synthase (UMPS) by PRPP attachment and decarboxylation of the resulting orotidine monophosphate forming uridine monophosphate (UMP) ^{131,132}.

A recent study showed that CAD, DHODH and UMPS form a protein complex connected by the voltage dependent anion channel 3 (VDAC3), that build up a metabolon termed pyrimidosome similar to the purinosome ¹³³. In contrast to purine synthesis, pyrimidine synthesis does not branch into two pathways at the monophosphate level, but instead continues to consecutively phosphorylate UMP by cytidine uridine kinase 1 (CMPK1) and a NDPK to form UTP ^{127,134}. Lastly, the synthesis of CTP is achieved by amination of UTP through the enzyme CTP synthase (CTPS) consuming an additional glutamine and ATP ¹³⁵.

1.2.2.3. The deoxyribonucleotide synthesis pathway

Deoxyribonucleotide synthesis is essentially a one-step reaction for three out of the four dNTPs and is catalyzed by a single protein complex. This complex is called ribonucleotide reductase (RNR) and represents an essential linchpin in nucleotide metabolism^{136,137}. Ribonucleotide flux through RNR sets the balance between rNTPs and dNTPs but, due to its intricate regulatory mechanism, also determines the intra dNTP pool composition. The RNR complex is a heterodimer composed of the constitutive RRM1 subunit and either the cell cycle dependent RRM2- or the DNA damage inducible RRM2B subunit^{138,139}. Three distinct nucleotide binding sites regulate enzyme activity, specificity and nucleotide reduction. RNR activity is stimulated by ATP binding to the A-site or inhibited by dATP binding. S-site occupation by different nucleotides modulates RNR substrate preference, that bind to the catalytic C-site and are reduced into deoxyribonucleotides¹⁴⁰. Deoxyribonucleotide synthesis occurs at the diphosphate level and thus branches off from the previously outlined ribonucleotide *de novo* synthesis pathway at the penultimate synthesis step (Figure 1.6).

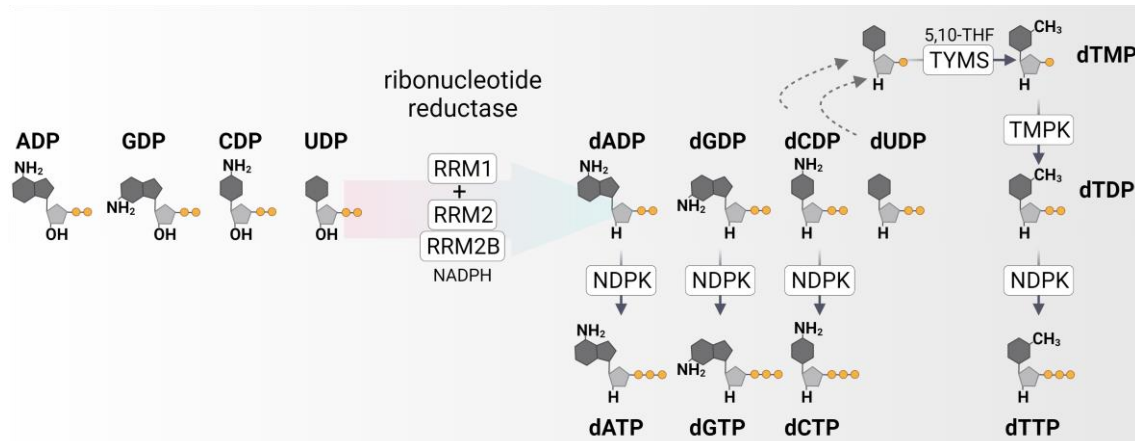


Figure 1.6 The deoxyribonucleotide synthesis pathway

The conversion of ribonucleoside diphosphates (left) into deoxyribonucleoside diphosphates (right) by the enzyme ribonucleotide reductase. Enzyme names indicated in white boxes, purine and pyrimidines indicated by their distinct ring structure and their defining chemical group, ribo- and deoxyribonucleotides indicated by the presence or absence of the 2' ribose hydroxyl group.

All ribonucleoside diphosphates are reduced at the 2' ribose carbon by removal of the hydroxyl group and converted into deoxyribonucleoside diphosphates (dNDPs)¹⁴⁰. Deoxy adenosine-, guanosine- and cytidine-diphosphate (dADP, dGDP and dCDP) are readily activated by a cytosolic NDPK, whereas the synthesis of deoxythymidine triphosphate (dTTP) requires additional processing

steps. Both, deoxyuridine diphosphate (dUDP) and dCDP can serve as precursors for dTTP synthesis. DTTP synthesis requires the dephosphorylation of dCDP and dUDP into their respective monophosphate forms. The resulting dCMP is then deaminated by deoxycytidylate deaminase (DCTD) to form dUMP that is methylated by thymidylate synthase (TYMS) into dTMP^{141–143}. dTTP synthesis is then completed by consecutive phosphorylation steps carried out by thymidylate monophosphate kinase (TMPK) and a cytosolic NDPK^{144,145}. Notably, the demand for dNTPs is not constant and fluctuates with the different phases of the cell cycle⁹⁹. During the G1- and S-phase, dNTP production is accelerated for the replication of the nuclear genome, while synthesis rates are reduced during the G2-phase in which dNTPs are mainly consumed for DNA damage repair and mtDNA synthesis⁹⁹. dNTP output is regulated through cell cycle dependent expression of rate-limiting enzymes. RRM2, TYMS and TYMK are highly expressed during the G1- and S-phase and efficiently degraded at the beginning of the G2-phase, thereby adapting dNTP production to the reduced demand^{139,146,147}.

In conclusion, nucleotide *de novo* synthesis is a complex energy-demanding metabolic process that maintains and adjusts the cellular nucleotide pools to meet the requirements for successful nuclear- and mitochondrial- genome replication and transcription.

1.2.3. The coordination of the mitochondrial and cytosolic nucleotide pools

The rNTPs and dNTPs that are constantly synthesized in the cytosol need to reach the sites of active replication and transcription within the cell. In the case of nuclear gene expression, cytosolic rNTPs and dNTPs can diffuse passively into the nucleus through the nuclear pores and can reach equilibrium with the cytosol^{102,103}. The mitochondrial gene expression machinery however, is sealed off from the cytosol by the nucleotide-impermeable IMM and can therefore not make direct use of the cytosolic nucleotide pools. Nucleotides need to be actively transported into the mitochondrial matrix by metabolite transporters that reside in the IMM. These transporters that belong to the solute carrier (SLC)-25-family are a major nucleotide supply route for mitochondria and connect the cytosolic nucleotide pools to the mitochondrial pools (**Figure 1.7**)^{148,149}.

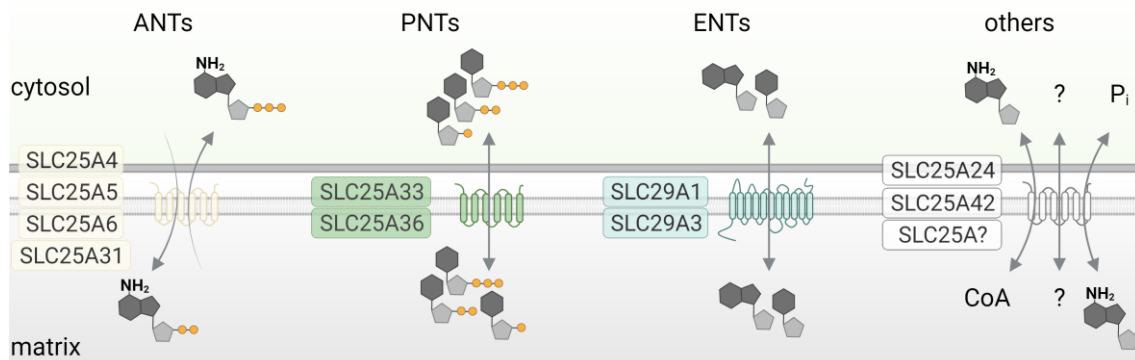


Figure 1.7 The nucleotide carriers of the inner mitochondrial membrane

Nucleotide carriers of the SLC25- and SLC29-family that localize to the inner mitochondrial membrane. Preferred substrates for the respective transporters are indicated. (ANT: adenine nucleotide transporter, PNT: pyrimidine nucleotide transporter, ENT: equilibrative nucleoside transporter).

Characteristic for SLC25-members are three domains that contain each two hydrophobic alpha helices that cross the IMM. The carriers are inserted in the IMM in a way that the N- and C-terminus face the IMS, which in some cases have additional domains, such as EF-hand motifs that are involved in regulation of the channel activity. The mode of transport varies for different transporters and includes antiporters, uniporters and symporters¹⁴⁹. 53 members of the SLC25-family have been identified, out of which at least ten have nucleotide transport activity¹⁴⁹.

Among the most well studied SLC25-family members are the adenine nucleotide transporters ANT1-4 (SLC25A4/5/6/31) which facilitate the export of ATP from the mitochondria to the cytosol by exchanging mitochondrial ATP for cytosolic ADP¹⁵⁰. This transport process is driven by the mitochondrial membrane potential. While SLC25A4/5/6 have a homology of 90% and 70% with SLC25A31, they possess distinct kinetic parameters and show tissue specific expression¹⁵⁰. Yet the functional differences between the isoforms are not understood in detail. Nucleotide transport of non-adenine species is carried out by the SLC25-family members SLC25A33 and SLC25A36 that have been identified as the main mitochondrial pyrimidine transporters. SLC25A33 and SLC25A36 are ~60% homologous and were both able to restore mtDNA levels in yeast cells that were depleted of the nucleotide carrier rim2^{151–153}. *In vitro* liposome experiments revealed that SLC25A33 exchanges ribo- and deoxyribo-pyrimidine di- and triphosphates in an antiport fashion. SLC25A36 exhibited additional monophosphate transport activity including guanosine and inosine nucleotides

that could be transported by an antiport as well as by a uniport mechanism ¹⁵¹. It should be noted however, that these experiments were performed as homo-exchange experiments under supra-physiological nucleotide concentrations and might therefore not fully reflect *in vivo* transport activities of these carriers.

Besides nucleotides, mitochondria also uptake the unphosphorylated precursor nucleosides that originate from DNA- and RNA-catabolism. These nucleosides enter the mitochondria via another set of solute carriers that belong to the SLC29-family and are referred to as equilibrative nucleoside transporters (ENTs). ENTs are generally expressed in the plasma membrane and play a pivotal role in maintaining nucleotide homeostasis in the body ^{154–156}. Two out of the four known ENTs have been also reported to localize to mitochondria where they drive the exchange of nucleosides depending on the concentration gradient. The mitochondrial ENT1 and 3 (SLC29A1 and SLC29A3) exhibit both purine and pyrimidine nucleoside transport activity ^{154,157,158}, which represents an additional exchange pathway for mitochondrial and cytosolic nucleosides. SLC29A1- and SLC29A3 transport activity also has implications for the efficacy of antiviral and anticancer nucleoside analogues ^{157,158}. Expression levels of SLC29A1 and SLC29A3 determined the mitochondrial toxicity of these drugs, which highlights the importance to understand the molecular underpinnings of mitochondrial and cytosolic nucleotide pool coordination.

Additional nucleotide trafficking is likely to occur via other solute carriers such as SLC25A24 and SLC25A42 that exchange nucleotides with other non-nucleotide metabolites and might tune nucleotide concentrations between the compartments and coordinate nucleotide metabolism with other pathways ^{159–161}. Lastly, other IMM-proteins such as MPV17L and multiple uncharacterized solute carriers, likely contribute to mitochondrial nucleotide homeostasis in so far undefined ways and should be subjected to further investigation ¹⁶².

In summary, mitochondrial and cytosolic nucleotide pools are synchronized in multiple ways by different solute carriers as well as unknown players that facilitate the active (SLC25-family) or passive (SLC29-family) exchange of nucleotides and nucleosides between the two compartments. Therefore, nucleotide uptake by solute carriers from the cytosolic site of production is a prerequisite for successful mitochondrial gene expression.

1.2.4. The mitochondrial deoxyribonucleotide salvage pathway

The reason why mitochondria also uptake the unphosphorylated precursor nucleosides, that cannot be readily incorporated into DNA, is their ability to salvage these nucleosides by converting them back into dNTPs ¹⁰⁴. This pathway is called the mitochondrial nucleotide salvage pathway and serves as an additional source by which mitochondria can maintain their nucleotide levels (Figure 1.8).

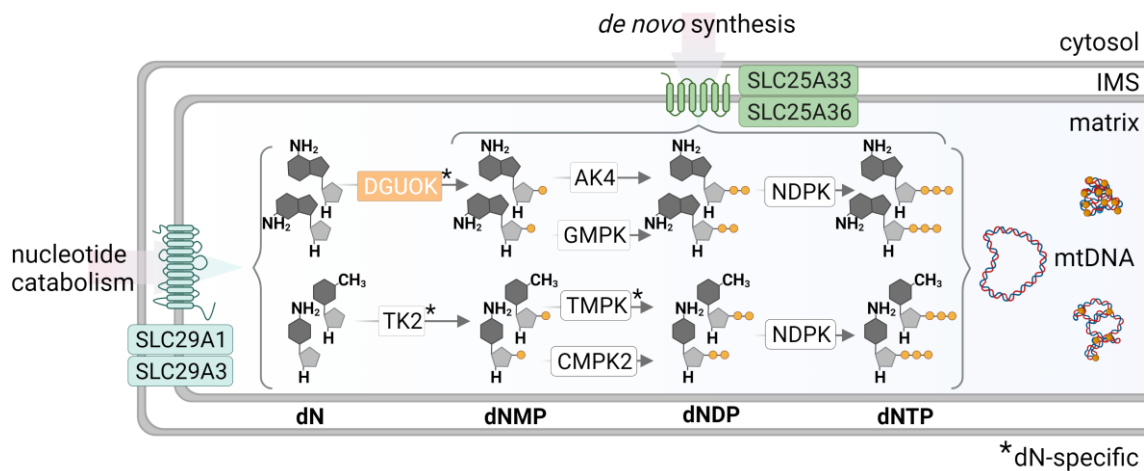


Figure 1.8 The mitochondrial deoxyribonucleotide salvage pathway

The recycling of deoxyribonucleotides within mitochondria from left to right.

Mitochondrial nucleotide recycling becomes particularly relevant, when *de novo* synthesis is reduced and the influx of cytosolic nucleotides is limited ¹⁰⁴. Mitochondria can then leverage their own nucleotide supply route to maintain their genome and their gene expression partially independent of cytosolic nucleotide availability. The mitochondrial nucleotide salvage pathway consists of three consecutive phosphorylation events that are carried out by mitochondria specific isoforms of enzymes that also operate in the cytosol. Even though this pathway is commonly referred to as the nucleotide salvage pathway, a more precise name would be the “mitochondrial deoxyribonucleotide salvage pathway” since ribonucleoside salvage activity has not yet been shown in mitochondria.

Purine and pyrimidine deoxyribonucleosides are converted into their respective monophosphate forms by the two mitochondrial matrix enzymes thymidine kinase 2 (TK2) and deoxyguanosine kinase (DGUOK). DGUOK preferentially phosphorylates deoxyguanosine (dG) and deoxyadenosine (dA) but exhibits deoxycytidine (dC) kinase activity as well ^{163,164}. TK2 is pyrimidine-specific and phosphorylates deoxy- uridine, cytidine and thymidine

(dC, dU and dT) ^{165–167}. The salvage of mitochondrial deoxyribonucleosides by TK2 and DGUOK is rate-limiting and also the only salvage-step that is strictly limited to deoxyribonucleosides. Subsequent phosphorylation steps are catalyzed by enzymes that are more promiscuous regarding the redox-state of the ribose and might act in the salvage of ribo- and deoxyribonucleosides respectively. These enzymes are the mitochondrial homologue of the cytosolic uridine-cytidine kinase (CMPK2) and, the mitochondrial adenylate kinase 4 (AK4) ^{168–171}. CMPK2, similar to its cytosolic counterpart CMPK1 was shown to phosphorylate UMP and CMP *in vitro*, but exhibited even higher affinity towards dCMP. This is in line with a rate-limiting CMPK2 function in mtDNA synthesis in lipopolysaccharide (LPS) stimulated macrophages ¹⁷². Interestingly, CMPK2 was also reported to act as a NDPK, that could use ATP and GTP as phosphate donors and therefore might fulfill multiple roles in mitochondrial nucleotide salvage ¹⁷¹. DGDP is synthesized by guanosine monophosphate kinase (GMPK) which is also the cytosolic guanylate kinase but is annotated as a mitochondrial protein as well ^{173,174}. Whether a specific isoform of GMPK localizes to mitochondria is not clear and the mitochondrial GMPK function has not been studied in detail. The fourth enzyme that phosphorylates dNMPs in mitochondria is the thymidylate kinase (DTYMK) that is dually localized to the cytosol and mitochondria and converts exclusively dTMP into dTDP ^{144,175,176}.

The last phosphorylation reaction in mitochondrial deoxyribonucleotide salvage is thought to be performed by a mitochondrial NDPK. Three NDPKs localize to mitochondria and exhibit kinase activity ^{127,177–180}. NME3 associates with the outer mitochondrial membrane (OMM), NME4 and NME6 localize to the mitochondrial matrix, however several reports also identified NME4 associated to the IMM facing the IMS ^{73,180–183}. Surprisingly, none of the mitochondrial NDPKs has been studied directly in the context of nucleotide metabolism and mitochondrial gene expression. Similar to the cytosolic NDPKs, NME4 and NME6 could act as the convergence point of mitochondrial ribo- and deoxyribonucleotide synthesis due to their broad substrate spectrum. NDPKs are nonspecific towards the base moiety and the 2'-hydroxyl group of the ribose and thus can phosphorylate all purine and pyrimidine ribonucleoside diphosphates as well as all deoxyribonucleoside diphosphates ¹⁸⁴.

The reaction mechanism is described as a ping-pong reaction that involves the transfer of the γ -phosphate from a donor NTP (usually ATP due to its abundance) to a catalytic histidine residue of the enzyme. The donor NTP is released as a NDP from the enzyme and the binding pocket is then occupied by the acceptor (d)NDP. The acceptor (d)NDP receives the phosphate from the phospho-histidine intermediate and is thereby converted into a (d)NTP ^{127,184}.

It is compelling to assume that mitochondrial NDPKs catalyze the final reaction of mitochondrial nucleotide salvage, however evidence that NME4 or NME6 is required for mitochondrial gene expression is scarce. So far only NME4 has been indirectly linked to affect mitochondrial gene expression. Firstly, NME4 was shown to form a complex with the succinyl-CoA synthase and the mitochondrial matrix protein ABAT that is required for mitochondrial deoxyribonucleotide salvage and maintenance of mtDNA copy number ^{185,186}. However, NME4-requirement for nucleotide salvage was not verified in this study ¹⁸⁵. Secondly, NME4 was shown to support mtDNA synthesis in LPS-stimulated macrophages, a process required for NLRP3-inflammasome activation ¹⁷². A subsequent study confirmed NME4-requirement for mtDNA synthesis and inflammasome licensing, but also linked this process to NME4-dependent cardiolipin exposure to the OMM and TNF receptor-associated factor 6 (TRAF6) recruitment to the OMM ¹⁸⁷. In summary, NME4 and also NME6 are likely candidates to catalyze the final reaction of mitochondrial nucleotide salvage, however their specific contribution to nucleotide homeostasis and mitochondrial gene expression awaits further experimental validation.

Only deoxyribonucleotide salvage capacity has been demonstrated in mitochondria so far. The existence of a second salvage pathway for ribonucleotides is an intriguing possibility, as also two dedicated salvage pathways for ribo- and deoxyribonucleotide recycling exist in the cytosol. Purine nucleobases are salvaged by the cytosolic enzymes adenosine phosphoribosyl transferase (APRT), hypoxanthine guanine phosphoribosyl transferase (HPRT) whereas pyrimidine nucleosides are salvaged by uridine-cytidine kinase 1 and 2 (UCK1/2) ^{188–191}. Specifically, these initial phosphorylation reactions of ribonucleosides have not yet been reported to be catalyzed by any mitochondrial enzyme. It remains to be seen whether mitochondrial homologues of

APRT/HPRT and UCK1/2 exist and whether mitochondria possess *bona fide* ribonucleotide salvage capacity.

In conclusion, the mitochondrial deoxyribonucleotide salvage pathway is an alternative source to sustain dNTP levels in mitochondria. Mitochondrial genome maintenance relies on mitochondrial dNTP recycling particularly when cytosolic *de novo* synthesis is limited.

1.3. Mitochondrial gene expression and disease

The expression of mitochondrial genes is essential for cellular and organismal health. The previous chapters have outlined various aspects of the mechanistic and metabolic requirements for mitochondrial gene expression. The importance of the factors that govern mitochondrial gene expression is reflected in their association with different pathologies that are summarized as mitochondrial diseases^{192,193}. Mitochondrial diseases are pleiotropic in nature and have been linked to numerous mutations in the nuclear- as well as the mitochondrial genome. With a disease prevalence of ~1:5000 mitochondrial diseases represent the most common group of congenital metabolic disorders^{192,193}. Diagnosis and treatment of mitochondrial diseases are notoriously challenging due to their diverse clinical manifestations. Typical features include seizures, hearing loss, encephalopathies, general weakness, myopathies and exercise intolerance, as well as metabolic dysfunctions such as lactic acidosis and diabetes mellitus. Mitochondrial diseases can occur at any age and often affect multiple tissues and organs, but symptoms generally develop most strongly in tissues with elevated energy requirements such as brain, heart and skeletal muscle^{192,193}. If a disease-causing mutation occurs on the mtDNA, its prevalence among the total mtDNA content in a cell and a tissue becomes a determining factor for the severity and progression of the disease. This phenomenon is called heteroplasmy and represents a unique hallmark of mitochondrial diseases that are caused by mtDNA mutations¹⁹⁴.

Besides mtDNA mutations that directly affect the expression of mitochondrial encoded proteins, several mutations in nuclear encoded genes have been reported to affect the process of mtDNA maintenance and thereby become pathogenic¹⁷. Mutations in these genes cause either mtDNA depletion or mtDNA deletions that lead to a dysfunctional ETC. These mitochondrial DNA

maintenance defect (MDMD) causing genes mostly include genes that are either part of the mtDNA replication machinery such as *POLG*, *TFAM*, *TWINKLE* and *MGME1* (see 1.1) or genes that regulate mitochondrial dNTP homeostasis such as *TK2*, *DGUOK*, *RRM2B* and *SLC25A4* (see 1.2) ¹⁷.

Mutations in these nucleotide homeostasis genes lead to a depletion of deoxyribonucleotides required for mtDNA replication. Mutations of *TK2* and *DGUOK*, directly affect the mitochondrial deoxyribonucleotide salvage capacity that can lead to mtDNA depletion or mtDNA deletions ¹⁹⁵. A *DGUOK* deficient mouse model was reported to exhibit mtDNA depletion across different tissues, alongside a reduction of the mitochondrial encoded complex IV subunit COX1. This phenotype was particularly pronounced in the liver and reflects features of *DGUOK*-deficient patients ¹⁹⁶. Other patients were reported to suffer from rhabdomyolysis, myopathies and progressive external ophthalmoplegia (PEO) ¹⁹⁷. Autosomal recessive PEO was also linked to two mutations in the *TK2* gene in patients that presented with multiple mtDNA depletions ¹⁹⁸. A *TK2*-deficient mouse model was rescued by the transgenic expression of a nuclear nucleoside kinase from *Drosophila melanogaster* (*Dm-dNK*) ¹⁹⁹. These transgenic mice exhibited elevated mtDNA levels and increased dTTP pools compared to *TK2*-deficient mice proving that mitochondrial deoxyribonucleotide salvage deficiency can be rescued by external dTMP synthesis ¹⁹⁹. This conclusion is also supported by the fact that *RRM2B* is a MDMD-causing gene. Notably, *RRM2B* is one of the few non-mitochondrial proteins reported so far that leads to MDMD ^{17,104}. *RRM2B* is the cell cycle independent subunit of the RNR complex and mainly responsible for the cytosolic ribonucleotide reduction in postmitotic cells and tissues. Mutations in *RRM2B* have been reported to lead to multiple mtDNA deletions causing mitochondrial disease phenotypes such as myopathies, PEO, and fatigue ^{200,201}. This emphasizes the notion that the mitochondrial deoxyribonucleotide salvage pathway cannot solely supply sufficient dNTPs for mtDNA replication and that mitochondria in postmitotic tissues still rely on cytosolic *de novo* synthesis of dNTPs ²⁰².

The importance of a functional nucleotide exchange between the cytosol and the mitochondria is also illustrated by mutations of *SLC25A4* leading to mtDNA deletions that have been described to cause cardio-myopathy and hypertrophy as well as PEO ^{150,203}. Mutations in another mitochondrial nucleotide carrier,

SLC25A36, have recently been reported in patients with hyperinsulinism/hyperammonemia syndrome (HI/HA) ¹⁵³. Further characterization of these mutations in HeLa cells revealed reduced mitochondrial GTP, CTP and mtDNA levels ¹⁵³. This illustrates that impaired mitochondrial nucleotide homeostasis and reduced mtDNA content can lead to pleiotropic disease phenotypes that not necessarily resemble mitochondrial disease phenotypes.

Altered mtDNA maintenance or mitochondrial nucleotide homeostasis can affect cellular and organismal health beyond mitochondrial function and has been linked to inflammation, DNA damage and premature ageing *in vitro* and *in vivo*. Loss of the mitochondrial protease YME1L interferes with nucleotide synthesis and nucleotide distribution causing mtDNA release into the cytosol and an innate immune response which could be blunted by exogenous supply of pyrimidines or depletion of SLC25A33 ¹⁰⁶. Interestingly, exogenous deoxynucleoside supplementation also proved to be beneficial in a model for impaired mtDNA replication. Deoxynucleoside supplementation rescued reduced mtDNA repopulation rates in human POLG-deficient fibroblasts treated with ethidium bromide ²⁰⁴. It was previously shown that mutations in *POLG* lead to increased but defective mtDNA replication and a concomitant dNTP pool imbalance that caused nuclear replication stress, DNA double strand breaks and premature ageing *in vivo* ¹⁰⁵. Mutagenic dNTP pools were also observed in another mtDNA replication deficiency model. Distinct mutations in the mitochondrial helicase TWINKLE lead to either mtDNA deletions or depletions that were accompanied by dNTP pool expansion or reduction respectively ²⁰⁵. These studies emphasize the intimate link between mtDNA maintenance and cellular nucleotide homeostasis. Impaired nucleotide homeostasis can be a cause and consequence of numerous mitochondrial diseases but impinges on cellular functions in general and has implications for non-mitochondrial diseases and organismal health as well. Thus, a comprehensive view on the cellular nucleotide metabolism is required to understand and potentially treat human disorders such as mitochondrial diseases in the future.

1.4. Aims of the thesis

Mitochondrial genome maintenance and gene expression is essential to sustain the numerous functions mitochondria fulfill in almost all eukaryotic cells. In humans, defective mitochondrial gene expression can lead to devastating pathologies that are difficult to diagnose and treat. Numerous disease-causing mutations have been identified in nucleotide metabolizing genes which underscore the important role that nucleotide metabolism plays in mitochondrial gene expression. However, the current understanding of how different nucleotide metabolizing genes impinge on mitochondrial gene expression remains incomplete.

Therefore, the aim of this thesis is to further explore mitochondrial nucleotide metabolism and its impact on mitochondrial gene expression.

1. We will test to what extent mitochondrial gene expression relies on the uptake of cytosolic pyrimidines by depleting the two known pyrimidine nucleotide carriers SLC25A33 and SLC25A36.
2. We will characterize how the loss of pyrimidine uptake will affect the mitochondrial nucleotide landscape, whether mitochondria undergo proteomic adaptations under these conditions and to what extent mitochondrial gene expression can be maintained.
3. We will devise an unbiased screening approach to identify novel nucleotide metabolizing genes that regulate mitochondrial gene expression if pyrimidine uptake is impaired.
4. Putative candidate genes will be further characterized and tested for their effects on mitochondrial nucleotide metabolism and mitochondrial gene expression.

2. Results

Successful mitochondrial gene expression requires sufficient amounts of ribo- and deoxyribonucleotides for mitochondrial transcription and replication, respectively. A major supply route for mitochondrial nucleotides is the uptake of cytosolic nucleotides facilitated by mitochondrial solute carrier proteins. We decided to further investigate the role of nucleotide uptake on mitochondrial gene expression. SLC25A33 and SLC25A36 have been identified as the mammalian mitochondrial pyrimidine transporters (see **1.2.3**)¹⁵¹. Loss of either carrier affects mitochondrial nucleotide levels, but the overlapping substrate affinities of SLC25A33 and SLC25A36 likely compensate partially for the reduced exchange rate if only one carrier is present¹⁵¹.

We decided to address this issue by simultaneously targeting SLC25A33 and SLC25A36. Depleting both nucleotide carriers simultaneously, compared to the previously studied single knockouts, bears the advantage that compensatory nucleotide influx into mitochondria is prevented more comprehensively. This allows us to explore alternative routes for nucleotide pool maintenance in mitochondria and facilitates the study of mitochondrial nucleotide metabolism and its effect on mitochondrial gene expression.

2.1. Loss of SLC25A33 and SLC25A36 causes mitochondrial nucleotide depletion

We generated *SLC25A33/SLC25A36* double knockout (DKO) HeLa cells using CRISPR-Cas9 gene editing technology. We selected two clones (#1; #2) that exhibited complete depletion of SLC25A33 and SLC25A36 for further experiments (**Figure 2.1A**). Loss of SLC25A33 or SLC25A36 individually reduces mitochondrial UTP, GTP and CTP levels, which is in line with the reported *in vitro* transport activities^{151,153,206}.

To test whether the *SLC25A33/SLC25A36* DKO HeLa cells exhibit a similar phenotype, we measured the steady-state nucleotide levels of mitochondria enriched fraction by liquid chromatography-mass spectrometry (LC-MS). We isolated mitochondria from cell extracts using density-gradient centrifugation, as this has been done previously to study mitochondrial nucleotide pools^{207–209}. The

purity of the isolated fractions was confirmed by immunoblot analysis. Mitochondria enriched fractions contained increased amounts of the mitochondrial OXPHOS components ATP5A, UQCRC2, SDHB and NDUFB8, whereas the cytosolic protein Vinculin was depleted from these fractions (**Figure 2.1B**).

Dimensionality reduction by principal component analysis (PCA) revealed separation of the cell extracts from the mitochondria enriched fractions, as well as a separation of the genotypes within the mitochondrial fraction (**Figure 2.1C**). This indicates a distinct and reproducible metabolite profile of the isolated fractions as well as a genotype-dependent adaptation within the mitochondrial fraction. Loss of SLC25A33 and SLC25A36 led to a depletion of mitochondrial GTP and CTP by ~75% and UTP by 50% in both tested clones (**Figure 2.1D**). The precursor mono- and diphosphates were equally affected as their respective triphosphates, except UMP, which was reduced by 30%. These findings are in accordance with the previously reported transport capacities of these carriers and confirm SLC25A33 and SLC25A36 as a major entry route of nucleotides into mitochondria^{151,153,206}. ATP, in contrast to the other three NTPs, is produced in large quantities by complex V of the ETC and is exported from the mitochondria into the cytosol via a dedicated set of ANTs (SLC25A4/5/6/31)¹⁵⁰. ATP and its precursors were only mildly depleted in clone #1 and completely unaffected in clone #2 compared to HeLa WT cells. This corroborates the previous finding that mitochondrial ATP levels are not affected by loss of SLC25A33 and is consistent with the existence of an adenosine nucleotide-specific exchange route through SLC25A4/5/6 or SLC25A31 respectively^{150,206}.

In line with deoxyribonucleotides transport capacity of SLC25A33 and SLC25A36¹⁵¹, mitochondrial ribonucleotide depletion in *SLC25A33/SLC25A36* DKO cells was accompanied by a depletion of deoxyribonucleotides (**Figure 2.1E**). Similar to their ribo-counterparts, mitochondrial dGTP and dTTP pools were depleted by more than 50%. Mitochondrial dCTP pool size was most strongly affected and reduced by 90% in both tested clones. Further, dATP levels were mildly reduced in clone #1 and unchanged in clone #2.

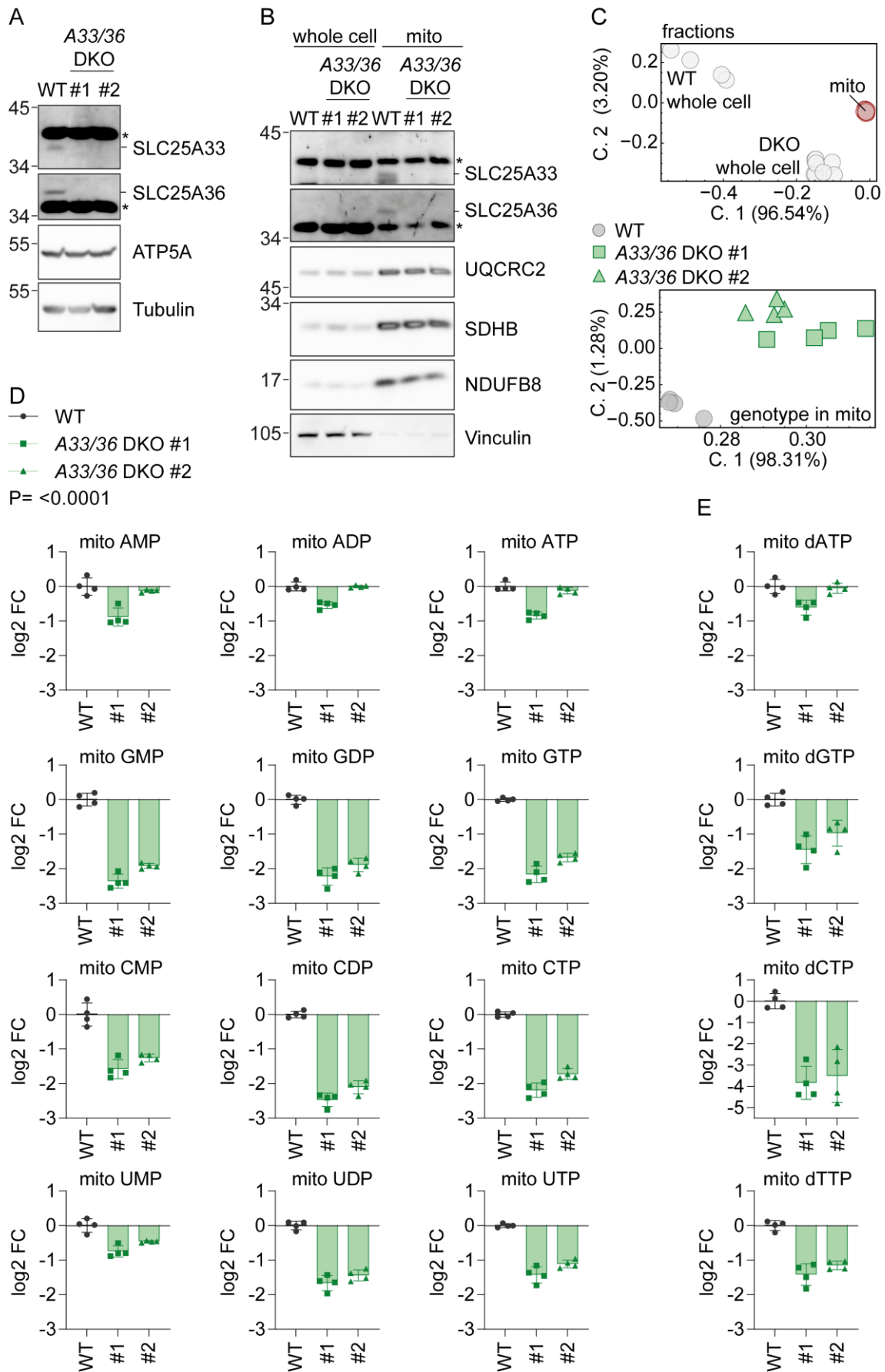


Figure 2.1 Loss of SLC25A33 and SLC25A36 causes mitochondrial nucleotide depletion

(A) Representative immunoblot of HeLa WT and *SLC25A33/SLC25A36* double knockout (DKO) cells.

(B) Representative immunoblot analysis comparing whole cell extracts and mitochondria enriched fractions of HeLa WT and *SLC25A33/SLC25A36* DKO cells used for LC-MS based metabolomics analysis.

(C) Dimensionality reduction analysis by principal component analysis (PCA) resolved for whole cell extracts (grey) and mitochondria enriched fractions (red) (top) and genotypes (WT in grey; DKO in green) within the mitochondrial fraction (bottom).

(D) Relative ribonucleotide levels of mitochondria enriched fractions from *SLC25A33/SLC25A36* DKO cells (clone #1 and #2) compared to HeLa WT cells as determined by quantitative mass spectrometry. P-value for D and E: two-way ANOVA; P-value (genotype) = <0.0001; P-value (metabolite) = <0.0001; P-value (interaction) = <0.0001. (log₂ fold change; n = 4 independent cultures).

(E) Relative deoxyribonucleotide levels of mitochondria enriched fractions from *SLC25A33/SLC25A36* DKO cells (clone #1 and #2) compared to HeLa WT cells as determined by quantitative mass spectrometry. (log₂ fold change; n = 4 independent cultures).

We measured other mitochondrial non-nucleotide metabolites to rule out the possibility that loss of SLC25A33 and SLC25A36 leads to a general depletion of mitochondrial metabolites.

The TCA-cycle intermediates citrate, aconitate, isocitrate and α -ketoglutarate were either unchanged or accumulated mildly in *SLC25A33/SLC25A36* DKO cells, confirming that loss of the nucleotide carriers specifically affects nucleotides and not mitochondrial metabolites in general (**EV 7A**). Concomitant with the mitochondrial nucleotide pools, nucleotide levels of whole cell extracts were also reduced in *SLC25A33/SLC25A36* DKO cells, yet to a lesser extent (**EV 7B**). Since whole cell extracts include mitochondrial nucleotide pools that contribute to total nucleotide levels, a statement about the cytosolic nucleotide levels cannot be made. Interrupted nucleotide exchange between mitochondria and the cytosol might affect *de novo* nucleotide synthesis and or nucleotide salvage directly, which could be an additional contributing factor to the depletion of total nucleotide levels.

Taken together, the combined loss of SLC25A33 and SLC25A36 leads to a significant depletion of the mitochondrial nucleotides GTP, CTP and UTP and their deoxy-analogues, corroborating previous *in vitro* studies^{151,153}.

2.2. *SLC25A33/SLC25A36* DKO cells sustain mitochondrial gene expression

We reasoned that the limited mitochondrial nucleotide influx, should affect processes that rely on an adequate supply of ribo- and deoxyribonucleotides. Therefore, we measured mtDNA and mtRNA steady state levels in WT and *SLC25A33/SLC25A36* DKO cells by real-time quantitative polymerase chain reaction (qPCR). Surprisingly, mtDNA levels were only reduced by 20% in response to the combined loss of *SLC25A33* and *SLC25A36* (**Figure 2.2A**)²¹⁰. Hence, although mtDNA replication depends on the supply of deoxyribonucleotides, loss of the known mitochondrial pyrimidine carriers affected mtDNA levels on moderately. Conversely, mitochondrial transcripts were either unaffected by the loss of *SLC25A33* and *SLC25A36* or were significantly increased (**Figure 2.2B**). This indicates that the remaining mitochondrial ribonucleotides are sufficient to sustain transcription. Largely functional mitochondrial gene expression in *SLC25A33/SLC25A36* DKO HeLa cells was further confirmed by Seahorse experiments.

The oxygen consumption rate (OCR) and the extracellular acidification rate (ECAR) were only mildly reduced in the *SLC25A33/SLC25A36* DKO cells, indicative of an intact ETC and a normal glycolysis rate (**Figure 2.2C**). Depletion of *SLC25A33* and *SLC25A36* had a modest impact on cellular fitness in standard culture conditions. Incucyte live cell imaging growth assays revealed a growth rate reduction of 10% (**Figure 2.2D**).

Together, these data demonstrate that despite a general depletion of mitochondrial nucleotide pools by >50%, *SLC25A33/SLC25A36* DKO HeLa cells are able to maintain mitochondrial gene expression that suffices to prevent severe OXPHOS deficiency and to prevent a metabolic shift towards glycolysis. Our data leads to the conclusion that mitochondrial nucleotides are present in excess and not a rate-limiting factor for mitochondrial gene expression under steady state conditions in proliferating HeLa cells.

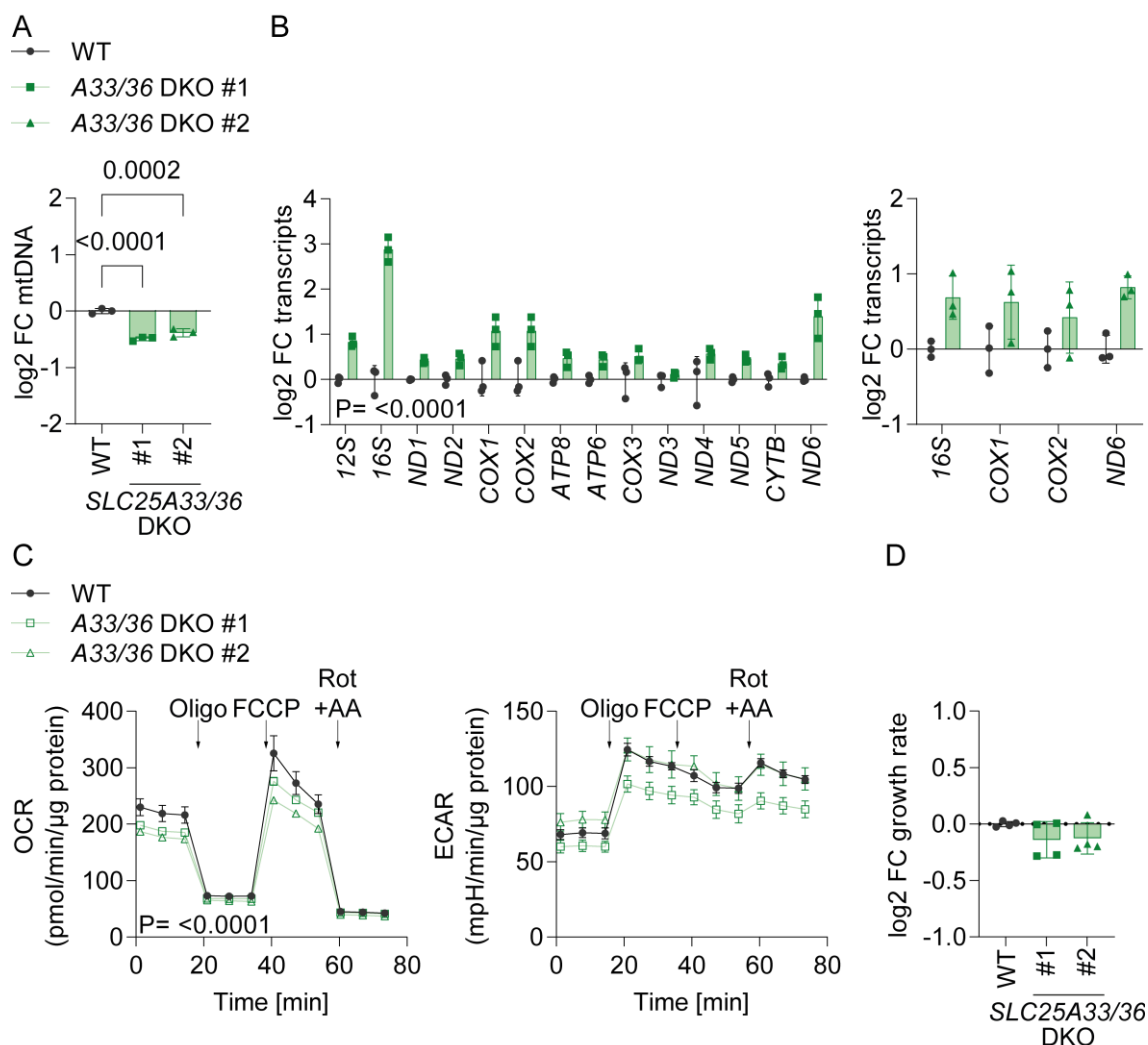


Figure 2.2 *SLC25A33/SLC25A36* DKO cells sustain mitochondrial gene expression

(A) Relative mtDNA levels of HeLa WT and *SLC25A33/SLC25A36* DKO cells (clone #1 and #2) as determined by qPCR. P-values: one-way ANOVA. (log₂ fold change; n = 3 independent cultures).

(B) Relative mitochondrial transcript levels of HeLa WT and *SLC25A33/SLC25A36* DKO cells (clone #1 left and #2 right) as determined by qPCR. P-value: two-way ANOVA. P-value (genotype) = <0.0001; P-value (transcript) = <0.0001; P-value (interaction) = <0.0001. (log₂ fold change; n = 3 independent cultures).

(C) Oxygen consumption rates (OCR) and extracellular acidification rates (ECAR) HeLa WT and *SLC25A33/SLC25A36* DKO cells (clone #1 and #2) during a mitochondrial stress test with inhibitor treatments at the indicated time points. P-values for OCR: two-way ANOVA P-value (time) = <0.0001, P-value (genotype) = <0.0001, P-value (interaction) = <0.0001. (n = 3 independent cultures).

(D) Relative growth rates of HeLa WT and *SLC25A33/SLC25A36* DKO cells (clone #1 and #2), (log₂ fold change; n = 4 independent cultures).

2.3. Mitochondrial proteome profiling of *SLC25A33/SLC25A36* DKO cells

To investigate whether loss of *SLC25A33* and *SLC25A36* leads to adaptations in the mitochondrial proteome, that could support mitochondrial gene expression upon nucleotide depletion, we performed LC-MS based proteomics in HeLa WT and *SLC25A33/SLC25A36* DKO cells.

In total 10729 proteins were identified out of which 971 were annotated as mitochondrial proteins by MitoCarta3.0, thereby covering 85% of the mitochondrial proteome (**Figure 2.3A**)¹⁷³. Loss of *SLC25A33* or *SLC25A36* has been associated with an increase in mitochondrial biogenesis and thereby mitochondrial mass^{153,211}. Comparing total protein abundance and mitochondrial protein abundance between HeLa WT cells and *SLC25A33/SLC25A36* DKO cells revealed a slight accumulation of mitochondrial proteins, which was significant in clone #2, supporting previous studies. However, accumulation of mitochondrial proteins was not linked to a specific mitochondrial process.

1D-enrichment pathway analysis for mitochondrial pathways according to MitoCarta3.0 did not identify a systematic change of proteins that can be mapped to a specific mitochondrial function¹⁷³. Mitochondrial pathways, that are associated with mitochondrial gene expression, such as “nucleotide metabolism”, “mtDNA- and mtRNA-maintenance” and “*SLC25A* family” were not systematically regulated in *SLC25A33/SLC25A36* DKO cells compared to HeLa WT cells (**Figure 2.3B**).

Therefore, we looked at the regulation of individual mitochondrial proteins, annotated by volcano plot analysis. Significant protein changes, based on multiple testing correction by permutation based false discovery rate (FDR), that occurred in both clones included *SLC25A24*, *SLC25A42* and *AK4* (**Figure 2.3C**). The common feature of these proteins is their role in mitochondrial adenine nucleotide homeostasis. *AK4*, which accumulated in both clones catalyzes the phosphorylation of AMP and dAMP into ADP and dADP in the mitochondrial matrix. Like other adenylate kinases, *AK4* exhibits NDPK-activity and can convert (d)NDPs into their respective (d)NTPs, thereby supporting mitochondrial nucleotide metabolism^{169,171,212}. Increased levels of *SLC25A24* leads to increased adenine nucleotide import in exchange for inorganic phosphate, that has been reported to improve Ca²⁺-handling in cancer cells^{159,160}. *SLC25A42* exchanges cytosolic Coenzyme A (CoA) for mitochondrial adenine nucleotides.

Reduced SLC25A42 levels in *SLC25A33/SLC25A36* DKO cells, thus limit mitochondrial efflux of adenine species and CoA uptake¹⁶¹. The observed changes of these proteins favor the accumulation of adenine nucleotides within the mitochondrial matrix and likely contribute to the mild phenotype observed for adenine nucleotides (**Figure 2.1D/E**). Additionally, stronger regulation of these proteins in clone #2 correlates with increased mitochondrial adenine species observed in this clone.

TFB2M, is an essential component of the transcription initiation machinery and increased levels have been shown to promote transcription *in vitro*³⁶. Hence, it is conceivable that elevated TFB2M levels in *SLC25A33/SLC25A36* DKO cells boost mitochondrial transcription and contribute to steady mitochondrial gene expression in these cells.

In summary, loss of SLC25A33 and SLC25A36 leads to a differential regulation of several mitochondrial proteins, but not to a pathway-specific adaptation of the mitochondrial proteome. Changes observed in proteins that are involved in adenine nucleotide homeostasis and mitochondrial transcription likely support mitochondrial gene expression if the supply of nucleotides from the cytosol is limited.

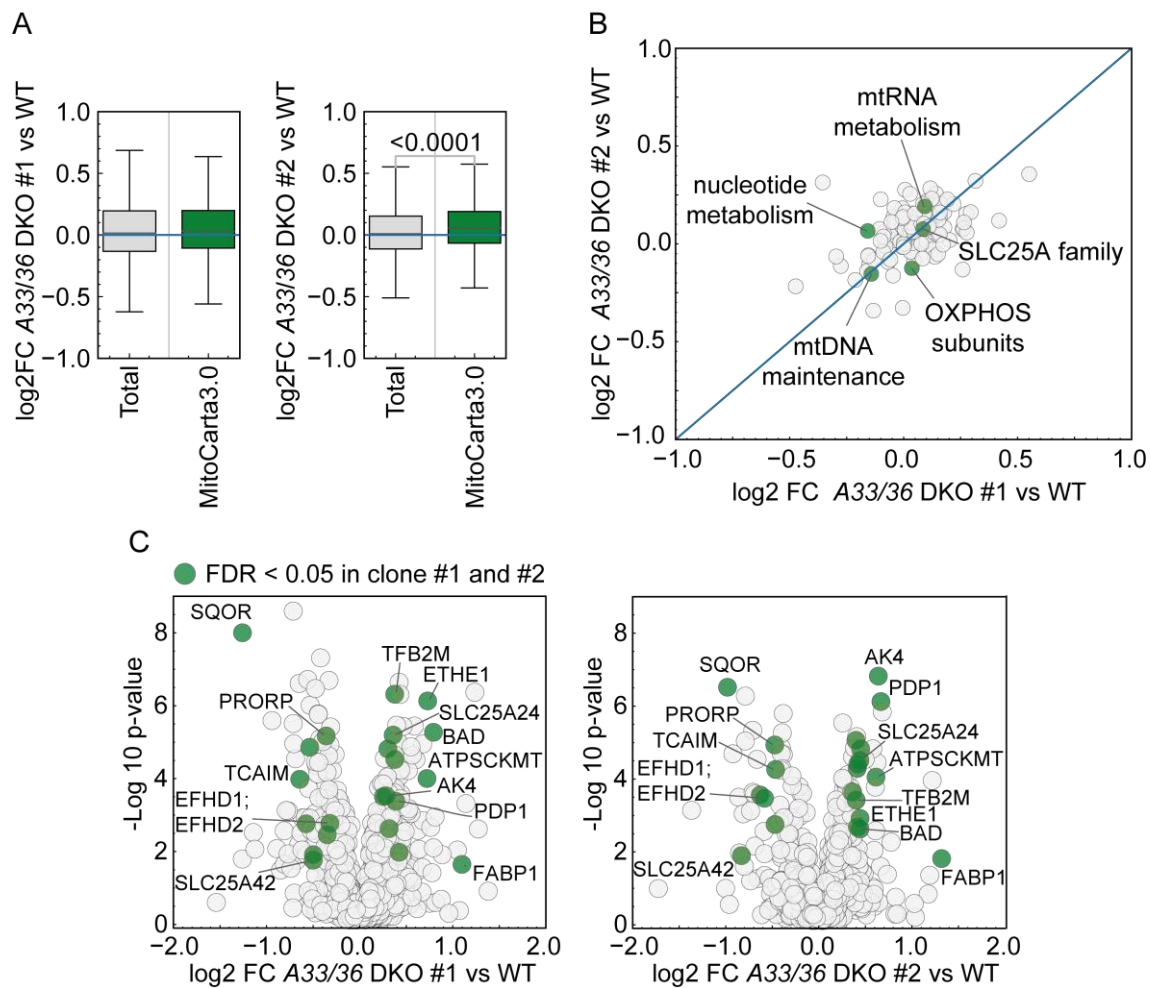


Figure 2.3 Mitochondrial proteome profiling of *SLC25A33/SLC25A36* DKO cells

(A) Box plot analysis of log₂ fold change in protein intensities in *SLC25A33/SLC25A36* DKO cells compared to WT HeLa cells. Distribution of the complete set of quantified protein groups Total (10729 proteins detected) and MitoCarta3.0 positive (971 proteins detected) (Box limits denote 25- and 75% quartile, line denotes the median, whiskers denote 1.5 x interquartile range deviation from the median), (P-value: Welch's t-test; log₂ fold change; n = 6 independent cultures).

(B) 1D-enrichment pathway analysis for MitoPathways according to MitoCarta3.0 annotation of HeLa WT and *SLC25A33/SLC25A36* DKO cells (clone #1 and #2). Each dot represents the median log₂ fold change compared to WT of a MitoPathway category. Annotated selection highlighted in green (log₂ fold change).

(C) Volcano plot representation of log₂ fold change in mitochondrial protein abundance of *SLC25A33/SLC25A36* DKO cells (clone #1 left, and #2 right) compared to HeLa WT cells. FDR-significant (<0.05) protein changes in both clones in green, with selected annotation (log₂ fold change, false discovery rate, n = 6 independent cultures).

2.4. Loss of *DGUOK* is not rate-limiting for mitochondrial gene expression

Our data supports the notion that *SLC25A33* and *SLC25A36* are a major factor for mitochondrial nucleotide homeostasis, however additional nucleotide sources must exist, that account for the remaining mitochondrial nucleotides of *SLC25A33/SLC25A36* DKO cells. The mitochondrial deoxyribonucleotide salvage pathway represents a second source for mitochondrial nucleotides. In contrast to *SLC25A33* and *SLC25A36* that facilitate the import of mono- di- or triphosphorylated nucleosides, the mitochondrial salvage pathway recycles unphosphorylated deoxynucleosides. The primary enzymes in this pathway, TK2 and *DGUOK*, catalyze the conversion of dC, dT, and dG and dA into their respective monophosphate forms^{165,213,214}. In contrast to *SLC25A33* and *SLC25A36*, mutation in TK2 and *DGUOK* have been linked to mitochondrial DNA depletion syndrome (MDS) in patients^{17,195,197}.

We therefore decided to use *DGUOK* KO HeLa cells to test whether inhibition of the nucleotide salvage rather than the inhibition of nucleotide import affects mitochondrial gene expression.

We targeted *DGUOK* by CRISPR Cas9 and selected two clones that showed complete depletion of *DGUOK* by immunoblot analysis. (**Figure 2.4A**). Depletion of *DGUOK* did not affect steady state mtDNA levels and did not significantly change expression of selected mitochondrial transcripts (**Figure 2.4B/C**). We further confirmed the functional expression of mitochondrial genes by testing OCR and ECAR in both *DGUOK* KO clones (**Figure 2.4D**). Respiratory- and glycolytic-rates were similar to WT rates, which confirms that blocking the nucleotide salvage pathway by *DGUOK* depletion does not impact mitochondrial gene expression in proliferating HeLa cells. This was in line with WT-level growth rates in these clones and LC-MS based proteomics experiments confirmed that loss of *DGUOK* does not alter the mitochondrial proteome in a pathway-specific manner (**Figure 2.4E/F/G; EV 8**).

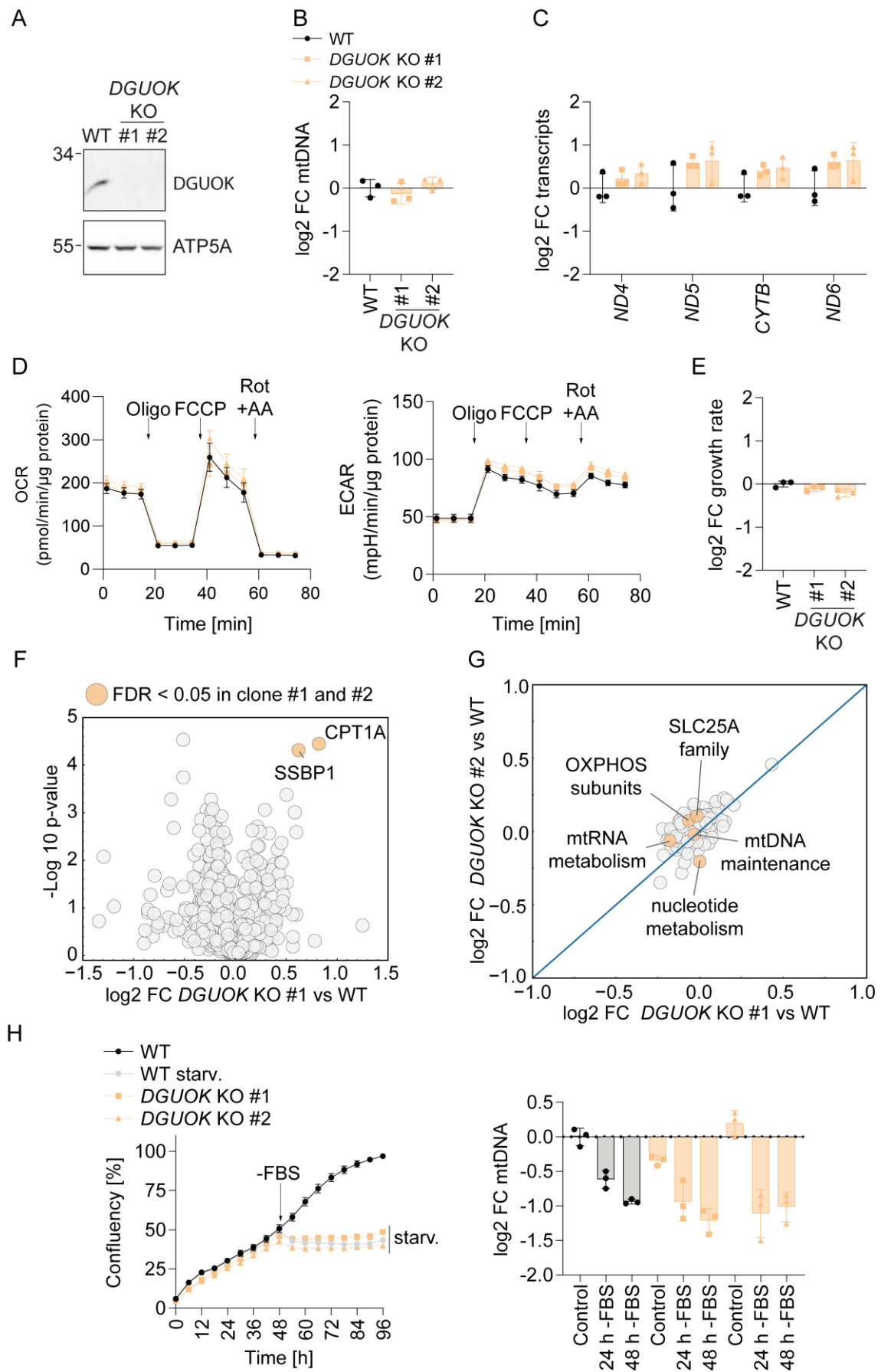


Figure 2.4 Loss of DGUOK is not rate-limiting for mitochondrial gene expression

- (A) Representative immunoblot of *DGUOK* knockout (KO) (clone #1 and #2) and WT HeLa cells.
- (B) Relative mtDNA levels of HeLa WT and *DGUOK* KO (clone #1 and #2) cells as determined by qPCR (log₂ fold change; n = 3 independent cultures).
- (C) Relative mitochondrial transcript levels of HeLa WT and *DGUOK* KO (clone #1 and #2) cells as determined by qPCR (log₂ fold change; n = 3 independent cultures).
- (D) Oxygen consumption rates (OCR) and extracellular acidification rates (ECAR) HeLa WT and *DGUOK* KO (clone #1 and #2) cells during a mitochondrial stress test with inhibitor treatments at the indicated time points.
- (E) Relative growth rates of HeLa WT and *DGUOK* KO (clone #1 and #2) cells (log₂ fold change; n = 3 independent cultures).
- (F) Volcano plot representation of log₂ fold change in mitochondrial protein abundance of *DGUOK* KO cells (clone #1) compared to HeLa WT cells. FDR-significant (<0.05) protein changes in both clones in orange, with selected annotation (log₂ fold change, false discovery rate, n = 3 independent cultures).
- (G) 1D-enrichment pathway analysis for MitoPathways according to MitoCarta3.0 annotation of HeLa WT and *DGUOK* KO cells (clone #1 and #2). Each dot represents the median log₂ fold change compared to WT of a MitoPathway category. Annotated selection highlighted in orange (log₂ fold change).
- (H) Growth curve of HeLa WT and *DGUOK* KO (clone #1 and #2) cells after serum withdrawal (-FBS) alongside mtDNA levels as determined by qPCR at the indicated time points. (log₂ fold change; n = 3 independent cultures).

In proliferating cells, such as HeLa cells, the cellular demand for dNTPs is high and the *de novo* synthesis rate increases to expand the deoxyribonucleotide pools required for replication of the genome^{100,104,139}. Increased cytosolic dNTP levels also fuel mitochondrial dNTP demands and hence the reliance on the mitochondrial salvage of dNTPs is reduced under these conditions. On the contrary, in non-proliferating cells, *de novo* synthesis rate is reduced and cytosolic provision of dNTPs to the mitochondria is limited. Mitochondria replicate their genome independently of the cell cycle and mitigate the reduced influx of cytosolic dNTPs by using their deoxyribonucleotide salvage pathway to sustain mitochondrial dNTP pools¹⁰⁴.

We decided to test whether loss of DGUOK becomes an essential factor for mtDNA maintenance when cytosolic *de novo* dNTP synthesis is limited. Therefore, we induced cell cycle arrest by serum starvation in *DGUOK* KO clones and monitored proliferation rates by Incucyte-based live cell imaging. Proliferation was successfully stopped within 6 hours of serum starvation (**Figure 2.4H**)²¹⁵. We measured mtDNA levels 24 h and 48 h after induction of cell cycle arrest. HeLa WT and *DGUOK* KO cells reduced their mtDNA content over time, however no genotype specific difference could be observed. This indicates that DGUOK is not rate limiting for mtDNA maintenance in non-proliferating HeLa cells.

In summary, these data show that neither inhibition of nucleotide import nor inhibition of nucleotide salvage via DGUOK depletion is sufficient to affect

mitochondrial nucleotide pools in HeLa cells in such a way that mitochondrial gene expression is affected. This remarkable plasticity of mitochondrial nucleotide homeostasis raises the question as to what extent these two pathways operate in parallel and whether alternative, yet unknown, factors of mitochondrial nucleotide metabolism contribute to the observed plasticity.

2.5. Mitochondrial nucleotide import and salvage synergize to maintain mtDNA levels

Our data indicate that redundant pathways partially sustain mitochondrial nucleotide levels in the absence of SLC25A33 and SLC25A36. We argue that *SLC25A33/SLC25A36* DKO cells are a useful system to discover synthetic gene dependencies in mitochondrial nucleotide metabolism.

As a proof of this concept, we decided to test whether the mitochondrial nucleotide salvage pathway fulfills a redundant role in this system.

Therefore, we combined our two previously characterized models and generated *SLC25A33/SLC25A36/DGUOK* triple knockout (TKO) cells, to monitor mitochondrial gene expression upon combined interference with nucleotide uptake and salvage. Strikingly, mitochondrial proteins of the ETC were not changed, including the mitochondrial encode complex IV subunit COX1, as shown by immunoblot analysis (**Figure 2.5A**). Unchanged mitochondrial ETC proteins, were accompanied by increased levels of mitochondrial transcripts in *SLC25A33/SLC25A36/DGUOK* TKO cells, suggesting functional mitochondrial gene expression in these cells (**Figure 2.5B**). However, the combined depletion of SLC25A33/SLC25A36 and DGUOK led to a reduction of mtDNA by 50% compared to HeLa WT cells (**Figure 2.5C**). Indicating that both, nucleotide import and nucleotide salvage synergize to provide sufficient dNTPs for mtDNA maintenance.

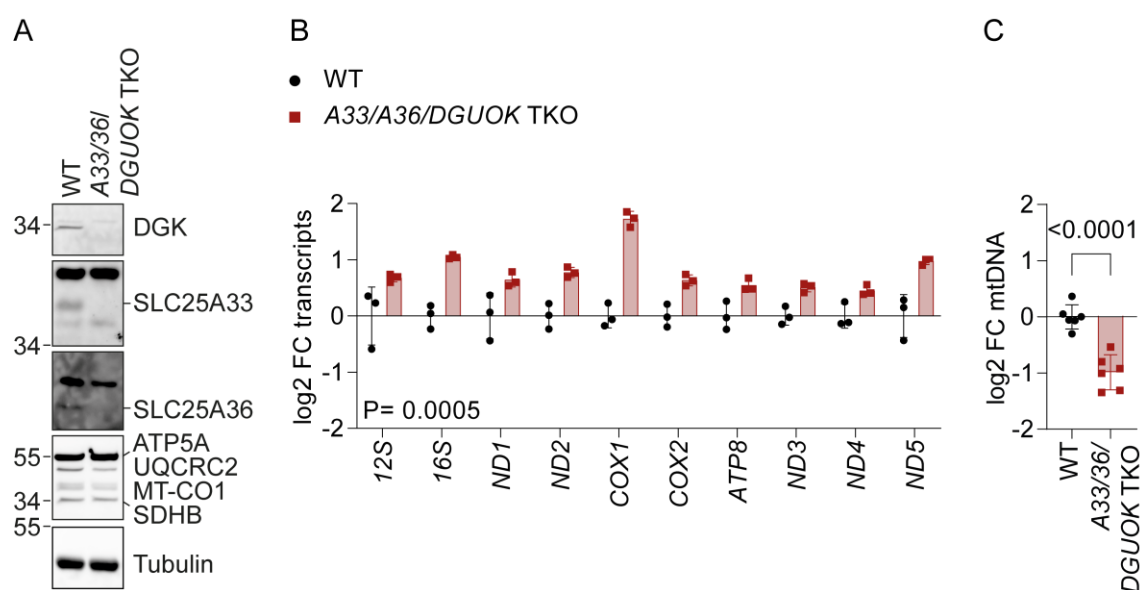


Figure 2.5 Mitochondrial nucleotide import and salvage synergize to maintain mtDNA levels

(A) Representative immunoblot of HeLa WT and *SLC25A33/SLC25A36/DGUOK* triple knockout (TKO) cells.

(B) Relative mitochondrial transcript levels of HeLa WT and *SLC25A33/SLC25A36/DGUOK* TKO cells as determined by qPCR. P-values: two-way ANOVA, P-value (genotype) = <0.0001; P-value (transcript) = 0.0005; P-value (interaction) = 0.0005 (log₂ fold change; n = 3 independent cultures).

(C) Relative mtDNA levels of HeLa WT *SLC25A33/SLC25A36/DGUOK* TKO cells and as determined by qPCR. P-value: unpaired t-test (log₂ fold change; n = 6 independent cultures).

The effect of DGUOK depletion on mtDNA but not on mtRNA in the *SLC25A33/SLC25A36* DKO background is in line with DGUOK specificity for deoxyribonucleosides²¹⁴. Even though mtDNA levels were depleted by 50%, mitochondrial gene expression remained unaffected due to sufficient transcript levels, in line with other mtDNA depletion models^{216,217}. Increased transcript levels suggests that ribonucleotide pools in *SLC25A33/SLC25A36/DGUOK* TKO cells have not reached rate-limiting concentrations for mitochondrial transcription. We conclude that indeed different factors of mitochondrial nucleotide homeostasis synergize to facilitate mitochondrial gene expression and that individual contributions of these factors can be revealed by combined interference. The fact that mtDNA was still maintained at 50% and mtRNA was increased in *SLC25A33/SLC25A36/DGUOK* TKO cells points to additional mitochondrial sources for dNTPs and rNTPs respectively. We decided to try to identify these sources with an unbiased CRISPR-screen approach.

2.6. Ribonucleotide synthesis by NME6 fuels mitochondrial gene expression

The following chapter of this thesis has already been published and represents the main work of my PhD. This publication was a collaborative effort of multiple authors. My personal contributions to the publication included:

Conceptualization; data curation; formal analysis; validation; investigation; visualization; methodology; writing – original draft; writing – review and editing.

The reader may continue with section 2.6.1

“The maintenance of mtDNA depends on NME6 when pyrimidine nucleotide import is blocked”

SOURCE
DATATRANSPARENT
PROCESSOPEN
ACCESS

Ribonucleotide synthesis by NME6 fuels mitochondrial gene expression

Nils Grotehans¹ , Lynn McGarry¹ , Hendrik Nolte¹, Vanessa Xavier², Moritz Kroker¹,
Álvaro Jesús Narbona-Pérez¹ , Soni Deshwal¹ , Patrick Gialvalisco¹, Thomas Langer^{1,3} &
Thomas MacVicar^{2,*}

Abstract

Replication of the mitochondrial genome and expression of the genes it encodes both depend on a sufficient supply of nucleotides to mitochondria. Accordingly, dysregulated nucleotide metabolism not only destabilises the mitochondrial genome, but also affects its transcription. Here, we report that a mitochondrial nucleoside diphosphate kinase, NME6, supplies mitochondria with pyrimidine ribonucleotides that are necessary for the transcription of mitochondrial genes. Loss of NME6 function leads to the depletion of mitochondrial transcripts, as well as destabilisation of the electron transport chain and impaired oxidative phosphorylation. These deficiencies are rescued by an exogenous supply of pyrimidine ribonucleosides. Moreover, NME6 is required for the maintenance of mitochondrial DNA when the access to cytosolic pyrimidine deoxyribonucleotides is limited. Our results therefore reveal an important role for ribonucleotide salvage in mitochondrial gene expression.

Keywords mitochondria; mitochondrial DNA; mitochondrial transcription; NME6; nucleotide metabolism

Subject Categories Organelles; Translation & Protein Quality

DOI 10.15252/embj.2022113256 | Received 11 December 2022 | Revised 7 June 2023 | Accepted 19 June 2023

The EMBO Journal (2023) e113256

Introduction

Oxidative phosphorylation (OXPHOS) drives the synthesis of ATP during aerobic respiration and regulates broad cellular functions including redox homeostasis and cell death (Winter *et al*, 2022). The OXPHOS protein complexes at the inner mitochondrial membrane are predominantly composed of nuclear DNA-encoded subunits that are imported into mitochondria. However, the correct assembly and activity of complexes I, III, IV and V also depend on the integration of subunits encoded by mitochondrial DNA (mtDNA)

in the mitochondrial matrix (Fernandez-Vizarra & Zeviani, 2021). The compact and circular mtDNA encodes 13 OXPHOS subunits, two ribosomal RNAs (rRNAs) and 22 transfer RNAs (tRNAs) in mammalian cells and is maintained at a high, yet variable, copy number across tissues and developmental stages (Filograna *et al*, 2021).

The replication of mtDNA and synthesis of mitochondrial RNA (mtRNA) require a constant supply of deoxyribonucleoside triphosphates (dNTPs) and ribonucleoside triphosphates (rNTPs), respectively (Gustafsson *et al*, 2016; D'Souza & Minczuk, 2018). Disturbances in the nucleotide supply lead to mtDNA depletion and/or deletions causing mitochondrial disease (Vafai & Mootha, 2012; Russell *et al*, 2020). Mammalian cells synthesise dNTPs and rNTPs either *de novo* in the cytosol from multiple carbon and nitrogen sources or, in a process termed nucleotide salvage, from (deoxy)ribonucleosides via a series of phosphorylation reactions within the cytosol or within mitochondria (Lane & Fan, 2015). Mitochondria therefore depend on the import of dNTPs and rNTPs or of precursor (deoxy)ribonucleosides across the inner mitochondrial membrane (Mathews & Song, 2007; Wang, 2016) (Fig 1A).

The predominant source and supply route of dNTPs for mtDNA replication is defined by the cell cycle and tissue type (Wang, 2016). Within proliferating cells, mitochondria import *de novo* synthesised dNTPs from the cytosol, while quiescent cells have a greater dependence on mitochondrial nucleotide salvage as a consequence of downregulated cytosolic dNTP synthesis (Ferraro *et al*, 2005; Mathews & Song, 2007). Accordingly, patients with mutations in the mitochondrial pyrimidine salvage pathway enzyme thymidine kinase 2 (*TK2*) show severe depletion of mtDNA in the skeletal muscle (Saada *et al*, 2001; Suomalainen & Isohanni, 2010). Disturbances in mitochondrial nucleotide metabolism also impact cellular nucleotide balance with striking consequences for cellular signalling. Expression of proofreading-deficient mtDNA polymerase gamma enhances the uptake of mitochondrial dNTPs, which results in the depletion of cytosolic dNTPs and nuclear genomic instability (Hamalainen *et al*, 2019). This was observed in mouse stem cells but not in whole mouse embryos, pointing to cell type specific

¹ Max Planck Institute for Biology of Ageing, Cologne, Germany

² The CRUK Beatson Institute, Glasgow, UK

³ Cologne Excellence Cluster on Cellular Stress Responses in Aging-Associated Diseases (CECAD), University of Cologne, Cologne, Germany

*Corresponding author. Tel: +49 221 37 970 500; E-mail: tlanger@age.mpg.de

**Corresponding author. Tel: +44 0141 330 2066; E-mail: thomas.macvicar@glasgow.ac.uk

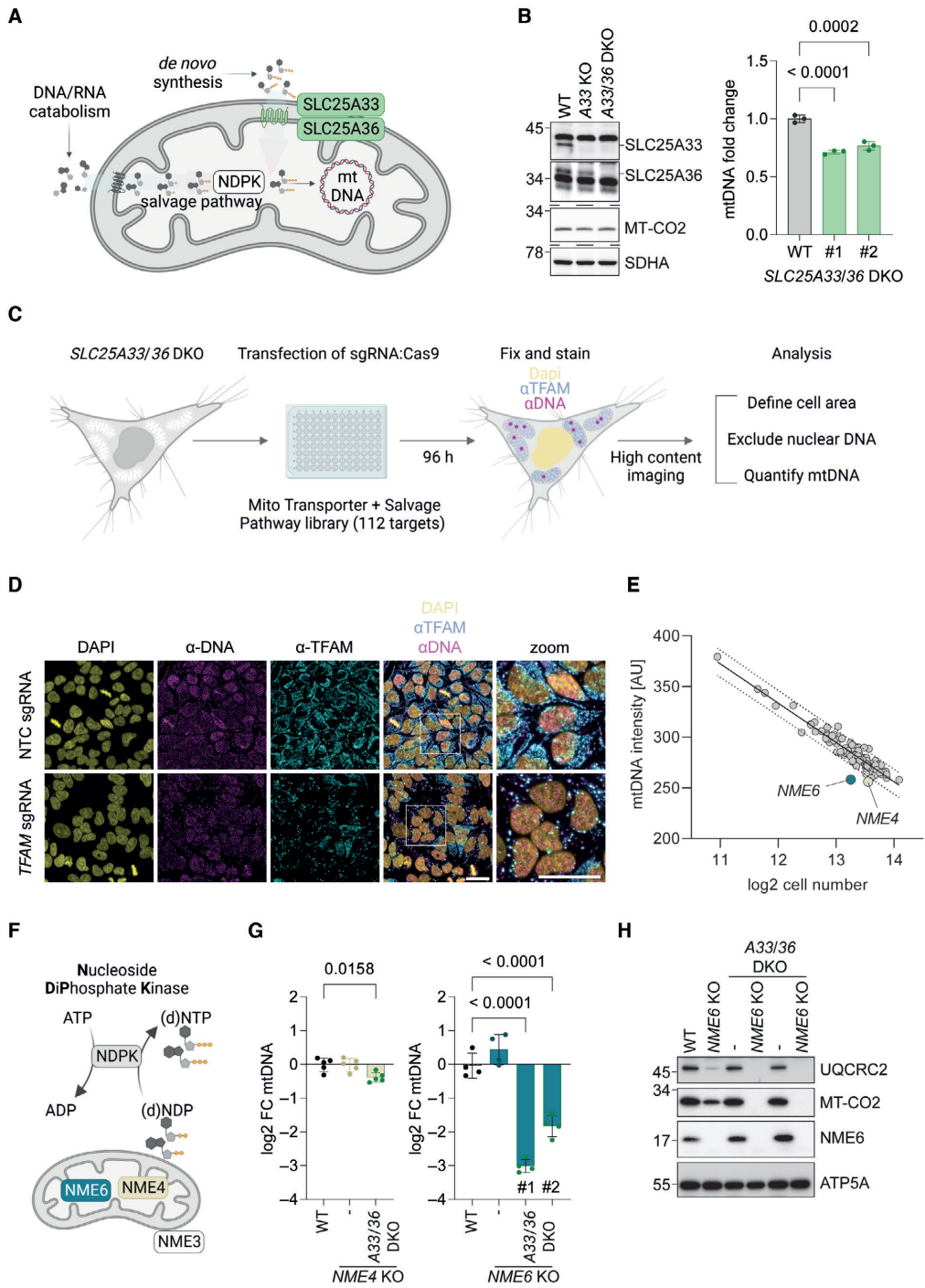


Figure 1.

Figure 1. NME6 is required for the maintenance of mtDNA when mitochondrial pyrimidine import is blocked.

- A Scheme of the routes by which mitochondria obtain and metabolise pyrimidine nucleotides.
- B Immunoblot analysis of SLC25A33 and SLC25A36 depletion in the indicated knockout (KO) and double knockout (DKO) HeLa cells (left) alongside the relative mtDNA levels of two monoclonal SLC25A33/SLC25A36 DKO cell lines calculated by qPCR (*CYTB/ACTB*; right) ($n = 3$ independent cultures).
- C Experimental flow chart of the arrayed CRISPR-SpCas9 screen to identify regulators of mtDNA levels in the absence of mitochondrial pyrimidine import.
- D Representative images taken from the arrayed CRISPR-SpCas9 screen of SLC25A33/SLC25A36 DKO cells showing one field of view from wells transfected with non-targeting control (NTC) sgRNA or TFAM sgRNA (scale bar = 20 μm).
- E The result of the CRISPR-SpCas9 screen plotted as the mean mtDNA intensity values against the mean log₂ cell number from each sgRNA target. The values for cells transfected with NME6 sgRNA and NME4 sgRNA lie below the 95% prediction bands (Least-squares regression; $R^2 = 0.90$; $n = 3$ independent experiments; AU, arbitrary units).
- F Scheme of nucleoside diphosphate kinase (NDPK) enzymatic activity and the reported locations of the mitochondrial NDPKs: NME3, NME4 and NME6.
- G Relative mtDNA levels in NME4 KO and NME4/SLC25A33/SLC25A36 triple KO HeLa (left) or NME6 KO and two clones of NME6/SLC25A33/SLC25A36 triple KO HeLa (right). MtDNA calculated by qPCR (*CYTB/ACTB*) and presented as log₂ fold change compared to levels in WT HeLa cells ($n = 4-5$ independent cultures).
- H Representative immunoblot analysis of the indicated HeLa cell lines (UQCRC2, Ubiquinol-cytochrome C reductase core protein 2; MT-CO2, mitochondrial-encoded cytochrome c oxidase II; ATP5A, ATP synthase F1 subunit alpha).

Data information: P-values were calculated using one-way analysis of variance (ANOVA) with Tukey's multiple comparison test (B, G). FC, fold change. Data are means \pm standard deviation (SD).

Source data are available online for this figure.

regulation of mitochondrial dNTP levels (Sharma *et al*, 2020). An enhanced uptake of mitochondrial pyrimidines promotes mtDNA replication, but can also trigger mtDNA release from mitochondria and mtDNA-dependent inflammatory pathways (Sprenger *et al*, 2021). The mitochondrial dNTP salvage pathway also contributes to innate immune signalling. Stimulation of macrophages induces the expression of the mitochondrial cytidine/uridine monophosphate kinase 2 (CMPK2), which drives the rapid synthesis of mtDNA and supports inflammasome activation (Zhong *et al*, 2018; Ernst *et al*, 2021).

While it has been demonstrated that the mitochondrial dNTP supply can tune mtDNA replication, how mitochondria obtain rNTPs for RNA synthesis, which is required for both transcription and mtDNA replication, remains unclear. By interrogating mitochondrial nucleotide supply pathways, we show here that the nucleoside diphosphate kinase, NME6, is a mitochondrial nucleotide salvage pathway enzyme, which is required for mRNA synthesis and OXPHOS function, highlighting the critical role of mitochondrial ribonucleotide metabolism in mitochondrial gene expression.

Results

To address how nucleotide supply regulates mitochondrial gene maintenance and expression, we explored the routes by which mitochondria obtain cytosolic pyrimidine nucleotides for mtDNA and mRNA synthesis in proliferating cells. We decided to focus on the mitochondrial supply of pyrimidines, since we and others have observed that enhanced mitochondrial import or salvage of pyrimidines is sufficient to increase the abundance of mtDNA (Favre *et al*, 2010; Zhong *et al*, 2018; Sprenger *et al*, 2021). While several mitochondrial solute carriers are known to exchange adenine nucleotides across the inner membrane, only two mitochondrial pyrimidine (deoxy)ribonucleotide carriers (SLC25A33 and SLC25A36) have been identified in mammalian cells (Floyd *et al*, 2007; Di Noia *et al*, 2014), both of which also transport guanine nucleotides *in vitro* (Di Noia *et al*, 2014). Loss of the single homologue of SLC25A33 and SLC25A36 in yeast, Rim2, leads to mtDNA depletion and blocks growth on non-fermentable carbon sources (Van Dyck *et al*, 1995). We generated HeLa cells lacking

SLC25A33 and SLC25A36 by CRISPR-SpCas9 mediated genome editing and monitored mtDNA levels. To our surprise, mtDNA levels were only reduced by 20% in these cells (Fig 1B), suggesting that mitochondria can obtain pyrimidine dNTPs via an alternative route when the pyrimidine nucleotide carriers are missing.

The maintenance of mtDNA depends on NME6 when pyrimidine nucleotide import is blocked

To identify genes that regulate mtDNA content in cells lacking the canonical mitochondrial pyrimidine transporters SLC25A33 and SLC25A36, we performed an arrayed CRISPR-SpCas9 knockout high-content microscopy screen. HeLa cells lacking both pyrimidine nucleotide carriers were transfected with SpCas9 nuclease and an arrayed CRISPR library, wherein each well contained three sgRNAs targeting individual genes with proposed roles in mitochondrial metabolite transport or pyrimidine nucleotide salvage (112 genes) (Dataset EV1). We visualised mtDNA 96 h following transfection by immunofluorescence with an anti-DNA antibody and quantified the mean fluorescence intensity per cell after exclusion of the nuclear DNA signal (Fig 1C and D). The mtDNA level inversely correlated with cell confluency in each well, which led us to plot the mean fluorescence intensity of mtDNA against cell number to identify potential outliers (Fig 1E). Two outliers corresponded to sgRNA targeting the mitochondrial nucleoside diphosphate kinases (NDPK), NME4 and NME6, which suggested that their loss renders cells unable to maintain mtDNA levels when pyrimidine nucleotide import is blocked (Fig 1E). The library also included sgRNA targeting mitochondrial transcription factor A (TFAM), a mtDNA-binding protein that is essential for the packaging of mtDNA into compact nucleoids (Garrido *et al*, 2003; Legros *et al*, 2004). Although TFAM protein level correlates closely with the abundance of mtDNA (Larsson *et al*, 1998; Ekstrand *et al*, 2004; Kanki *et al*, 2004; Bonekamp *et al*, 2021) and TFAM was selectively and efficiently depleted in our screen (Fig 1D), TFAM sgRNA did not register as an outlier in our mtDNA fluorescence intensity analysis (Fig 1E). It should be noted, however, that the residual TFAM condensed with mtDNA in enlarged nucleoids in line with previous observations in cells transiently depleted of TFAM (West *et al*, 2015; Feric *et al*, 2022). We calculated the area of mtDNA puncta as an

additional readout of mtDNA homeostasis and found that, analogous to the mean fluorescence intensity, the total area of mtDNA also declined with cell confluency (Fig EV1A). The total area of mtDNA puncta per cell was diminished in cells transfected with *TFAM* sgRNA and reduced modestly in cells transfected with *NME6* sgRNA (Fig EV1A).

The non-metastatic (NME) gene family of NDPKs generate dNTPs by transferring the terminal phosphate group predominantly from ATP to dNDPs or rNDPs via a transient phospho-histidine intermediate (Fig 1F) (Boissan et al, 2018). Three NME family members are reported to reside at mitochondria in different subcompartments; NME3 is located at the mitochondrial surface (Chen et al, 2019), NME4 has been detected in both the intermembrane space and matrix (Milon et al, 2000; Tokarska-Schlattner et al, 2008) and NME6 is present in the mitochondrial matrix (Proust et al, 2021). The results from our CRISPR screen indicated that NME4 and NME6 maintain mtDNA in the absence of pyrimidine nucleotide transport. We therefore deleted *NME4* and *NME6* by CRISPR/Cas9-mediated genome editing in WT cells and in cells lacking *SLC25A33* and *SLC25A36* and determined mtDNA levels by real-time quantitative PCR (qPCR). Loss of NME4 or NME6 did not alter mtDNA levels (Fig 1G). However, the combined knockout of *NME6*, *SLC25A33* and *SLC25A36* caused a dramatic loss of mtDNA to 15–25% of WT levels (Fig 1G) and resulted in the loss of the mtDNA-encoded protein cytochrome c oxidase II (MT-CO2; Fig 1H). In contrast, deletion of *NME4* did not affect the accumulation of mtDNA in the absence of *SLC25A33* and *SLC25A36* (Fig 1G). We therefore conclude that NME6 but not NME4 is required for pyrimidine nucleotide salvage in these cells. To further validate our findings, we depleted *SLC25A33* and *SLC25A36* individually and together in WT and *NME6* knockout cells using short interfering RNA (esiRNA). Knockdown of the pyrimidine carriers significantly depleted mtDNA in cells lacking NME6 but not in WT cells (Fig EV1B and C). NME6 is ubiquitously expressed in humans and catalyses phosphotransfer through a conserved histidine residue within an NDPK consensus motif at position 137 (H137) (Tsuiji et al, 1999). Importantly, mtDNA levels were maintained in *NME6* knockout cells expressing WT NME6-MycFlag but not in cells expressing kinase inactive mutant NME6 (*NME6*^{H137N}-MycFlag) (Fig EV1B). Collectively, these data demonstrate that NME6 maintains the mitochondrial genome, if the supply of pyrimidine nucleotides from the cytosol is limited, and indicate that NME6 generates dNTPs within mitochondria (Fig 1A).

NME6 supports cell proliferation independent of mtDNA synthesis

Although the loss of NME6 did not affect mtDNA levels in WT cells, we observed reduced growth of NME6-deficient cells on glucose medium (Fig 2A). This is consistent with the fitness dependency of many cancer cell lines on *NME6* revealed by a DepMap analysis of CRISPR knockout screens (Fig 2B). The growth defect of *NME6* knockout cells was more severe in galactose medium, when cell growth increasingly depends on glutaminolysis and OXPHOS (Reitzer et al, 1979; Rosignol et al, 2004) (Fig 2C). *NME6* was recently identified in a CRISPR-SpCas9 screen as essential for survival in human plasma like medium (HPLM) (Rossiter et al, 2021) and, consistently, we observed that NME6 depleted HeLa cells could

not survive in HPLM for extended periods (Fig 2D). This was likely due to glucose exhaustion in the HPLM of *NME6* knockout HeLa cells since glucose supplementation could restore the viability of NME6-depleted cells in HPLM (Fig EV2). The increased dependency on NME6 in galactose or HPLM medium was independent of mtDNA levels, which remained normal in cells lacking NME6 regardless of the growth medium (Fig 2E and F). These growth assays thus demonstrate that proliferating cells require NME6, even when the mitochondrial import of dNTPs is normal and the maintenance of mtDNA does not depend on NME6.

Mitochondrial respiration and OXPHOS subunit homeostasis depend on NME6

Consistent with the impaired growth in galactose medium (Fig 2C), the loss of NME6 strongly reduced cellular oxygen consumption rates (OCR) and resulted in a concomitant increase in the extracellular acidification rate (ECAR) (Fig 3A). Enhanced ECAR is indicative of upregulated glycolysis, which likely explains the greater glucose dependency in cells lacking NME6 (Fig EV2). Normal OCR and ECAR were restored in *NME6* knockout cells upon the expression of WT NME6-MycFlag but not *NME6*^{H137N}-MycFlag, demonstrating that mitochondrial function requires NME6 kinase activity (Fig 3A).

To explore why mitochondrial respiration depends on NME6, we examined mitochondrial protein homeostasis by quantitative proteomics and analysed mitochondrial proteins (MitoCarta 3.0) (Rath et al, 2021) that were significantly altered in an NME6-dependent manner by unsupervised hierarchical clustering (Fig EV3A). While 20 mitochondrial proteins accumulated in *NME6* knockout cells (Fig EV3A), the largest cluster consisted of 55 mitochondrial proteins that were significantly depleted in cells lacking NME6 compared to WT and NME6-MycFlag complemented cells (Fig 3B; Dataset EV2). Remarkably, 47 of the 55 mitochondrial proteins were OXPHOS subunits, resulting in the collective depletion of OXPHOS proteins relative to other mitochondrial proteins, which was also revealed by unbiased 1D-enrichment driven pathway analysis (Fig 3C and D). These data demonstrate that OXPHOS subunit homeostasis depends on NME6, while overall mitochondrial mass is unaffected by NME6 loss (Fig 3C). Immunoblotting of selected OXPHOS subunits revealed that the abundance of OXPHOS subunits in *NME6* knockout cells was restored upon expression of NME6 but not in the presence of the kinase dead variant *NME6*^{H137N} (Fig 3E). Thus, respiration depends on enzymatically active NME6 (Fig 3A).

We next expanded our analysis to liver cancer cell lines, since the expression of NME6 is increased in these cell lines relative to other cancer types (Fig EV3B). The expression of NME6 correlates with an unfavourable prognosis in liver cancer patients (Fig EV3C). OXPHOS subunits were diminished in two out of three *NME6* knockout human liver cancer cell lines (Fig 3F), while the abundance of mtDNA was not affected (Fig 3G). The absence of NME6 in HLE and Huh6 cells, but not HepG2 cells, also resulted in a significant growth defect (Fig 3H), which was consistent with publicly available CRISPR screening data (Fig EV3D; depmap.org/portal) and correlated with the levels of OXPHOS subunits in these cell lines (Fig 3F). Finally, complementation of *NME6* knockout HLE cells with WT NME6-MycFlag but not *NME6*^{H137N}-MycFlag restored OXPHOS homeostasis (Fig EV3E), thus confirming the requirement for NME6 kinase activity in these cells. Collectively, we conclude that NME6 is

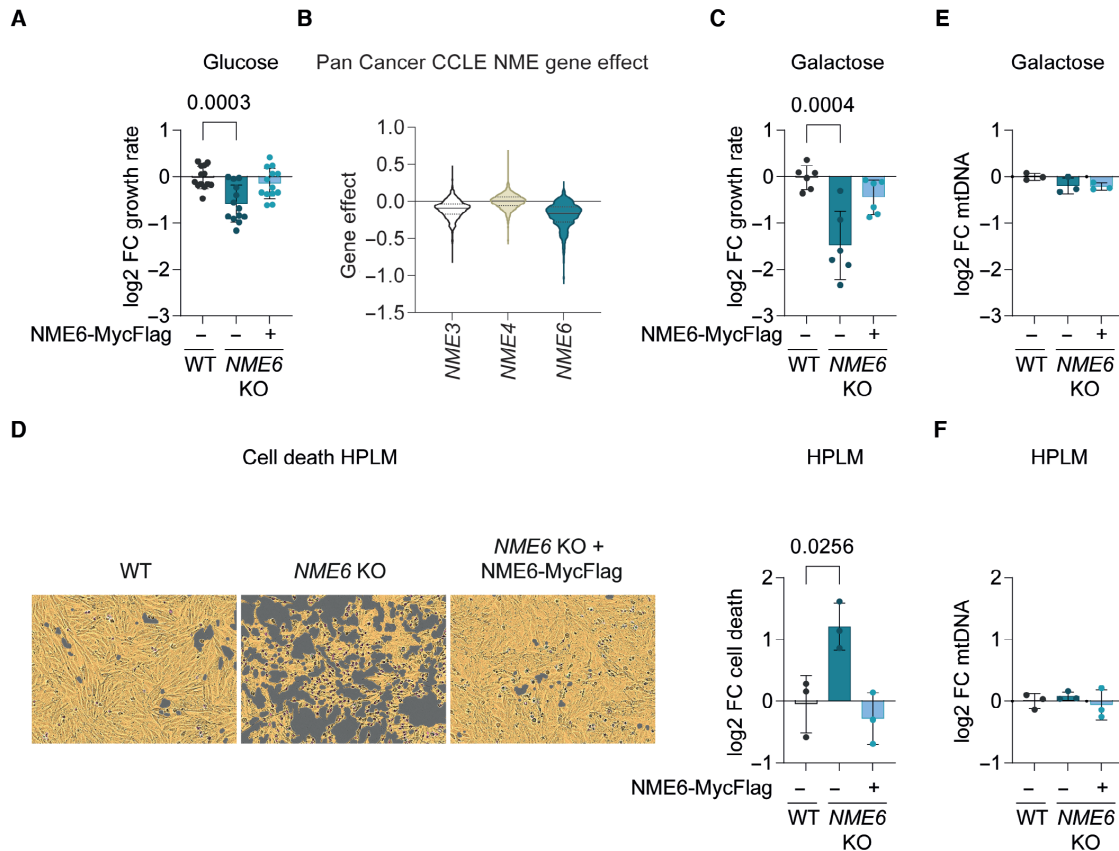


Figure 2. NME6 supports cell proliferation independent of mtDNA synthesis.

- A The growth rate of *NME6* KO and *NME6* KO + *NME6*-MycFlag HeLa relative to WT HeLa cells incubated in DMEM containing 25 mM glucose (\log_2 ; $n = 13$ independent cultures).
- B Violin plot of gene effects of *NME3*, *NME4* or *NME6* depletion in 1,086 cell lines from the Cancer Cell Line Encyclopaedia (CCLE) determined by CRISPR screening (DepMap 22Q2 Public+Score, Chronos; solid line denotes median, dotted line denotes 25% quartile).
- C The growth rate of *NME6* KO and *NME6* KO + *NME6*-MycFlag HeLa relative to WT HeLa cells incubated in DMEM containing 10 mM galactose (\log_2 ; $n = 6$ independent cultures).
- D Representative live-cell images of the indicated cell lines grown in Human Plasma-Like Medium (HPLM) (left) and calculated cell death after 96 h (right). Cell confluency is depicted with the yellow mask and dead cells are identified by SYTOX green staining in purple ($n = 3$ independent cultures).
- E MtDNA level monitored by qPCR (*CYTB/ACTB*) in *NME6* KO and *NME6* KO + *NME6*-MycFlag HeLa relative to WT HeLa cells in DMEM containing 10 mM galactose ($n = 3$ independent cultures).
- F MtDNA level monitored by qPCR (*CYTB/ACTB*) in *NME6* KO and *NME6* KO + *NME6*-MycFlag HeLa relative to WT HeLa cells in HPLM ($n = 3$ independent cultures).

Data information: *P*-values were calculated using one-way ANOVA with Tukey's multiple comparison test (A, C–F). FC, fold change. Data (except B) are means \pm SD. Source data are available online for this figure.

required for respiration and the maintenance of OXPHOS subunits independent of its role in mtDNA synthesis.

Mitochondrial gene expression depends on NME6

The depletion of mtDNA-encoded proteins within complex I, III, IV and V (Fig 3D) in *NME6* knockout cells prompted us to monitor mitochondrial protein synthesis *in vitro*. We observed reduced

synthesis of mtDNA-encoded subunits in mitochondria lacking *NME6* (Fig 4A and B), indicating defective mitochondrial transcription or translation in the absence of *NME6*. Consistently, gene coessentiality network analysis across hundreds of heterogenous cancer cell lines using the FIREWORKS (Fitness Interaction Ranked nEtWORKS) web tool (Amici *et al*, 2021) revealed that the top coessential genetic interactors with *NME6* are regulators of mtDNA replication, transcription, mitochondrial tRNA maturation and

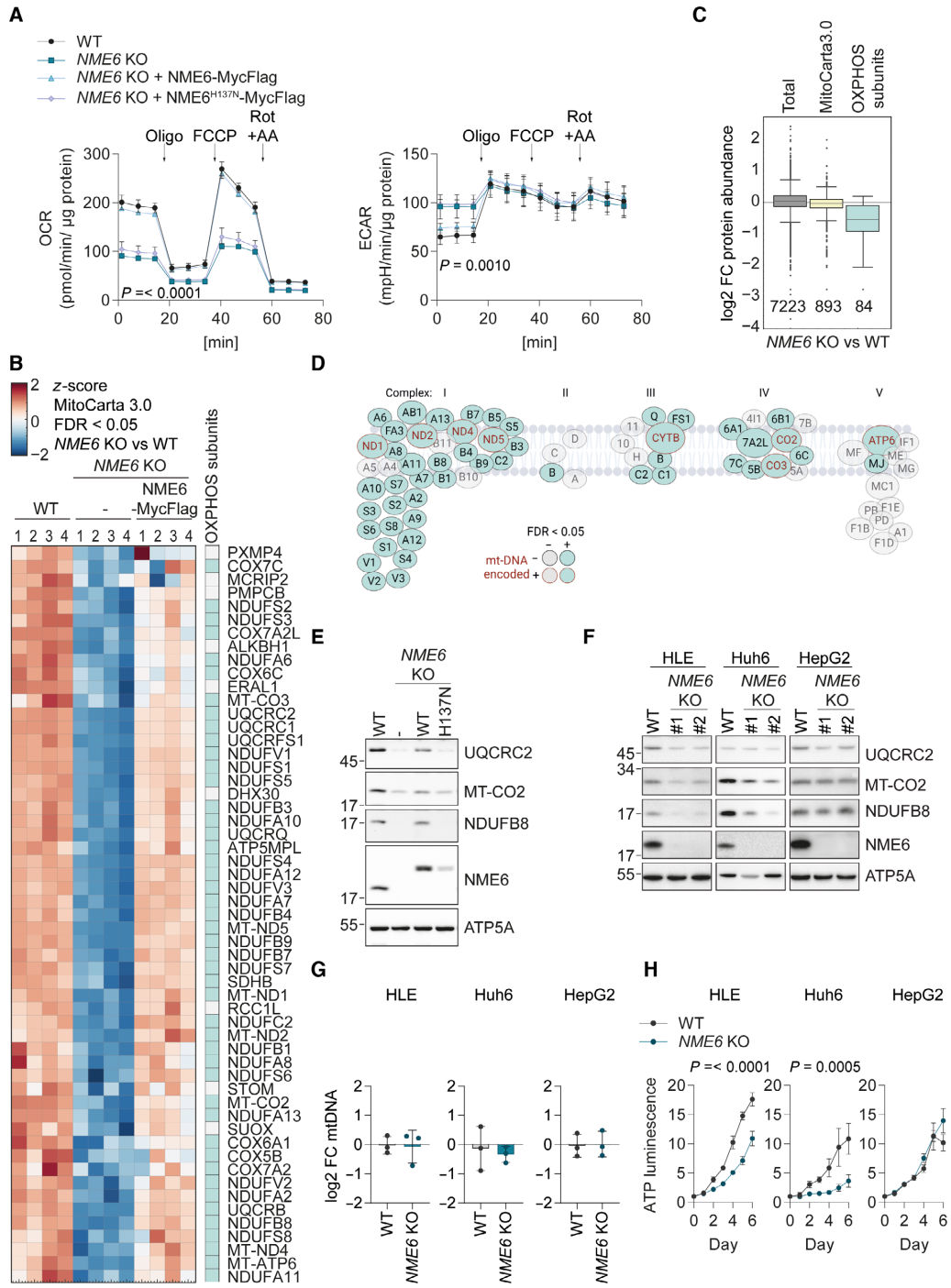


Figure 3.

Figure 3. Mitochondrial respiration and OXPHOS depend on NME6.

- A Oxygen consumption rates (OCR) and extracellular acidification rates (ECAR) of the indicated HeLa cell lines during a mitochondrial stress test with inhibitor treatments at the indicated timepoints. *P*-values for OCR: two-way ANOVA *P*-value (time) = < 0.0001, *P*-value (genotype) = < 0.0001, *P*-value (interaction) = < 0.0001; *P*-values for ECAR: two-way ANOVA *P*-value (time) = < 0.0001, *P*-value (genotype) = < 0.001, *P*-value (interaction) = 0.0517; *P*-values for genotype are shown (Oligo, oligomycin; FCCP, carbonyl cyanide-*p*-trifluoromethoxyphenylhydrazone; Rot + AA, rotenone and antimycin A; *n* = 3 independent experiments).
- B Heat map representation of *z*-scores of log₂-transformed protein intensities determined by quantitative mass spectrometry and filtered for mitochondrial proteins according to MitoCarta 3.0 (Rath et al, 2021) (cluster four of Fig EV3A). The proteins shown clustered together due to their significant (permutation-based FDR < 0.05, *s*₀ = 0.1) depletion in *NME6* KO HeLa cells compared to WT and *NME6* KO + *NME6*-MycFlag HeLa cells. OXPHOS subunits are indicated in the right column (*n* = 4 independent cultures).
- C Box plot analysis of log₂ fold change in protein intensities in *NME6* KO compared to WT HeLa cells. Distribution of the complete set of quantified protein groups: Total (7,223 proteins detected), MitoCarta 3.0 positive (893 proteins detected) and OXPHOS subunits (CI – CV of the MitoCarta 3.0 pathway annotations; 84 proteins detected). Box limits denote 25- and 75% quartile, line denotes the median, whiskers denote 1.5 × interquartile range deviation from the median.
- D Graphical representation of all respiratory complex subunit proteins detected in our proteomic assay to highlight the respiratory complexes most affected by loss of *NME6* as also shown in B. OXPHOS subunits depleted in *NME6* KO cells compared to WT and *NME6* KO + *NME6*-MycFlag HeLa cells are in teal. MtDNA-encoded OXPHOS subunits are labelled in red. Subunits that were not significantly altered between genotypes are in grey.
- E Immunoblot analysis of WT HeLa cells, *NME6* KO cells and *NME6* KO cells expressing *NME6*-MycFlag (WT) or *NME6*^{H137N}-MycFlag (H137N).
- F Immunoblot analysis of WT cells and two *NME6* KO clones (#1, #2) generated in three different liver cancer cell lines: HLE, Huh6 and HepG2.
- G MtDNA level monitored by qPCR (*CYTB/ACTB*) in *NME6* KO relative WT cells in the indicated liver cancer cell lines (*n* = 3 independent cultures).
- H The relative growth of WT and *NME6* KO liver cancer cell lines monitored on each day (d) using an ATP luminescence assay. *P*-values for HLE cells: two-way ANOVA *P*-value (time) = < 0.0001, *P*-value (genotype) = < 0.0001, *P*-value (interaction) = < 0.0001; *P*-values for Huh6 cells: two-way ANOVA *P*-value (time) = < 0.0001, *P*-value (genotype) = 0.0005, *P*-value (interaction) = < 0.0001; *P*-values for genotype are shown (*n* = 4 independent cultures).
- Data information: FC, fold change. Data (except C) are means ± SD.
Source data are available online for this figure.

mitochondrial ribosome (mitoribosome) biogenesis, which is unique within the *NME* gene family (Fig EV4A).

Immunoprecipitation of *NME6*-MycFlag coupled with mass spectrometry identified the putative mitoribosome assembly factor, RCC1L, to be the only high confidence interaction partner of *NME6* (Fig EV4B; Dataset EV3). This is in line with previous proximity labelling and immunoprecipitation assays (Floyd et al, 2016; Antonicka et al, 2020; Proust et al, 2021). The depletion of RCC1L by CRISPR-Cas9 resulted in a concomitant depletion of *NME6* (Fig EV4C). RCC1L-FLAG colocalises with mtRNA granules (Antonicka et al, 2017) and our confocal fluorescence imaging revealed that endogenous *NME6* forms puncta that overlap partially with mtDNA nucleoids and mtRNA granules (Fig 4C). However, unlike cells depleted of RCC1L (Reyes et al, 2020), we did not observe any disruption of mitoribosome proteins in cells lacking *NME6* (Figs 3B and EV3A), which argues against *NME6* being required for mitoribosome assembly.

Mitochondrial transcription is initiated from a single promoter on the heavy-strand and two promoters on the light-strand of mtDNA to yield polycistronic transcripts that are further processed to individual mitochondrial messenger (m)RNAs, transfer (t)RNAs and ribosomal (r)RNAs (Miranda et al, 2022; Tan et al, 2022) (Fig 4D).

We measured the levels of mitochondrial messenger RNA (mRNA) and ribosomal RNA (rRNA) by qPCR and observed a striking pattern of mitochondrial mRNA depletion in cells lacking *NME6* that correlated with the distance from the heavy strand promoter (Fig 4D and E). Heavy-strand mRNAs from *ATP8* onwards, as well as *ND6* on the light-strand, were significantly lower in the absence of *NME6* compared to WT and *NME6*-MycFlag complemented cells (Fig 4E). Mitochondrial transcripts were also depleted in *NME6* knockout HLE cells and the fold change reduction of heavy-strand transcripts was greatest for those furthest from the promoter (Fig EV4D). The transcript levels of nuclear DNA encoded OXPHOS subunits were unaffected by the loss of *NME6* (Fig 4F) despite their reduced protein levels (Fig 3D). Collectively, these data highlight a crucial role for *NME6* in the maintenance of mitochondrial transcripts, which could explain the OXPHOS deficiency in cells lacking *NME6*.

NME6 supplies rNTPs for mitochondrial transcription

The synthesis of the almost genome-length polycistronic transcripts by POLRMT requires an adequate supply of rNTPs. To test whether *NME6* supplies rNTPs for mitochondrial transcription, we supplemented

Figure 4. NME6 regulates mitochondrial gene expression.

- A Representative mitochondrial translation assay monitored by the incorporation of ³⁵S methionine and cysteine into the indicated mtDNA-encoded proteins followed by autoradiography (top panel). MtDNA encoded proteins are labelled according to expected size and *NME6* and SDHA immunoblots are shown below.
- B Quantification of ³⁵S methionine and cysteine incorporation into all mtDNA-encoded proteins labelled in (B) relative to WT HeLa cells at 15 min (log₂; mitochondrial preparations from *n* = 3 independent cultures).
- C Immunofluorescence of *NME6* with mtDNA (top) or bromouridine (BrU) labelled nascent mtRNA (bottom) in HeLa cells imaged by confocal microscopy. Relative fluorescence intensities were calculated from linescans generated within the mitochondrial regions indicated by dotted lines.
- D Scheme of human mtDNA organisation with the heavy strand promoter (HSP) represented by an arrow on the outside and the light strand promoters (LSP) by two arrows on the inside. Heavy strand -transcripts are labelled in blue, light strand-transcript is labelled in green, tRNAs are labelled in grey.
- E MtDNA-encoded transcript levels analysed by qRT-PCR in *NME6* KO and *NME6* KO + *NME6*-MycFlag cells relative to WT HeLa cells. *P*-values for mtDNA-encoded transcripts: two-way ANOVA *P*-value (transcript) = < 0.0001, *P*-value (genotype) = < 0.0001, *P*-value (interaction) = < 0.0001 (log₂; *n* = 3 independent cultures).
- F Nuclear DNA-encoded transcript levels analysed by qRT-PCR in *NME6* KO and *NME6* KO + *NME6*-MycFlag HeLa cells relative to WT (log₂; *n* = 3 independent cultures).
- Data information: FC, fold change. Data are means ± SD.
Source data are available online for this figure.

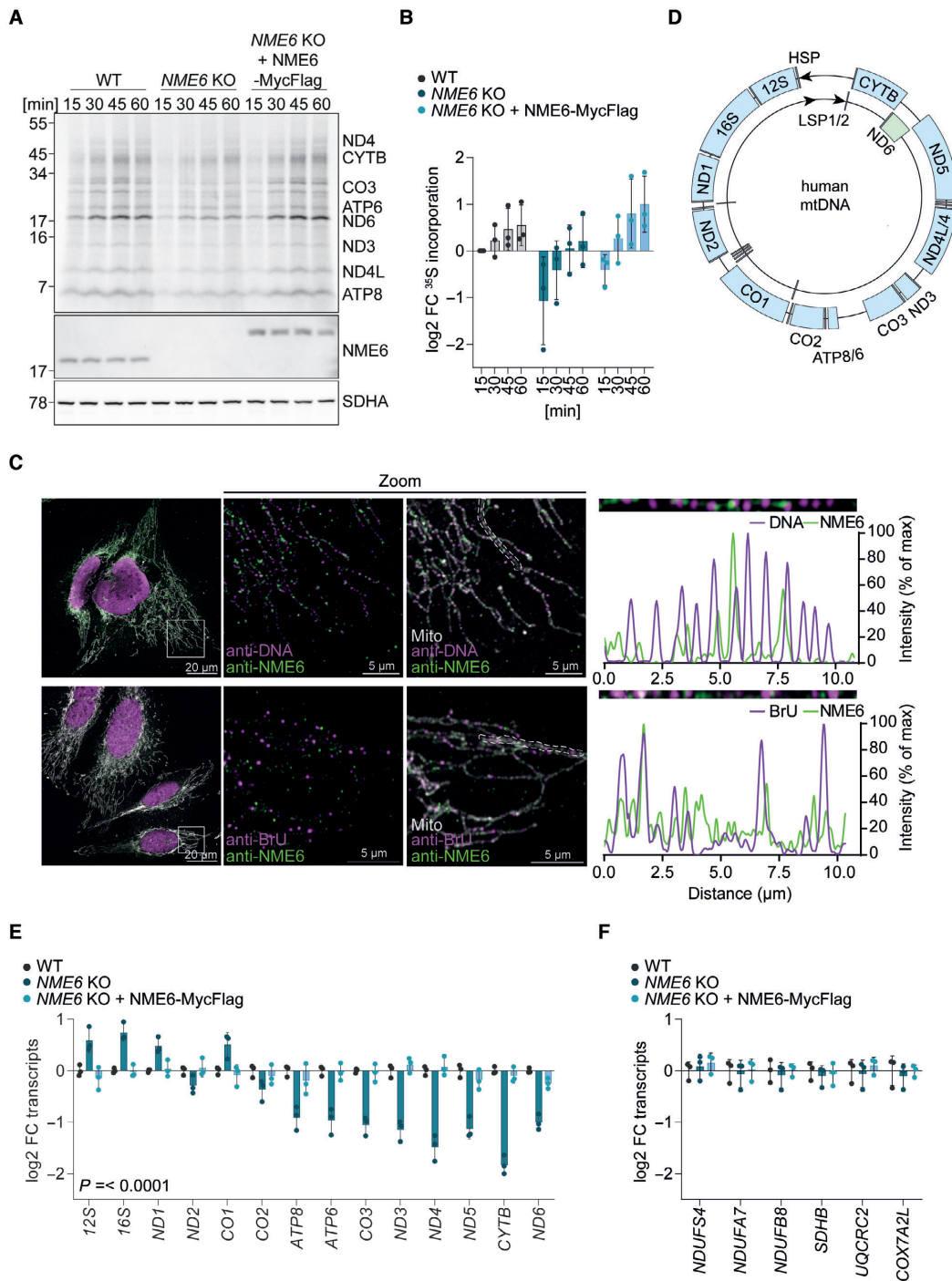


Figure 4.

NME6 knockout cells with rNTPs or dNTPs and measured mitochondrial transcript levels by qPCR. Strikingly, mitochondrial mRNAs were restored to WT levels in *NME6* knockout cells treated with rNTPs, while supplementation with dNTPs had no effect (Fig 5A). Proteomic analysis confirmed that supplementation with rNTPs, was sufficient to increase the levels of OXPHOS subunits in *NME6* knockout cells (Fig 5B; Dataset EV4). Exogenous rNTPs are likely hydrolysed by ectonucleotidases prior to cell uptake as ribonucleosides (Zimmermann, 1999; Pastor-Anglada & Perez-Torras, 2018). We therefore treated cells with a mix of nucleosides that included the four ribonucleosides cytidine, uridine, guanosine and adenosine and the deoxyribonucleoside thymidine. Similar to rNTP treatment, nucleoside supplementation resulted in the complete rescue of mitochondrial transcript levels in cells lacking *NME6* (Fig 5C). The rescue of mitochondrial transcripts by nucleoside treatment correlated with a complete restoration of normal OCR and ECAR in *NME6* knockout cells (Fig 5D), demonstrating that exogenous nucleoside supply is sufficient to maintain OXPHOS in the absence of *NME6*.

We reasoned that exogenous nucleosides must be phosphorylated via the cytosolic salvage pathway prior to entry into the mitochondria as rNTPs in order to bypass the requirement for *NME6* (Fig EV5A). Indeed, nucleoside treatment no longer restored mitochondrial transcript levels in *NME6* knockout cells that were depleted of the cytosolic uridine-cytidine kinase 2 (UCK2), which is essential for pyrimidine nucleoside salvage by phosphorylating uridine and cytidine (Figs 5E and EV5A and B). In contrast, combined depletion of the purine nucleoside salvage enzymes, hypoxanthine-guanine phosphoribosyl-transferase (HPRT)

and adenine phosphoribosyltransferase (APRT), did not prevent the restoration of mitochondrial transcripts in *NME6* knockout cells treated with nucleosides (Fig EV5C). Together, these data demonstrate that *NME6* is required to generate pyrimidine rNTPs for mitochondrial transcription and OXPHOS.

We next quantified the abundance of nucleotide species in whole-cell extracts and mitochondrial fractions by liquid chromatography-mass spectrometry (LC-MS; Figs 5F and EV5D). Mitochondria lacking *NME6* had significantly reduced levels of CTP (down by 70%) and dCTP (down by 90%), which were restored in cells re-expressing *NME6*. Conversely, UTP and GTP levels were barely affected, while ATP and dATP were even moderately increased in mitochondria lacking *NME6* (Fig 5F). This result suggested that *NME6* is predominantly required for the maintenance of mitochondrial cytidine triphosphates. Consistently, treatment of cells with cytidine or uridine restored mitochondrial transcript levels in the absence of *NME6*, whereas purine nucleosides did not (Figs 5G and EV5E). Uridine treatment can increase both cellular UTP and CTP levels (Pooler *et al*, 2005), since UTP is readily converted to CTP by the cytosolic enzyme CTP synthetase (CTPS). We quantified mitochondrial nucleotides in cells supplemented with cytidine or uridine by LC-MS and confirmed that both treatments elevated mitochondrial CTP and dCTP levels in *NME6* knockout cells (Fig 5H; Appendix Fig S1A–D). Neither nucleoside could fully restore mitochondrial CTP/dCTP in *NME6* knockout cells however, which may explain the partial improvement in cell growth upon treatment with cytidine or uridine (Fig EV5F).

Finally, we tested the impact of individual nucleoside supplementation on mitochondrial respiration and observed that cytidine

Figure 5. *NME6* maintains pyrimidine ribonucleotide triphosphates for mitochondrial transcription.

- A Heat map of log₂ transformed mean mitochondrial transcript levels of WT and *NME6* KO HeLa cells incubated with 100 μM rNTPs or dNTPs for 48 h relative to untreated WT cells analysed by qRT-PCR (*n* = 3 independent cultures).
- B Volcano plot representation of log₂ fold change in proteins between *NME6* KO cells treated with 100 μM rNTPs for 120 h and untreated *NME6* KO HeLa cells determined by quantitative mass spectrometry. OXPHOS subunits are highlighted in teal (*n* = 3 independent cultures).
- C Heat map of log₂ transformed mean mitochondrial transcript levels of WT and *NME6* KO HeLa cells incubated with 100 μM nucleosides for 48 h relative to untreated WT cells analysed by qRT-PCR (*n* = 3 independent cultures).
- D Oxygen consumption rates (OCR) and extracellular acidification rates (ECAR) of WT and *NME6* KO HeLa cells incubated with or without nucleosides (100 μM) for a minimum of 120 h. Mitochondrial stress test was performed as in Fig 3A (*n* = 3 independent experiments). *P*-values for OCR: two-way ANOVA *P*-value (time) = < 0.0001, *P*-value (genotype) = 0.0011, *P*-value (interaction) = < 0.0001; *P*-values for ECAR: two-way ANOVA *P*-value (time) = < 0.0001, *P*-value (genotype) = 0.8994, *P*-value (interaction) = < 0.0001.
- E *CYT8* transcript levels analysed by qRT-PCR in WT and *NME6* KO HeLa cells transfected with the indicated esiRNA and incubated with or without nucleosides (100 μM) for 72 h (log₂; *n* = 4 independent cultures). *P*-values were calculated using a one-way ANOVA.
- F Nucleotide levels in whole cell (left) and mitochondria enriched fractions (right) from *NME6* KO and *NME6* KO + *NME6*-MycFlag (WT) cells compared to WT HeLa cells as determined by quantitative mass spectrometry. The NTPs (top) and dNTPs (bottom) are shown except for dGTP which was not detected in our analysis. *P*-values for whole cell rNTPs: two-way ANOVA *P*-value (rNTP) = 0.0018, *P*-value (genotype) = < 0.0001, *P*-value (interaction) = 0.0027; *P*-values for mito enriched fraction rNTPs: two-way ANOVA *P*-value (rNTP) = < 0.0001, *P*-value (genotype) = < 0.0001, *P*-value (interaction) = < 0.0001; *P*-values for whole cell dNTPs: two-way ANOVA *P*-value (dNTP) = 0.0096, *P*-value (genotype) = < 0.0001, *P*-value (interaction) = 0.0027; *P*-values for mito enriched fraction dNTPs: two-way ANOVA *P*-value (dNTP) = < 0.0001, *P*-value (genotype) = < 0.0001, *P*-value (interaction) = < 0.0001; Significant multiple comparison *P*-values are shown (log₂; *n* = 4 independent cultures).
- G *CYT8* (top) and *ND5* (bottom) transcript levels analysed by qRT-PCR in WT and *NME6* KO HeLa cells incubated with the indicated nucleoside species for 48 h. *P*-values were calculated using a one-way ANOVA (A, adenosine; G, guanosine; C, cytidine; U, uridine; log₂; 100 μM; *n* = 4 independent cultures).
- H CTP (top) and dCTP (bottom) levels in the mitochondria enriched fraction of WT and *NME6* KO HeLa cells incubated with the indicated nucleoside species for 120 h as determined by quantitative mass spectrometry. *P*-values for CTP: two-way ANOVA *P*-value (supplementation) = < 0.0001, *P*-value (genotype) = < 0.0001, *P*-value (interaction) = 0.3179; *P*-values for dCTP: two-way ANOVA *P*-value (supplementation) = < 0.0001, *P*-value (genotype) = < 0.0001, *P*-value (interaction) = 0.0569; *P*-values for supplementation are shown (C, cytidine; U, uridine; log₂; 100 μM; *n* = 4 independent cultures).
- I Basal (top) and maximal (bottom) oxygen consumption rates of WT and *NME6* KO HeLa cells incubated with the indicated nucleoside species for a minimum of 120 h relative to untreated WT cells (A, adenosine; G, guanosine; C, cytidine; U, uridine; log₂; 100 μM; *n* = 4 independent experiments). Basal and maximal rates were calculated from Fig EV5G. *P*-values were calculated using a one-way ANOVA.

Data information: FC, fold change. Data are means ± SD.

Source data are available online for this figure.

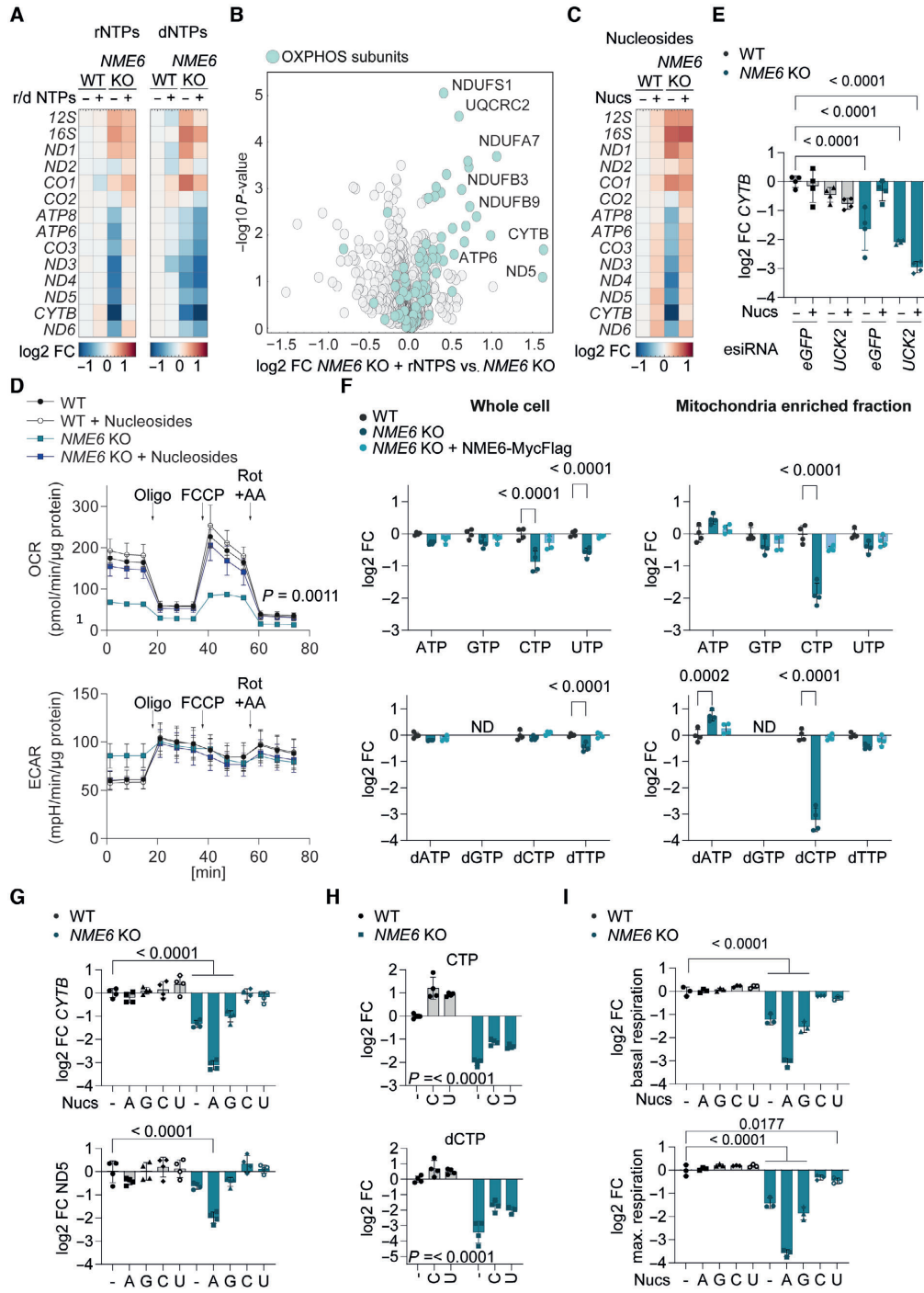


Figure 5.

or uridine treatment resulted in near complete restoration of OCR in *NME6* knockout HeLa cells (Figs 5I and EV5G). The ECAR in *NME6* knockout cells was also normalised upon treatment with the pyrimidine nucleosides, likely reflecting a deceleration of glycolysis (Figs 5I and EV5G). Conversely, treatment of these cells with guanosine did not restore mitochondrial respiration or ECAR, while adenosine treatment resulted in a more severe inhibition of mitochondrial respiration and a further increase in ECAR in cells lacking *NME6*. The bioenergetic impact of each nucleoside correlated remarkably with their individual effects on mitochondrial transcript levels in *NME6* knockout cells (Figs 5G and EV5E) and nucleoside treatment had no impact on the bioenergetics (Figs 5I and EV5G) or mitochondrial transcript levels in WT HeLa cells (Figs 5G and EV5E). These results highlight a specific dependency on *NME6* for the maintenance of mitochondrial pyrimidine nucleotides required to drive mitochondrial gene expression and OXPHOS in proliferating cells (Fig 6).

Discussion

We reveal the dual function of the nucleoside diphosphate kinase *NME6* in mitochondrial nucleotide metabolism. *NME6* supplies pyrimidine rNTPs for mitochondrial transcription and is required for the maintenance of mtDNA when pyrimidine dNTP import from the cytosol is limited. The loss of *NME6* or of its kinase activity impairs mitochondrial gene expression and OXPHOS function, despite normal levels of mtDNA. Therefore, while previous research has focused on the supply of deoxyribonucleotides for mtDNA synthesis, our study highlights the importance of mitochondrial ribonucleotide metabolism for healthy mitochondrial function.

The inhibition of *NME6* kinase activity results in mitochondrial cytidine nucleotide depletion and loss of OXPHOS subunits, which

likely reflects the degradation of non-assembled OXPHOS subunits upon a primary loss of mtDNA-encoded subunits (Deshwal *et al.*, 2020; Szczepanowska & Trifunovic, 2021). The specific depletion of CTP and dCTP in *NME6* knockout HeLa cells is surprising given the reported lack of base moiety specificity of NDPK enzymes (Lascu & Gonin, 2000). Interestingly, *in vitro* kinase assays that describe *NME6* as an active NDPK used CDP as the γ -phosphate acceptor with recombinant *NME6* (Tsuiki *et al.*, 1999), whereas no NDPK activity was detected for recombinant *NME6* when dTDP was used as the γ -phosphate acceptor (Proust *et al.*, 2021). It remains to be seen whether the contribution of *NME6* to the steady-state levels of mitochondrial ribonucleotides differs between cell and tissue types, as indicated by the different effects of *NME6* in various liver cancer cell lines. The depletion of mitochondrial CTP may lead to the stalling of the mitochondrial RNA polymerase, analogous to DNA polymerase stalling upon the depletion of dNTPs, and ultimately perturb transcription efficiency (Edenberg *et al.*, 2014). The strongest effect of *NME6* loss on mitochondrial transcripts furthest from the heavy-strand promoter likely reflects progressive CTP depletion with ongoing transcription and argues against a general role for *NME6* in mRNA stabilisation. For comparison, all heavy-strand mRNA transcripts are depleted in mitochondria lacking the mRNA stabilising factor, leucine-rich pentatricopeptide repeat containing (LRPPRC) protein (Gohil *et al.*, 2010; Ruzzenente *et al.*, 2012). Nevertheless, mRNA stability will contribute to the steady state levels of transcripts after *NME6* depletion and may explain the subtle differences we observed in relative mRNA changes upon *NME6* loss between HeLa and HLE cells. Interestingly, our proteomic analysis revealed that the levels of four mitochondrial proteins associated with mitochondrial RNA granules (MRGs) are reduced in the absence of *NME6*: ALKBH1, ERAL1, DHX30 and RCC1L (Antonicka & Shoubridge, 2015; Antonicka *et al.*, 2017; Zaganelli *et al.*, 2017; Wagner *et al.*, 2019). MRGs are

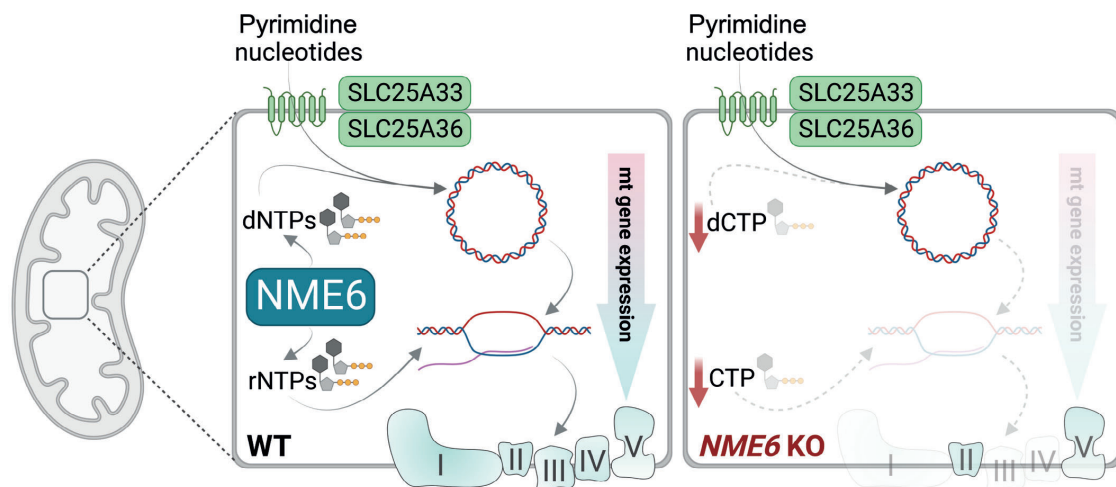


Figure 6. Mitochondrial pyrimidine nucleotide synthesis is required for mitochondrial gene expression.
Schematic depiction of the central role played by *NME6* in mitochondrial nucleotide metabolism.

The reader may continue with section 2.7.

“Adenosine feeding exacerbates the nucleotide imbalance in *NME6* KO cells”

hubs for the processing and maturation of nascent RNA and are associated with the assembly of mitoribosomes (Xavier & Martinou, 2021). In light of the critical role of NME6 for transcription, it is intriguing to consider that its interaction with RCC1L may allow spatial coordination of mitochondrial transcription with translation.

NME6 is not required for the maintenance of mtDNA in the cell lines we tested despite a significant reduction in mitochondrial dCTP levels detected in NME6 knockout HeLa cells. Mitochondria contain asymmetric pools of dNTPs and HeLa cells have been reported to have low levels of dCTP in comparison to other dNTP species (Song et al, 2003). Depletion of dCTP is also linked to mtDNA depletion in mitochondrial neurogastrointestinal encephalomyopathy (MNGIE) caused by mutations in thymidine phosphorylase (TYMP) (González-Vioque et al, 2011). We speculate that proliferating cells lacking NME6 are still able to maintain sufficient dCTP supply for mtDNA replication via the import of cytosolic dCTP. NME6 nevertheless becomes essential for the maintenance of mtDNA in cells lacking the mitochondrial pyrimidine transporters, SLC25A33 and SLC25A36. It remains to be seen whether NME6 is required for mtDNA synthesis in quiescent tissues that suppress *de novo* synthesis of deoxyribonucleotides and depend on mitochondrial nucleotide salvage for the provision of dNTPs for mtDNA synthesis (Ferraro et al, 2005; Mathews & Song, 2007; Pontarin et al, 2007). Reduced

mitochondrial dCTP may also cause multiple mutations and deletions in the mtDNA of proliferating cells (Song et al, 2003; González-Vioque et al, 2011), which should be explored in future studies alongside the absolute concentrations of mitochondrial dNTPs in the presence and absence of NME6.

Synthesis of mitochondrial pyrimidines by NME6 has broad implications for the control of OXPHOS and mitochondrial signalling. For instance, NME6 is upregulated along with the mitochondrial transcription machinery in certain cases of liver cancer and has been linked to negative prognosis (Jiang et al, 2019; Fei et al, 2020; Wan et al, 2021). It will also be important to consider how NME6 may influence mitochondrial signalling in innate immunity. Altered mitochondrial pyrimidine metabolism can trigger inflammation (Sprenger et al, 2021) and NME6 was recently identified as a positive regulator of the inflammasome in a mouse macrophage cell line, along with NME4 and NME3 (Ernst et al, 2021). Expanding our understanding of mitochondrial nucleotide metabolism will be essential to understand how mitochondrial nucleotide supply impacts ageing and disease associated with dysregulation of the mitochondrial genome and OXPHOS function. We propose that mitochondrial ribonucleotide salvage and mtRNA synthesis should be considered alongside mtDNA synthesis pathways in the context of diseases associated with defective mitochondrial nucleotide metabolism.

Materials and Methods

Reagents and Tools table

Reagent/Resource	Source	Identifier/Catalog number
Antibodies		
Human SLC25A33	Origene	TA309042
Human SLC25A36	Gene Tex	GTX119934
Human MT-CO2	Abcam	ab110258
Human SDHA	Abcam	ab14715
Human Oxphos-Cocktail	Abcam	ab110411
Human NME6	Sigma	HPA017909
Human RCC1L	Proteintech	13796-1-AP
Human TFAM	Proteintech	22586-1-AP
DNA	Sigma	CBL186
BrdU	Abcam	ab6326
HRP-conjugated secondary anti rabbit	BioRad	170-6515
HRP-conjugated secondary anti mouse	BioRad	170-6516
Alexa 488-conjugated secondary anti rabbit	Invitrogen	A11034
Alexa 568-conjugated secondary anti mouse (IgM)	Invitrogen	A21043
Alexa 568-conjugated secondary anti rat	Invitrogen	A11077
qPCR oligonucleotides		
MT-ND1	Thermo Fisher Scientific	Hs02596873_s1
MT-ND2	Thermo Fisher Scientific	Hs02596874_g1
MT-ND3	Thermo Fisher Scientific	Hs02596875_s1
MT-ND4	Thermo Fisher Scientific	Hs02596876_g1

Reagents and Tools table (continued)

Reagent/Resource	Source	Identifier/Catalog number
MT-ND5	Thermo Fisher Scientific	Hs02596878_g1
MT-ND6	Thermo Fisher Scientific	Hs02596879_g1
MT-CYTB	Thermo Fisher Scientific	Hs02596867_s1
MT-CO1	Thermo Fisher Scientific	Hs02596864_g1
MT-CO2	Thermo Fisher Scientific	Hs02596865_g1
MT-CO3	Thermo Fisher Scientific	Hs02596866_g1
MT-ATP6	Thermo Fisher Scientific	Hs02586862_g1
MT-RNR1	Thermo Fisher Scientific	Hs02596859_g1
MT-RNR2	Thermo Fisher Scientific	Hs02596860_s1
B2M	Thermo Fisher Scientific	Hs00187842_m1
Genomic GAPDH	Thermo Fisher Scientific	Hs02786624_g1
Genomic ACTB (actin β)	Thermo Fisher Scientific	Hs03023880_g1
NDUFA7	Thermo Fisher Scientific	Hs01561430_m1
NDUFS4	Thermo Fisher Scientific	Hs00159589_m1
NDUFB8	Thermo Fisher Scientific	Hs00922353_g1
UQCRB	Thermo Fisher Scientific	Hs00559884_m1
COX7A2L	Thermo Fisher Scientific	Hs01059547_g1
MT-7S (Dloop)	Thermo Fisher Scientific	Hs02596861_s1
UCK2	Thermo Fisher Scientific	Hs00989900_m1
APRT	Thermo Fisher Scientific	Hs00975727_g1
HPRT	Thermo Fisher Scientific	Hs02800695_m1
esiRNA oligonucleotides		
Human UCK2 esiRNA	Sigma	EHU153241
Human SLC25A33	Sigma	EHU160961
Human SLC25A36	Sigma	EHU036611
Human APRT	Sigma	EHU1236681
Human HPRT	Sigma	EHU078931
EGFP	Sigma	EHUEGFP
Plasmid oligonucleotides		
SLC25A33 gRNA px459v2	Genscript	U7363GD130_1
SLC25A36 gRNA px459v2	Genscript	U721DGA050_1
NME6 gRNA px459v2	Genscript	U197WGG080_2
NME4 gRNA	This study	gaccggagcggaccctgg
RCC1L gRNA #1	This study	caccgcatgttacgaaagtctgg
RCC1L gRNA #2	This study	caccgagggctacagatgtgt
hNME6-MYC-FLAG pCMV6-Entry	Origene	RC20051
pLVX-puro	Takara	632164
hNME6-MYC-FLAG pLVX-puro	This study	
hNME6 H137N-MYC-FLAG pLVX-puro	This study	
Cell lines		
HeLa	ATCC	CCL2
HLE	Japanese Collection of Research Biosources	JCRB0404
Huh6	Japanese Collection of Research Biosources	JCRB0401
HepG2	ATCC	HB-8065
LentiX HEK293T	Takara	632180

Reagents and Tools table (continued)

Reagent/Resource	Source	Identifier/Catalog number
Cell culture reagents		
Dulbecco's Modified Eagle's Medium	Gibco	61965
Dulbecco's Modified Eagle's Medium (glucose free)	Gibco	11966
Human Plasma Like Medium	Gibco	A48991-01
Fetal Bovine Serum	Gibco	10270
Dialyzed FBS	Gibco	26400-044
Galactose	Serva	22020.02
Glucose	Sigma	G7021
Glutamine	Gibco	25030-081
Sodium Pyruvate	Gibco	11360
rNTPs	New England BioLabs	N0466S
dNTPs	New England BioLabs	N0446S
EmbryoMax 100× Nucleosides	Millipore	ES-008-D
Adenosine	Sigma	A4036
Guanosine	Sigma	G6264
Cytidine	Sigma	C4654
Uridine	Sigma	U3003
Lipofectamine RNAi MAX	Thermo Fisher Scientific	13778150
Lipofectamine CRISPR MAX	Thermo Fisher Scientific	CMAX00008
SYTOX green	Invitrogen	S7020
³⁵ S Methionine and Cysteine	Hartmann Analytics	ARS-0110A
HCS CellMask Deep Red Stain	Thermo Fisher Scientific	H32721
DAPI	Sigma	D9542
MitoTracker Deep Red	Thermo Fisher Scientific	M22426
Other		
TaqMan PCR master mix	Thermo Fisher Scientific	4324020
Cell Titer Glo	Promega	G9241
Mitochondrial Stress Test	Agilent	103015-100
NucleoSpin RNA	Machery-Nagel	740955.250
DNeasy Blood and Tissue Kit	Qiagen	69506
GoScript Reverse Transcription	Promega	A2791
Bio-Rad Protein Assay Kit	Bio-Rad	5000001
Pierce Protein Assay Reagent	Thermo Fisher Scientific	22660
FluorSave Reagent	Millipore	345789

Methods and Protocols

Reagents

Antibodies, qPCR oligonucleotides, esiRNA oligonucleotides, plasmids, cell lines, cell culture reagents and commercial assays used in this study are listed in the [Reagents and Tools table](#).

Cell culture

HeLa, HLE, HepG2 and Huh6 cells were grown in Dulbecco's Modified Eagle's Medium (DMEM) containing 10% foetal bovine serum (FBS) and maintained at 37°C and 5% CO₂, if not stated otherwise.

Alternatively, cells were cultured in either glucose free DMEM supplemented with 10% FBS, 10 mM galactose and uridine (200 µg/ml), or in human plasma-like medium (HPLM) supplemented with 10% dialysed FBS. All cultured cell lines were routinely tested for *Mycoplasma* contamination and authenticated by STR profiling.

For supplementation experiments, nucleosides (100 µM), rNTPs (100 µM) or dNTPs (100 µM) were added to the medium for at least 48 h. RNA interference experiments were performed by reverse transfection of 2×10^5 cells with 5 µg esiRNA using Lipofectamine RNAiMax.

Generation of cell lines

Knockout (KO) cells were generated using CRISPR-SpCas9 mediated gene editing. SpCas9 and guide RNA (gRNA) were expressed using transient transfection of px459 v2 expression vector (Genscript). Polyclonal cultures were obtained by puromycin selection prior to monoclonal selection by serial dilution. Polyclonal cultures and individual clones were validated by immunoblotting and genomic sequencing. HeLa and HLE NME6 KO cells expressing NME6-MycFlag or NME6 H137N-Myc-Flag were generated by lentiviral transduction. Lenti-X HEK293T cells were transfected with either pLVX-NME6-Myc-Flag or pLVX-NME6^{H137N} Myc-Flag using Lenti-X Packaging Single Shots (Takara). The viral supernatant was collected after 48 h, cleared from cell debris by centrifugation and added to HeLa NME6 KO cells together with polybrene (4 µg/ml). Virus-containing medium was removed after 24 h and puromycin selection (1 µg/ml) was started after an additional 24–48 h.

Cell proliferation assays

HeLa cell proliferation was monitored by live cell imaging using the Incucyte S3 instrument (Sartorius). Image analysis was performed using Incucyte Software 2019 RevB. 5×10^3 cells per well were seeded onto a 96 well plate and confluency was assessed every 6 h by phase contrast imaging until 100% confluency was reached. Proliferation rates were determined from the slope of the exponential growth phase (24–72 h). Cell death was visualised by SYTOX green. SYTOX green was added to the assay medium (1:30,000) and relative cell death was calculated by area of SYTOX green puncta divided by phase contrast cell area. Relative growth of HLE, Huh6 and HepG2 cells was determined on each day after 5×10^3 cells were seeded per well of a 96-well plate. Total ATP luminescence was measured with the Cell Titer Glo viability assay (Promega) using a Glomax luminometer (Promega).

DNA extraction, RNA extraction and cDNA synthesis

For mitochondrial DNA (mtDNA) measurements, genomic DNA was isolated for cell pellets using the Blood and Tissue DNA extraction kit (Qiagen). RNA was isolated from cell pellets using the RNA extraction kit (Macherey-Nagel) and 1–2 µg of RNA was reverse transcribed into cDNA using GoScript (Promega).

Cell lysis and SDS-PAGE

Cells were collected in ice-cold phosphate-buffered saline (PBS). Cell pellets were lysed in RIPA buffer (50 mM Tris-HCl pH 7.4, 150 mM NaCl, 1% Triton X100, 0.5% DOC, 0.1% SDS and 1 mM EDTA) for 30 min at 4°C. Lysates were cleared by centrifugation at $20,000 \times g$ for 10 min at 4°C. Protein concentration was determined by Bradford assay (Bio-Rad). Protein lysates were mixed with 4× Laemmli buffer and analysed by 10% SDS-PAGE and immunoblot.

Quantitative PCR

For mtDNA measurements, 10 ng of genomic DNA were amplified using TaqMan PCR master mix (Thermo Fisher Scientific). MtDNA levels were assessed by the delta delta ct method using *MT-7S*, *CYTB* and *MT-ND6* as mitochondrial probes and *GAPDH* and *ACTB* as nuclear DNA controls. For the measurements of nuclear and mitochondrial transcripts, 10 ng of cDNA were amplified using TaqMan PCR master mix. Expression levels were calculated by the delta delta ct method, for which *B2M* was used as control.

Design of arrayed single guide RNA (sgRNA) library

The custom Mito Transporter and Salvage Pathway sgRNA library was purchased from Synthego and consisted of three sgRNA sequences designed to generate deletions in early exons of each target gene. The 116 target genes included all genes encoding proteins designated as “Small Molecule Transporters” in MitoCarta 3.0 (Rath et al, 2021) as well as putative mitochondrial metabolite carriers identified in a recent proteomic evaluation of mitochondria (Morgenstern et al, 2021) and solute carriers with proposed mitochondrial localisation (Meixner et al, 2020). Mitochondrial pyrimidine salvage pathway genes were selected in addition to *TFAM* and controls, including non-targeting sgRNA (*NTC1*) and Polo-like kinase 1 (*PLK1*). All target genes and sgRNA sequences are listed in Dataset EV1.

Arrayed CRISPR-SpCas9 screen

The sgRNA library was reconstituted to 5 µM in Tris-EDTA (pH 8.0) and distributed to 96-well daughter plates. Note that the volumes in the following procedure correspond to individual transfections per well and were scaled up for the entire library in triplicate. Cas9 solution (0.5 µl SpCas9 2NLS nuclease, 1 µl Lipofectamine Cas9 plus reagent, 10.5 µl OptiMEM) was added to each well containing 1 µl sgRNA using the XRD-384 automated reagent dispenser (Fluidix). The Cas9-sgRNA mix was next stamped onto Cell Carrier Ultra 96-well plates (PerkinElmer) in triplicate prior to addition of the transfection reagent (0.35 µl Lipofectamine CRISPRMax, 10.15 µl OptiMEM) using the XRD-384. Each plate was placed on an orbital shaker at 300 rpm for 10 min at room temperature. In parallel, a cell suspension of *SLC25A33/SLC25A36* DKO HeLa cells (clone #2) was prepared in DMEM + 10% FBS (4×10^4 cells/ml) and added (100 µl/well) to the sgRNA:Cas9:LipofectamineCRISPRMax transfection mixture. Cells were distributed and incubated at 37°C and 5% CO₂. After 6 h, the media and transfection mix was replaced with fresh media containing 150 µM uridine using a plate washer (BioTeKELx405) to aspirate and XRD-384 to dispense. At 96 h post-transfection, the media was replaced with 80 µl of 4% formaldehyde in DMEM for 10 min. The cells were then washed twice in 150 µl PBS and permeabilised with 0.1% Triton-TX100 in 80 µl PBS for 20 min prior to two further PBS washes. Primary antibody staining was performed sequentially with anti-TFAM (ProteinTech; 1:800) and anti-DNA (Sigma; 1:800) antibodies in 40 µl PBS for 30 min at room temperature. Secondary antibody staining was also performed sequentially with anti-rabbit IgG-Alexa 488 nm (Thermo Fisher Scientific; 1:1,000) and anti-mouse IgM-Alexa 568 nm (Thermo Fisher Scientific; 1:1,000) antibodies in 40 µl PBS for 30 min at room temperature. Each antibody staining was followed by three PBS washes. Finally, DAPI (Merk; 0.5 µg/ml) and HCS CellMask Deep Red (Thermo Fisher Scientific; 1:20,000) were combined in 200 µl PBS per well for 30 min prior to three final PBS washes. Plates were stored in the dark at 4°C with 200 µl PBS in each well prior to imaging.

Plates were imaged with an OperaPhenix High Content Analysis System (PerkinElmer) using a 20× objective (25 fields per well; single plane) and 63× water objective (24 fields per well; 5 Z-planes with 1 µm separation). Imaging was performed using 405 nm (DAPI), 488 nm (TFAM), 561 nm (DNA) and 640 nm (CellMask) excitation. Maximum intensity projections were generated in each channel using all planes and analysis was performed using

Harmony 4.9 High-Content Imaging and Analysis Software (PerkinElmer). Nuclei masks were defined as DAPI positive structures above $30 \mu\text{m}^2$ in area and were counted to determine cell number. The $20\times$ objective was used to calculate cell number per well and all other analysis was performed with the $63\times$ objective. MtDNA was measured within HCS CellMask stained cytoplasmic regions upon exclusion of the nuclei. MtDNA intensity was analysed using standard mean intensity and mtDNA puncta were identified and measured using the “Find Spots” algorithm (relative spot intensity: > 0.045 , splitting sensitivity: 1).

Across the three replicates, cell number was depleted by over 75% in cells transfected with the lethal control sgRNA (PLK1) compared to non-targeting control sgRNA, which confirmed efficient transfection with Cas9:sgRNA ribonucleoprotein complexes in our screen.

Immunofluorescence and confocal microscopy

Cells were seeded on glass coverslips and grown to a confluency of 50%. MitoTracker Deep Red (Thermo Fisher Scientific; 100 nM) and bromouridine BrUX were added 20 min prior to fixation with 4% paraformaldehyde at 37°C . Cells were permeabilised and blocked in PBS containing 5% normal goat serum and 0.15% Triton-X. Cells were stained with primary antibodies for 90 min (NME6 1:250; BrdU 1:200; DNA 1:200) followed by Alexa-488 or Alexa-568 conjugated secondary antibodies for 45 min (1:1,000). Coverslips were mounted onto glass slides using FluorSave Reagent (Millipore) and imaged using a Zeiss LSM 880 Airyscan Confocal microscope with Zen 2.3 SP1 acquisition software. The objective used was Plan-Apochromat $40\times/1.3$ Oil DIC M27 and all images were acquired with the following three lasers: 633 nm (BP 570–620 + LP 645), 561 nm (BP 420–480 + BP 495–620) and 488 nm (BP 420–480 + BP 495–550). Plot profiles of foci were measured with ImageJ Version 1.53t.

Oxygen consumption and extracellular acidification measurements

Mitochondrial ATP-linked respiration and extra cellular acidification rate was measured by the Seahorse XFe96 analyser using the Mito Stress Test kit (Agilent). 4×10^4 cells were seeded and grown for 24 h in DMEM containing 10% FBS. For supplementation experiments, cells were cultured for at least 48 h in nucleoside containing medium prior to the experiment. Growth medium was exchanged to assay medium containing, glutamine, pyruvate and glucose. Oligomycin (2 μM), FCCP (0.5 μM) and rotenone and antimycin A (0.5 μM each) injections were used to calculate basal respiration, ATP-linked ATP production and maximal respiration, respectively. Results were normalised to the amount of protein per well.

Mitochondrial isolation

Cells were collected in ice-cold PBS. Cell pellets were resuspended in 1 ml ice-cold mitochondrial isolation buffer (containing 220 mM mannitol, 70 mM sucrose, 5 mM HEPES-KOH pH 7.4 and 1 mM EGTA-KOH + complete protease inhibitor). Cells were lysed detergent-free, using 10 strokes of a 1-ml syringe equipped with a 27-g needle. Cell lysates were spun down at $600 \times g$ for 5 min at 4°C and the supernatant was separated from the remaining cell pellet. The supernatant was spun down for 10 min at $8,000 \times g$ at 4°C . Mitochondria-enriched pellets were used for IP-, proteomic- and

metabolomics experiments. Purity of the mitochondria-enriched fractions was verified by SDS-PAGE and immunoblot.

Immunoprecipitation

Mitochondria-enriched pellets of HeLa WT and NME6 KO + NME6-MycFlag expressing cells (500 μg) were resuspended in 500 μl IP buffer (60 mM Tris-HCl and 300 mM KAc-KOH pH 7.4). Mitochondria were solubilised with digitonin (5 g/g protein) for 30 min at 4°C while shaking on a ThermoMixer (shaking: 550 rpm). Mitochondrial lysates were spun down at $20,000 \times g$ for 15 min at 4°C . The supernatant was mixed with Flag-agarose beads (Sigma) and incubated for 2 h at 4°C . After 2 h, the supernatant was removed by centrifugation at $500 \times g$ for 30 s and the remaining beads were washed three times with wash buffer (IP buffer containing 0.1% digitonin). Bound proteins were eluted from the beads using 60 μl of $1\times$ Laemmli buffer, samples were incubated for 10 min at 40°C . The eluate was separated from the beads by centrifugation at $1,000 \times g$ for 3 min. Eluates were used for SDS-PAGE, immunoblot analysis and LC-MS-based proteomics.

Mitochondrial translation assay

Mitochondrial translation rates were monitored by incorporation rates of radioactive methionine and cysteine (^{35}S) (Hartmann Analytic) into mitochondrial encoded proteins. Therefore, 3×10^5 cells were cultured for 24 h. Growth medium was washed out and replaced with minimal medium depleted of methionine and cysteine. Cytosolic translation was blocked by emetine (100 $\mu\text{g}/\text{ml}$) for 30 min. ^{35}S methionine and cysteine (50 μCi each) was added to the medium for 15–60 min. Cells were lysed and protein extracts were subjected to SDS-PAGE. Incorporation rates were visualised by autoradiography using a Typhoon FLA9500 imager (GE healthcare). Mitochondrial proteins were labelled according to their respective molecular weight.

Extraction of polar metabolites

Cell pellets and mitochondrial pellets were resuspended in -20°C cold extraction buffer (HPLC-grade ultrapure 40% MeOH, 40% acetonitrile, 20% water and 0.1 $\mu\text{g}/\text{ml}$ ^{13}C labelled ATP). Pellets were dissolved by sonication at 4°C followed by an incubation for 30 min at 4°C while shaking at 1,500 rpm. The metabolite containing supernatant was cleared by centrifugation at $20,000 \times g$ for 10 min and subsequently transferred to a speedvac concentrator to fully evaporate the extraction buffer. The remaining protein pellet from the extraction was used to determine protein concentration of the sample.

Anion-exchange chromatography mass spectrometry (AEX-MS) for the analysis of nucleotides and deoxynucleotides

Extracted metabolites from crude- and mito-preparations were resuspended in 100 μl of UPLC/MS grade water (Biosolve) and transferred to polypropylene autosampler vials (Chromatography Accessories Trott, Germany).

The samples were analysed using a Dionex ionchromatography system (Integrion Thermo Fisher Scientific) as described previously (Schwaiger et al, 2017). In brief, 5 μl of polar metabolite extract were injected in push partial mode, using an overfill factor of 1, onto a Dionex IonPac AS11-HC column (2 mm \times 250 mm, 4 μm particle size, Thermo Fisher Scientific) equipped with a Dionex

IonPac AG11-HC guard column (2 mm × 50 mm, 4 µm, Thermo Fisher Scientific). The column temperature was held at 30°C, while the auto sampler was set to 6°C. A potassium hydroxide gradient was generated using a potassium hydroxide cartridge (Eluent Generator, Thermo Scientific), which was supplied with deionised water (Millipore). The metabolite separation was carried at a flow rate of 380 µl/min, applying the following gradient conditions: 0–3 min, 10 mM KOH; 3–12 min, 10–50 mM KOH; 12–19 min, 50–100 mM KOH; 19–22 min, 100 mM KOH, 22–23 min, 100–10 mM KOH. The column was re-equilibrated at 10 mM for 3 min.

For the analysis of metabolic pool sizes the eluting compounds were detected in negative ion mode using full scan measurements in the mass range m/z 77–770 on a Q-Exactive HF high resolution MS (Thermo Fisher Scientific). The heated electrospray ionisation (HESI) source settings of the mass spectrometer were: Spray voltage 3.2 kV, capillary temperature was set to 300°C, sheath gas flow 50 AU, aux gas flow 20 AU at a temperature of 330°C and a sweep gas flow of 2 AU. The S-lens was set to a value of 60.

The semi-targeted LC–MS data analysis was performed using the TraceFinder software (Version 5.1, Thermo Fisher Scientific). The identity of each compound was validated by authentic reference compounds, which were measured at the beginning and the end of the sequence. For data analysis the area of the deprotonated $[M-H]^{-1}$ or doubly deprotonated $[M-2H]^{-2}$ mono-isotopologue mass peaks of every required compound were extracted and integrated using a mass accuracy < 3 ppm and a retention time tolerance of < 0.05 min as compared to the independently measured reference compounds. These areas were then normalised to the internal standard, which was added to the extraction buffer, followed by a normalisation to the protein content of the analysed sample. Values were log2 transformed and normalised to the WT mean.

Sample preparation for mass spectrometry-based proteomics

For whole proteome analysis, 60 µl of 4% SDS in 100 mM HEPES-KOH (pH = 8.5) was pre-heated to 70°C and added to the cell pellet for further 10 min incubation at 70°C on a ThermoMixer (shaking: 550 rpm). The protein concentration was determined using the 660 nm Protein Assay (Thermo Fisher Scientific, #22660). 20 µg of protein was subjected to tryptic digestion. For immunoprecipitation analysis, the LDS buffer eluate was directly used. Proteins were reduced (10 mM TCEP) and alkylated (20 mM CAA) in the dark for 45 min at 45°C. Samples were subjected to an SP3-based digestion (Hughes et al, 2014). Washed SP3 beads (Sera-Mag (TM) Magnetic Carboxylate Modified Particles (Hydrophobic, GE44152105050250), Sera-Mag™ Magnetic Carboxylate Modified Particles (Hydrophilic, GE24152105050250) from Sigma Aldrich) were mixed equally, and 3 µl of bead slurry were added to each sample. Acetonitrile was added to a final concentration of 50% and washed twice using 70% ethanol ($V = 200$ µl) on an in-house made magnet. After an additional acetonitrile wash ($V = 200$ µl), 5 µl digestion solution (10 mM HEPES-KOH pH = 8.5 containing trypsin (0.5 µg, Sigma) and LysC (0.5 µg, Wako)) was added to each sample and incubated overnight at 37°C. Peptides were desalted on a magnet using 2 × 200 µl acetonitrile. Peptides were eluted in 10 µl 5% DMSO in LC–MS water (Sigma Aldrich) in an ultrasonic bath for 10 min. Formic acid and acetonitrile were added to a final concentration of 2.5 and 2%, respectively. Samples were stored at –20°C before subjection to LC–MS/MS analysis.

Liquid chromatography and mass spectrometry

LC–MS/MS instrumentation consisted of an Easy-LC 1200 (Thermo Fisher Scientific) coupled via a nano-electrospray ionisation source to an Exploris 480 mass spectrometer (Thermo Fisher Scientific, Bremen, Germany). An in-house packed column (inner diameter: 75 µm, length: 40 cm) was used for peptide separation. A binary buffer system (A: 0.1% formic acid and B: 0.1% formic acid in 80% acetonitrile) was applied as follows:

Whole proteome analysis

Linear increase of buffer B from 4 to 27% within 70 min, followed by a linear increase to 45% within 5 min. The buffer B content was further ramped to 65% within 5 min and then to 95% within 5 min. 95% buffer B was kept for a further 5 min to wash the column.

Immunoprecipitation analysis

Linear increase of buffer B from 4 to 27% within 40 min, followed by a linear increase to 45% within 5 min. The buffer B content was further ramped to 65% within 5 min and then to 95% within 5 min. 95% buffer B was kept for a further 5 min to wash the column.

Prior to each sample, the column was washed using 5 µl buffer A and the sample was loaded using 8 µl buffer A.

The RF Lens amplitude was set to 55%, the capillary temperature was 275°C and the polarity was set to positive. MS1 profile spectra were acquired using a resolution of 120,000 (at 200 m/z) at a mass range of 320–1,150 m/z and an AGC target of 1×10^6 .

For MS/MS independent spectra acquisition, 48 equally spaced windows were acquired at an isolation m/z range of 15 Th, and the isolation windows overlapped by 1 Th. The fixed first mass was 200 m/z . The isolation centre range covered a mass range of 357–1,060 m/z . Fragmentation spectra were acquired at a resolution of 15,000 at 200 m/z using a maximal injection time of 22 ms and stepped normalised collision energies (NCE) of 26, 28 and 30. The default charge state was set to 3. The AGC target was set to 3e6 (900% - Exploris 480). MS2 spectra were acquired in centroid mode.

Proteomics data analysis

DIA-NN (Data-Independent Acquisition by Neural Networks) v 1.8 (Demichev et al, 2020) was used to analyse data-independent raw files. The spectral library was created using the reviewed-only Uniprot reference protein (*Homo sapiens*, 20,350 entries, downloaded September 2019) with the “Deep learning-based spectra and RTs prediction” turned on. Protease was set to trypsin and a maximum of 1 miss cleavage was allowed. N-term M excision was set as a variable modification and carbamidomethylation at cysteine residues was set as a fixed modification. The peptide length was set to 7–30 amino acids and the precursor m/z range was defined from 340 to 1,200 m/z . The option “Quantitative matrices” was enabled. The FDR was set to 1% and the mass accuracy (MS2 and MS1) as well as the scan window was set to 0 (automatic inference via DIA-NN). Match between runs (MBR) was enabled. The Neuronal network classifier worked in “double pass mode” and protein interference was set to “Isoform IDs”. The quantification strategy was set to “robust LC (high accuracy)” and cross-run normalisation was defined as “RT-dependent”.

The “pg” (protein group) output (MaxLFQ intensities; Cox et al, 2014) was further processed using Instant Clue (Nolte

et al., 2018) including and pairwise comparison using an unpaired two-sided *t*-test or one-way ANOVA followed by a permutation-based FDR correction (5%).

MitoCarta 3.0 (Rath et al., 2021) and Uniprot-based Gene Ontology annotations were used for filtering. Hierarchical clustering, heatmaps and volcano plots were generated using the InstantClue software (Nolte et al., 2018) v. 0.10.10.

Data availability

The mass spectrometry proteomics data have been deposited to the ProteomeXchange Consortium via the PRIDE partner repository with the dataset identifier PXD038391 (Perez-Riverol et al., 2021).

Expanded View for this article is available [online](#).

Acknowledgements

We thank the MPI Biology of Ageing Metabolomics core facility, the Beatson Advanced Imaging Resource and Dominique Diehl for technical assistance. We thank Dusanka Milenkovic, Payam Gammage and Ryan Corbyn for helpful discussion and Catherine Winchester for comments on the manuscript. We thank Victor Villar and Saverio Tardito for providing liver cancer cell lines. NG and AJNP received support from the Cologne Graduate School of Ageing Research. This work was supported by funds of the Max-Planck-Society and from the Deutsche Forschungsgemeinschaft (DFG, German Research Foundation) – SFB1403 – Projektnummer (414786233) to TL and a Cancer Research UK Career Development Fellowship to TM (RCCFELCDF-May21\100001) and CRUK core funding to the CRUK Beatson Institute (A31287).

Author contributions

Thomas MacVicar: Conceptualization; resources; data curation; supervision; funding acquisition; validation; visualization; writing – original draft; project administration; writing – review and editing. **Thomas Langer:** Conceptualization; resources; supervision; funding acquisition; validation; writing – original draft; project administration; writing – review and editing. **Nils Grotehans:** Conceptualization; data curation; formal analysis; validation; investigation; visualization; methodology; writing – original draft; writing – review and editing. **Lynn McGarry:** Data curation; formal analysis; validation; visualization; methodology. **Hendrik Nolte:** Data curation; software; formal analysis; visualization; methodology; writing – review and editing. **Moritz Kroker:** Investigation; writing – review and editing. **Álvaro Jesús Narbona-Pérez:** Conceptualization; methodology; writing – review and editing. **Soni Deshwal:** Conceptualization; methodology; writing – review and editing. **Patrick Gialvalisco:** Conceptualization; data curation; formal analysis; validation; methodology; writing – review and editing. **Vanessa Xavier:** Data curation; visualization.

Disclosure and competing interests statement

The authors declare that they have no conflict of interest.

References

Amici DR, Jackson JM, Truica MI, Smith RS, Abdulkadir SA, Mendillo ML (2021) FIREWORKS: a bottom-up approach to integrative coessentiality network analysis. *Life Sci Alliance* 4: e202000882

Antonicka H, Shoubridge EA (2015) Mitochondrial RNA granules are centers for posttranscriptional RNA processing and ribosome biogenesis. *Cell Rep* 10: 920–932

Antonicka H, Choquet K, Lin ZY, Gingras AC, Kleinman CL, Shoubridge EA (2017) A pseudouridine synthase module is essential for mitochondrial protein synthesis and cell viability. *EMBO Rep* 18: 28–38

Antonicka H, Lin ZY, Janer A, Aaltonen MJ, Weraarpachai W, Gingras AC, Shoubridge EA (2020) A high-density human mitochondrial proximity interaction network. *Cell Metab* 32: e479

Boissan M, Schlattner U, Lacombe ML (2018) The NDPK/NME superfamily: state of the art. *Lab Invest* 98: 164–174

Bonekamp NA, Jiang M, Motori E, Garcia Villegas R, Koolmeister C, Atanassov I, Mesaros A, Park CB, Larsson N-G (2021) High levels of TFAM repress mammalian mitochondrial DNA transcription *in vivo*. *Life Sci Alliance* 4: e202101034

Chen C-W, Wang H-L, Huang C-W, Huang C-Y, Lim WK, Tu I-C, Koorapati A, Hsieh S-T, Kan H-W, Tzeng S-R et al (2019) Two separate functions of NME3 critical for cell survival underlie a neurodegenerative disorder. *Proc Natl Acad Sci USA* 116: 566–574

Cox J, Hein MY, Lubner CA, Paron I, Nagaraj N, Mann M (2014) Accurate proteome-wide label-free quantification by delayed normalization and maximal peptide ratio extraction, termed MaxLFQ. *Mol Cell Proteomics* 13: 2513–2526

Demichev V, Messner CB, Vernardis SI, Lilley KS, Ralser M (2020) DIA-NN: neural networks and interference correction enable deep proteome coverage in high throughput. *Nat Methods* 17: 41–44

Deshwal S, Fiedler KU, Langer T (2020) Mitochondrial proteases: multifaceted regulators of mitochondrial plasticity. *Annu Rev Biochem* 89: 501–528

Di Noia MA, Todisco S, Cirigliano A, Rinaldi T, Agrimi G, Iacobazzi V, Palmieri F (2014) The human SLC25A33 and SLC25A36 genes of solute carrier family 25 encode two mitochondrial pyrimidine nucleotide transporters. *J Biol Chem* 289: 33137–33148

D'Souza AR, Minczuk M (2018) Mitochondrial transcription and translation: overview. *Essays Biochem* 62: 309–320

Edenberg ER, Downey M, Toczyski D (2014) Polymerase stalling during replication, transcription and translation. *Curr Biol* 24: R445–R452

Ekstrand MI, Falkenberg M, Rantanen A, Park CB, Gaspari M, Hultenby K, Rustin P, Gustafsson CM, Larsson N-G (2004) Mitochondrial transcription factor A regulates mtDNA copy number in mammals. *Hum Mol Genet* 13: 935–944

Ernst O, Sun J, Lin B, Banoth B, Dorrington MG, Liang J, Schwarz B, Stromberg KA, Katz S, Vayttaden SJ et al (2021) A genome-wide screen uncovers multiple roles for mitochondrial nucleoside diphosphate kinase D in inflammasome activation. *Sci Signal* 14: eabe0387

Favre C, Zhdanov A, Leahy M, Papkovsky D, O'Connor R (2010) Mitochondrial pyrimidine nucleotide carrier (PNC1) regulates mitochondrial biogenesis and the invasive phenotype of cancer cells. *Oncogene* 29: 3964–3976

Fei ZY, Wang WS, Li SF, Zi JJ, Yang L, Liu T, Ao S, Liu QQ, Cui QH, Yu M et al (2020) High expression of the TEFM gene predicts poor prognosis in hepatocellular carcinoma. *J Gastrointest Oncol* 11: 1291–1304

Feric M, Sarfallah A, Dar F, Temiakov D, Pappu RV, Misteli T (2022) Mesoscale structure–function relationships in mitochondrial transcriptional condensates. *Proc Natl Acad Sci USA* 119: e2207303119

Fernandez-Vizcarra E, Zeviani M (2021) Mitochondrial disorders of the OXPHOS system. *FEBS Lett* 595: 1062–1106

Ferraro P, Pontarin G, Crocco L, Fabris S, Reichard P, Bianchi V (2005) Mitochondrial deoxynucleotide pools in quiescent fibroblasts: a possible

- model for mitochondrial neurogastrointestinal encephalomyopathy (MNGIE). *J Biol Chem* 280: 24472–24480
- Filigrana R, Mennuni M, Alsina D, Larsson NG (2021) Mitochondrial DNA copy number in human disease: the more the better? *FEBS Lett* 595: 976–1002
- Floyd S, Favre C, Lasorsa FM, Leahy M, Trigiante G, Stroebel P, Marx A, Loughran G, O'Callaghan K, Marobbio CM et al (2007) The insulin-like growth factor-I-mTOR signaling pathway induces the mitochondrial pyrimidine nucleotide carrier to promote cell growth. *Mol Biol Cell* 18: 3545–3555
- Floyd BJ, Wilkerson EM, Veling MT, Minogue CE, Xia C, Beebe ET, Wrobel RL, Cho H, Kremer LS, Alston CL et al (2016) Mitochondrial protein interaction mapping identifies regulators of respiratory chain function. *Mol Cell* 63: 621–632
- Garrido N, Griparic L, Jokitalo E, Wartiovaara J, van der Blik AM, Spelbrink JN (2003) Composition and dynamics of human mitochondrial nucleoids. *Mol Biol Cell* 14: 1583–1596
- Gohil VM, Nilsson R, Belcher-Timme CA, Luo B, Root DE, Mootha VK (2010) Mitochondrial and nuclear genomic responses to loss of LRPPRC expression. *J Biol Chem* 285: 13742–13747
- González-Vioque E, Torres-Torronteras J, Andreu AL, Martí R (2011) Limited dCTP availability accounts for mitochondrial DNA depletion in mitochondrial neurogastrointestinal encephalomyopathy (MNGIE). *PLoS Genet* 7: e1002035
- Gustafsson CM, Falkenberg M, Larsson N-G (2016) Maintenance and expression of mammalian mitochondrial DNA. *Annu Rev Biochem* 85: 133–160
- Hamalainen RH, Landoni JC, Ahlqvist KJ, Goffart S, Ryytty S, Rahman MO, Brillhante V, Icaý K, Hautaniemi S, Wang L et al (2019) Defects in mtDNA replication challenge nuclear genome stability through nucleotide depletion and provide a unifying mechanism for mouse progerias. *Nat Metab* 1: 958–965
- Hughes CS, Foehr S, Garfield DA, Furlong EE, Steinmetz LM, Krijgsvelde J (2014) Ultrasensitive proteome analysis using paramagnetic bead technology. *Mol Syst Biol* 10: 757
- Jiang Y, Sun A, Zhao Y, Ying W, Sun H, Yang X, Xing B, Sun W, Ren L, Hu B et al (2019) Proteomics identifies new therapeutic targets of early-stage hepatocellular carcinoma. *Nature* 567: 257–261
- Kanki T, Ohgaki K, Gaspari M, Gustafsson CM, Fukuoh A, Sasaki N, Hamasaki N, Kang D (2004) Architectural role of mitochondrial transcription factor a in maintenance of human mitochondrial DNA. *Mol Cell Biol* 24: 9823–9834
- Lane AN, Fan TW (2015) Regulation of mammalian nucleotide metabolism and biosynthesis. *Nucleic Acids Res* 43: 2466–2485
- Larsson N-G, Wang J, Wilhelmsson H, Oldfors A, Rustin P, Lewandoski M, Barsh GS, Clayton DA (1998) Mitochondrial transcription factor A is necessary for mtDNA maintenance and embryogenesis in mice. *Nat Genet* 18: 231–236
- Lascu I, Gonin P (2000) The catalytic mechanism of nucleoside diphosphate kinases. *J Bioenerg Biomembr* 32: 237–246
- Legros F, Malka F, Frachon P, Lombès A, Rojo M (2004) Organization and dynamics of human mitochondrial DNA. *J Cell Sci* 117: 2653–2662
- Mathews CK, Song S (2007) Maintaining precursor pools for mitochondrial DNA replication. *FASEB J* 21: 2294–2303
- Meixner E, Goldmann U, Sedlyarov V, Scorzoni S, Rebsamen M, Girardi E, Superti-Furga G (2020) A substrate-based ontology for human solute carriers. *Mol Syst Biol* 16: e9652
- Milon L, Meyer P, Chiadmi M, Munier A, Johansson M, Karlsson A, Lascu I, Capeau J, Janin J, Lacombe M-L (2000) The human nm23-H4 gene product is a mitochondrial nucleoside diphosphate kinase. *J Biol Chem* 275: 14264–14272
- Miranda M, Bonekamp NA, Kuhl I (2022) Starting the engine of the powerhouse: mitochondrial transcription and beyond. *Biol Chem* 403: 779–805
- Morgenstern M, Peikert CD, Lübbert P, Suppanz I, Klemm C, Alka O, Steiert C, Naumenko N, Schendzielorz A, Melchionda L et al (2021) Quantitative high-confidence human mitochondrial proteome and its dynamics in cellular context. *Cell Metab* 33: 2464–2483
- Nolte H, MacVicar TD, Tellkamp F, Kruger M (2018) Instant clue: a software suite for interactive data visualization and analysis. *Sci Rep* 8: 12648
- Nusinow DP, Szpyt J, Ghandi M, Rose CM, McDonald ER III, Kalocsay M, Jané-Valbuena J, Gelfand E, Schweppe DK, Jedrychowski M et al (2020) Quantitative proteomics of the cancer cell line encyclopedia. *Cell* 180: 387–402
- Pastor-Anglada M, Perez-Torras S (2018) Emerging roles of nucleoside transporters. *Front Pharmacol* 9: 606
- Perez-Riverol Y, Bai J, Bandla C, Garcia-Seisdedos D, Hewapathirana S, Kamatchinathan S, Kundu Deepti J, Prakash A, Frericks-Zipper A, Eisenacher M et al (2021) The PRIDE database resources in 2022: a hub for mass spectrometry-based proteomics evidences. *Nucleic Acids Res* 50: D543–D552
- Pontarin G, Ferraro P, Håkansson P, Thelander L, Reichard P, Bianchi V (2007) p53R2-dependent ribonucleotide reduction provides deoxyribonucleotides in quiescent human fibroblasts in the absence of induced DNA damage. *J Biol Chem* 282: 16820–16828
- Pooler AM, Guez DH, Benedictus R, Wurtman RJ (2005) Uridine enhances neurite outgrowth in nerve growth factor-differentiated PC12 [corrected]. *Neuroscience* 134: 207–214
- Proust B, Radic M, Vidacek NS, Cottet C, Attia S, Lamarche F, Ackar L, Mikulic VG, Tokarska-Schlattner M, Cetkovic H et al (2021) NME6 is a phosphotransfer-inactive, monomeric NME/NDPK family member and functions in complexes at the interface of mitochondrial inner membrane and matrix. *Cell Biosci* 11: 195
- Rath S, Sharma R, Gupta R, Ast T, Chan C, Durham TJ, Goodman RP, Grabarek Z, Haas ME, Hung WHW et al (2021) MitoCarta3.0: an updated mitochondrial proteome now with sub-organelle localization and pathway annotations. *Nucleic Acids Res* 49: D1541–D1547
- Reitzer LJ, Wice BM, Kennell D (1979) Evidence that glutamine, not sugar, is the major energy source for cultured HeLa cells. *J Biol Chem* 254: 2669–2676
- Reyes A, Favia P, Vidoni S, Petruzzella V, Zeviani M (2020) RCC1L (WBSCR16) isoforms coordinate mitochondrial ribosome assembly through their interaction with GTPases. *PLoS Genet* 16: e1008923
- Rossignol R, Gilkerson R, Aggeler R, Yamagata K, Remington SJ, Capaldi RA (2004) Energy substrate modulates mitochondrial structure and oxidative capacity in cancer cells. *Cancer Res* 64: 985–993
- Rossiter NJ, Huggler KS, Adelman CH, Keys HR, Soens RW, Sabatini DM, Cantor JR (2021) CRISPR screens in physiologic medium reveal conditionally essential genes in human cells. *Cell Metab* 33: 1248–1263
- Russell OM, Gorman GS, Lightowlers RN, Turnbull DM (2020) Mitochondrial diseases: hope for the future. *Cell* 181: 168–188
- Ruzzenente B, Metodiev MD, Wredenberg A, Bratic A, Park CB, Cámara Y, Milenkovic D, Zickermann V, Wibom R, Hulthenby K et al (2012) LRPPRC is necessary for polyadenylation and coordination of translation of mitochondrial mRNAs. *EMBO J* 31: 443–456
- Saada A, Shaag A, Mandel H, Nevo Y, Eriksson S, Elpeleg O (2001) Mutant mitochondrial thymidine kinase in mitochondrial DNA depletion myopathy. *Nat Genet* 29: 342–344

- Schwaiger M, Rampler E, Hermann G, Miklos W, Berger W, Koellensperger G (2017) Anion-exchange chromatography coupled to high-resolution mass spectrometry: a powerful tool for merging targeted and non-targeted metabolomics. *Anal Chem* 89: 7667–7674
- Sharma S, Koolmeister C, Tran P, Nilsson AK, Larsson N-G, Chabes A (2020) Proofreading deficiency in mitochondrial DNA polymerase does not affect total dNTP pools in mouse embryos. *Nat Metab* 2: 673–675
- Smith JC, Sheltzer JM (2022) Genome-wide identification and analysis of prognostic features in human cancers. *Cell Rep* 38: 110569
- Song S, Wheeler LJ, Mathews CK (2003) Deoxyribonucleotide pool imbalance stimulates deletions in HeLa cell mitochondrial DNA. *J Biol Chem* 278: 43893–43896
- Sprenger H-G, MacVicar T, Bahat A, Fiedler KU, Hermans S, Ehrentraut D, Ried K, Milenkovic D, Bonekamp N, Larsson N-G et al (2021) Cellular pyrimidine imbalance triggers mitochondrial DNA-dependent innate immunity. *Nat Metab* 3: 636–650
- Suomalainen A, Isohanni P (2010) Mitochondrial DNA depletion syndromes – many genes, common mechanisms. *Neuromuscul Disord* 20: 429–437
- Szczepanowska K, Trifunovic A (2021) Tune instead of destroy: how proteolysis keeps OXPHOS in shape. *Biochim Biophys Acta Bioenerg* 1862: 148365
- Tan BC, Mutti CD, Shi Y, Xie X, Zhu X, Silva-Pinheiro P, Menger KE, Diaz-Maldonado H, Wei W, Nicholls TJ et al (2022) The human mitochondrial genome contains a second light strand promoter. *Mol Cell* 82: 3646–3660
- Tokarska-Schlattner M, Boissan M, Munier A, Borot C, Mailleau C, Speer O, Schlattner U, Lacombe M-L (2008) The nucleoside diphosphate kinase D (NM23-H4) binds the inner mitochondrial membrane with high affinity to cardiolipin and couples nucleotide transfer with respiration. *J Biol Chem* 283: 26198–26207
- Tsuiki H, Nitta M, Furuya A, Hanai N, Fujiwara T, Inagaki M, Kochi M, Ushio Y, Saya H, Nakamura H (1999) A novel human nucleoside diphosphate (NDP) kinase, Nm23-H6, localizes in mitochondria and affects cytokinesis. *J Cell Biochem* 76: 254–269
- Vafai SB, Mootha VK (2012) Mitochondrial disorders as windows into an ancient organelle. *Nature* 491: 374–383
- Van Dyck E, Jank B, Ragnini A, Schweygen RJ, Duyckaerts C, Sluse F, Foury F (1995) Overexpression of a novel member of the mitochondrial carrier family rescues defects in both DNA and RNA metabolism in yeast mitochondria. *Mol Gen Genet* 246: 426–436
- Wagner A, Hofmeister O, Rolland SG, Maiser A, Aasumets K, Schmitt S, Schorpp K, Feuchtinger A, Hadian K, Schneider S et al (2019) Mitochondrial Alkbh1 localizes to mtRNA granules and its knockdown induces the mitochondrial UPR in humans and *C. elegans*. *J Cell Sci* 132: jcs223891
- Wan L, Wang Y, Zhang Z, Wang J, Niu M, Wu Y, Yang Y, Dang Y, Hui S, Ni M et al (2021) Elevated TEFM expression promotes growth and metastasis through activation of ROS/ERK signaling in hepatocellular carcinoma. *Cell Death Dis* 12: 325
- Wang L (2016) Mitochondrial purine and pyrimidine metabolism and beyond. *Nucleosides Nucleotides Nucleic Acids* 35: 578–594
- West AP, Khoury-Hanold W, Staron M, Tal MC, Pineda CM, Lang SM, Bestwick M, Duguay BA, Raimundo N, MacDuff DA et al (2015) Mitochondrial DNA stress primes the antiviral innate immune response. *Nature* 520: 553–557
- Winter JM, Yadav T, Rutter J (2022) Stressed to death: mitochondrial stress responses connect respiration and apoptosis in cancer. *Mol Cell* 82: 3321–3332
- Xavier VJ, Martinou J-C (2021) RNA granules in the mitochondria and their organization under mitochondrial stresses. *Int J Mol Sci* 22: 9502
- Zaganelli S, Rebelo-Guiomar P, Maundrell K, Rozanska A, Pierredon S, Powell CA, Jourdain AA, Hulo N, Lightowlers RN, Chrzanowska-Lightowlers ZM et al (2017) The pseudouridine synthase RPUSD4 is an essential component of mitochondrial RNA granules. *J Biol Chem* 292: 4519–4532
- Zhong Z, Liang S, Sanchez-Lopez E, He F, Shalapur S, Lin XJ, Wong J, Ding S, Seki E, Schnabl B et al (2018) New mitochondrial DNA synthesis enables NLRP3 inflammasome activation. *Nature* 560: 198–203
- Zimmermann H (1999) Two novel families of ectonucleotidases: molecular structures, catalytic properties and a search for function. *Trends Pharmacol Sci* 20: 231–236



License: This is an open access article under the terms of the [Creative Commons Attribution](https://creativecommons.org/licenses/by/4.0/) License, which permits use, distribution and reproduction in any medium, provided the original work is properly cited.

Expanded View Figures

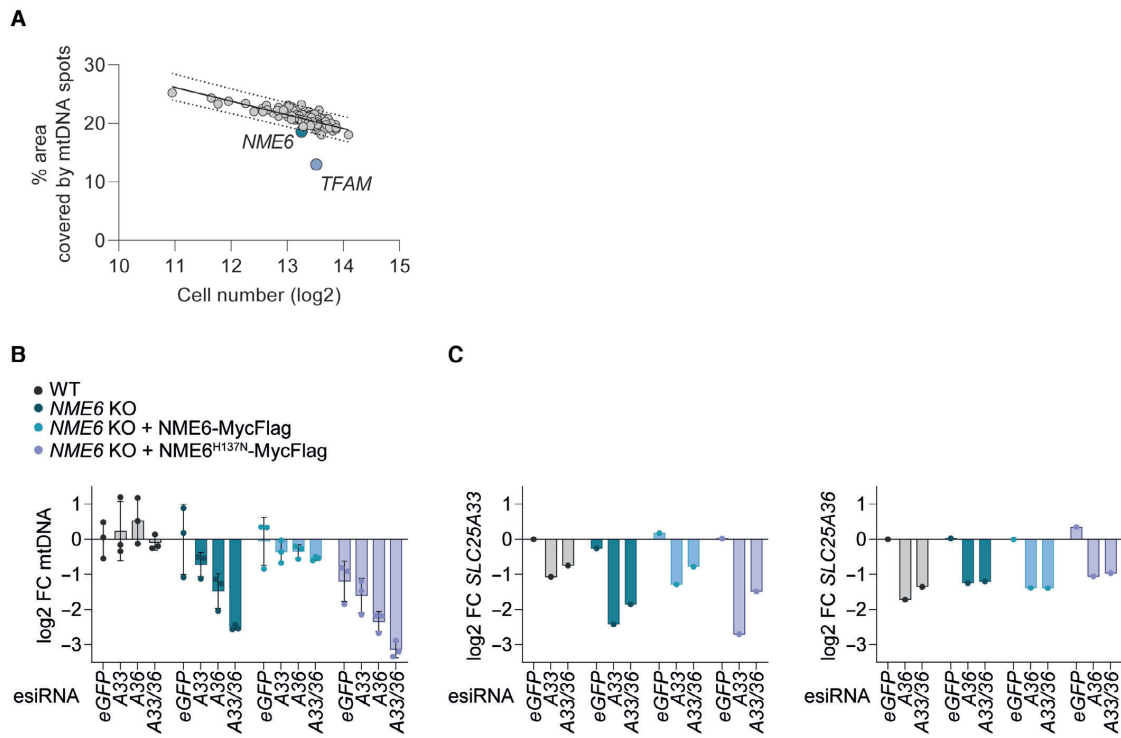


Figure EV1. CRISPR-SpCas9 screen analysis and validation by RNA interference.

A The result of the CRISPR-SpCas9 screen (Fig 1C) plotted as the percentage of cell cytoplasm area occupied by mtDNA spots against the mean log₂ cell number from each sgRNA target. The values for cells transfected with *NME6* sgRNA and *TFAM* sgRNA lie below the 95% prediction bands (least-squares regression; $R^2 = 0.52$; $n = 3$ independent experiments).

B MtDNA level monitored by qPCR (*CYTB/ACTB*) in the indicated HeLa cell lines treated with esiRNA targeting *GFP* (control), *SLC25A33* (A33), *SLC25A36* (A36) or *SLC25A33 + SLC25A36* (A33/A36) relative to WT cells (log₂; $n = 3$ independent cultures).

C *SLC25A33* (left) and *SLC25A36* (right) transcript levels in samples from a representative experiment in (B) monitored by qRT-PCR (log₂; $n = 1$).

Data information: FC, fold change. Data are means \pm SD.

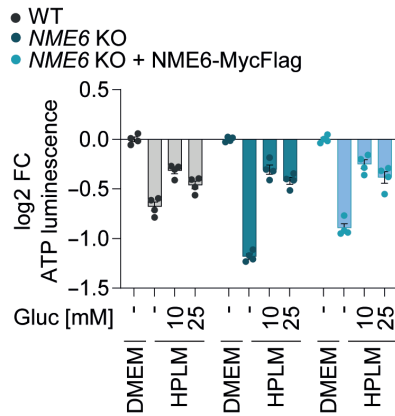


Figure EV2. Glucose is limiting for growth in HPLM.

Cell viability in WT, *NME6* KO and *NME6* KO + *NME6* MycFlag HeLa cells incubated in HPLM supplemented with different concentrations of glucose (standard HPLM contains 5 mM glucose). Cell viability was determined by ATP luminescence assay and analysed relative to DMEM (log₂; n = 4 independent cultures). FC, fold change. Data are means ± SD.

Figure EV3. Alterations to the proteome upon *NME6* depletion and further characterisation of *NME6* in liver cancer.

- A Extended unsupervised hierarchical row clustering (Euclidean distance, complete method) representation of significantly different proteins (FDR < 0.05) (*NME6* KO vs. WT) z-scores of log₂-transformed protein intensities determined by quantitative mass spectrometry and filtered for mitochondrial proteins according to MitoCarta 3.0 (Rath et al, 2021). The cluster presented in Fig 3B is visible at the top (C4). The bottom cluster (C1) is expanded here to reveal proteins that are significantly upregulated in *NME6* KO cells compared to WT and *NME6* KO + *NME6*-MycFlag HeLa cells (n = 4 independent cultures).
- B Relative *NME6* protein expression in cell lines across the indicated cancer types determined by quantitative proteomic profiling (Nusinow et al, 2020). Data obtained from depmap.org/portal (solid line = median, box limits = 25th and 75th percentile and whiskers = maxima and minima).
- C Kaplan–Meier plots showing patient survival in the indicated liver hepatocellular carcinoma cohorts (LIHC) from The Cancer Genome Atlas Program (TCGA) analysed using <http://www.tcgatoolbox.org>. P-values were determined using a log rank test (Smith & Sheltzer, 2022).
- D Stratification of the gene effect of *NME6* depletion from Fig 2A into cancer type (left, solid line = median, box limits = 25th and 75th percentile and whiskers = maxima and minima). Individual cell line *NME6* gene effects are also shown with HepG2 and Huh6 cell lines highlighted (right, note that HLE cells are not included in DepMap 22Q2 Public+Score, Chronos).
- E Immunoblot analysis of WT HLE cells, *NME6* KO cells and *NME6* KO cells expressing *NME6*-MycFlag (WT) or *NME6*^{H137N}-MycFlag (H137N).

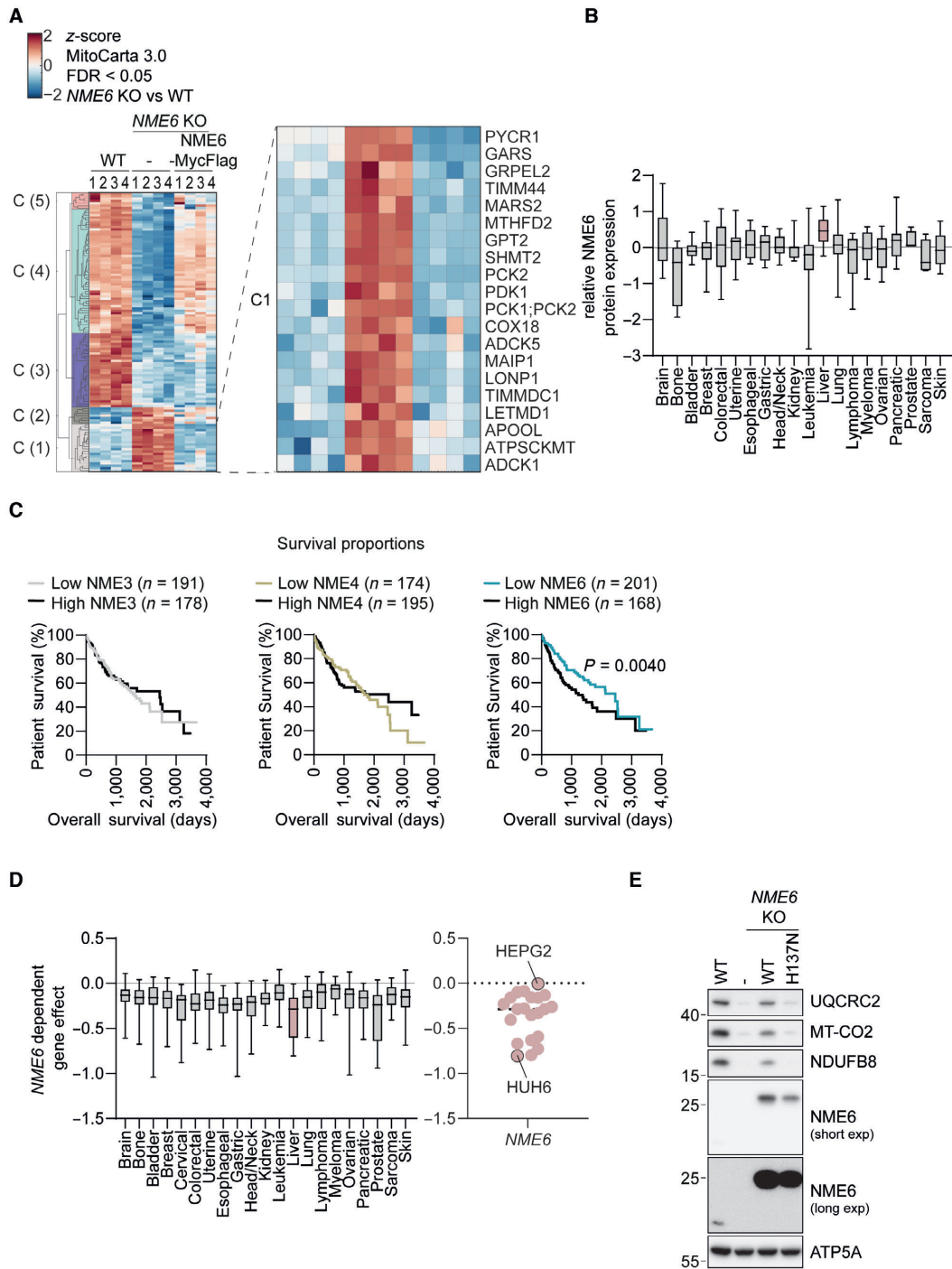


Figure EV3.

Figure EV4. Proteomic analysis of immunoprecipitates shows interaction between NME6 and RCC1L.

- A Pan-cancer gene coessentiality network visualisation of the top 15 positively correlated genes (solid lines) and five secondary node positive interactions (dotted lines) with all NME family members (*NME1-9*) using FIREWORKS (Amici et al, 2021) (left) and *NME6* correlated genes were grouped further into manually annotated mitochondrial functions (right).
- B Representative immunoblot (left) and proteomic analysis (right) following immunoprecipitation of *NME6*-MycFlag from HeLa cell mitochondrial lysates using a Flag antibody ($n = 4$ independent experiments). FC, fold change.
- C Immunoblot analysis of HeLa WT cells and two polyclonal *RCC1L* KO populations.
- D MtDNA-encoded transcript levels analysed by qRT-PCR in *NME6* KO, *NME6* KO + *NME6*-MycFlag and *NME6* KO H137N-MycFlag cells relative to WT HLE cells (\log_2 ; $n = 4$ independent cultures).

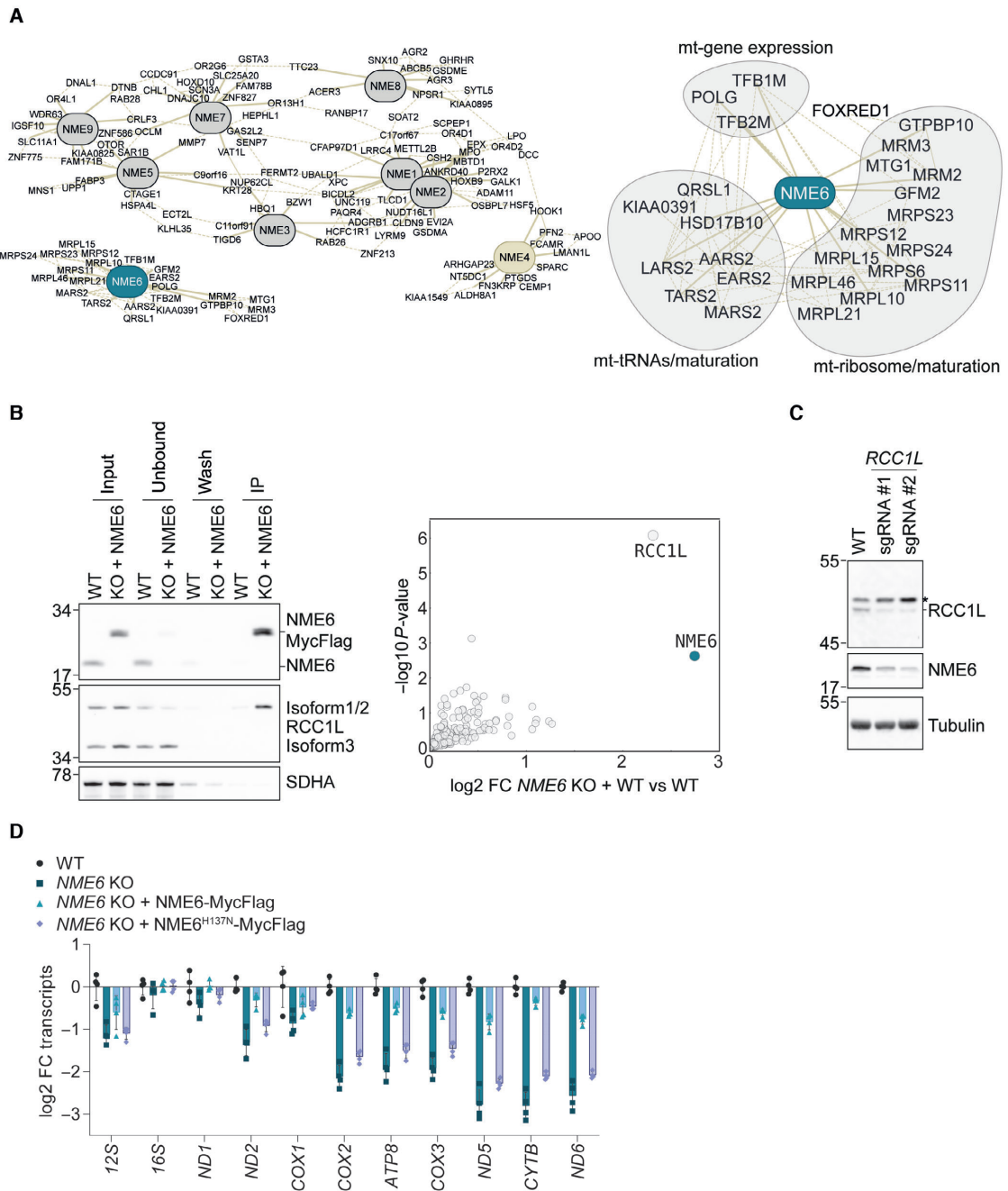


Figure EV4.

Figure EV5. NME6 supplies pyrimidines for mitochondrial transcription and OXPHOS.

- A Scheme of the cytosolic ribonucleotide salvage pathway.
- B *UCK2* and *ND5* transcript levels analysed by qRT-PCR in WT and *NME6* KO HeLa cells transfected with the indicated esiRNA and incubated with or without nucleosides (100 μ M) for 72 h (log2; $n = 3$ independent cultures from Fig 5E).
- C *CYTB*, *NDS*, *APRT* and *HPRT* transcript levels analysed by qRT-PCR in WT and *NME6* KO HeLa cells transfected with the indicated esiRNA and incubated with or without nucleosides (100 μ M) for 72 h (log2; $n = 3$ independent cultures).
- D Representative immunoblot showing the enrichment of mitochondrial proteins in crude mitochondrial fractions taken from the indicated HeLa cell lines during the isolation of mitochondria for LC-MS based metabolomics in Fig 5F. WC, whole cell; CM, crude mitochondria.
- E Mitochondrial transcript levels analysed by qRT-PCR in WT and *NME6* KO HeLa cells incubated with the indicated nucleoside species for 48 h as in Fig 5G (A, adenosine; G, guanosine; C, cytidine; U, uridine; log2 transformed; 100 μ M; $n = 4$ independent cultures).
- F The growth rates of HeLa WT and *NME6* KO cells supplemented with individual nucleosides (A, adenosine; G, guanosine; C, cytidine; U, uridine; log2 transformed; 100 μ M; $n = 6$ independent cultures).
- G Oxygen consumption rates (OCR) and extracellular acidification rates (ECAR) of WT and *NME6* KO HeLa cells incubated with or without individual nucleosides for a minimum of 120 h. Mitochondrial stress test was performed as in Fig 3A ($n = 3$ independent experiments). The basal and maximal respiration rates shown in Fig 5H were determined from OCR measurements before injection of oligomycin and after injection of FCCP respectively (A, adenosine; G, guanosine; C, cytidine; U, uridine; 100 μ M; $n = 3$ independent cultures).

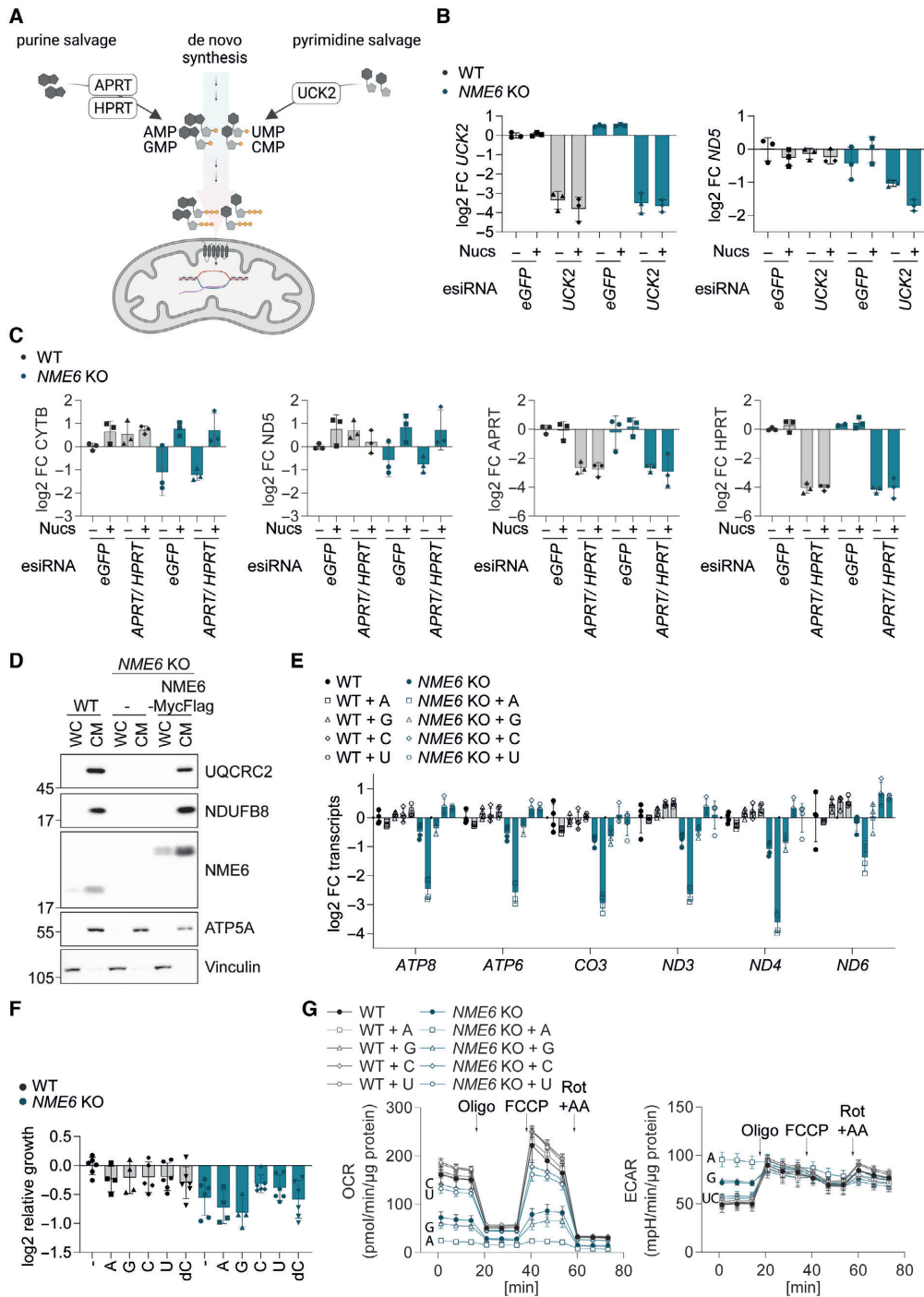


Figure EV5.

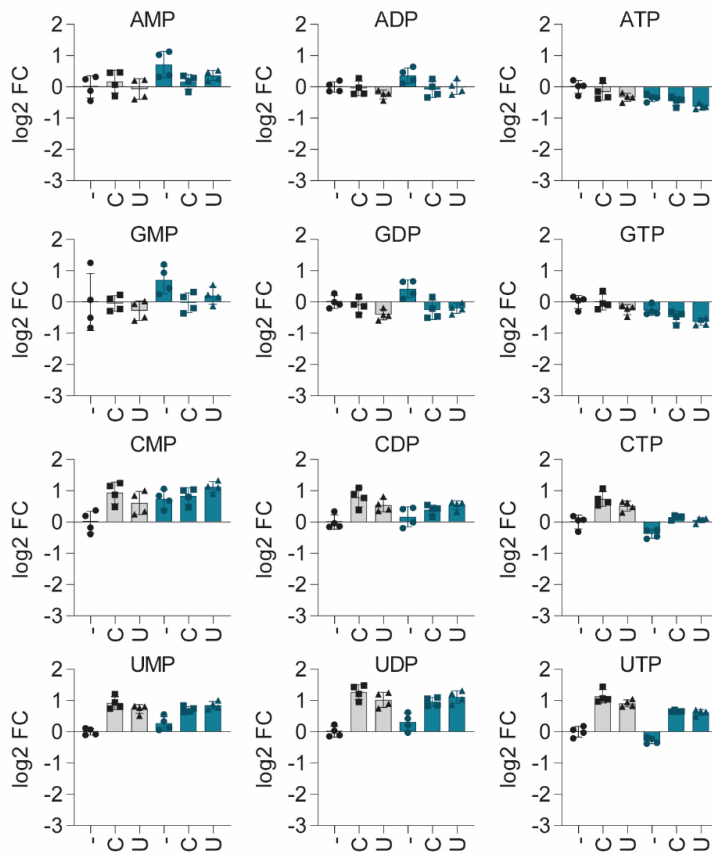
Table of contents

Appendix S1	2
Figure legend Appendix S1	3

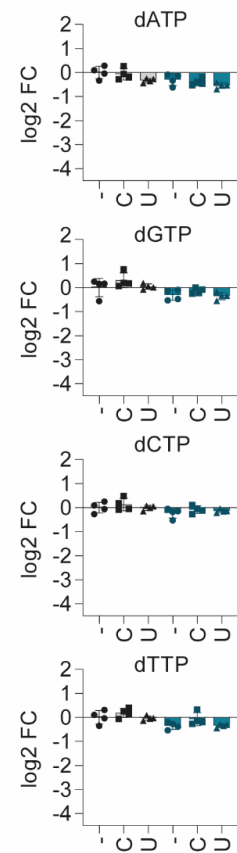
Appendix S1

- WT
- NME6 KO

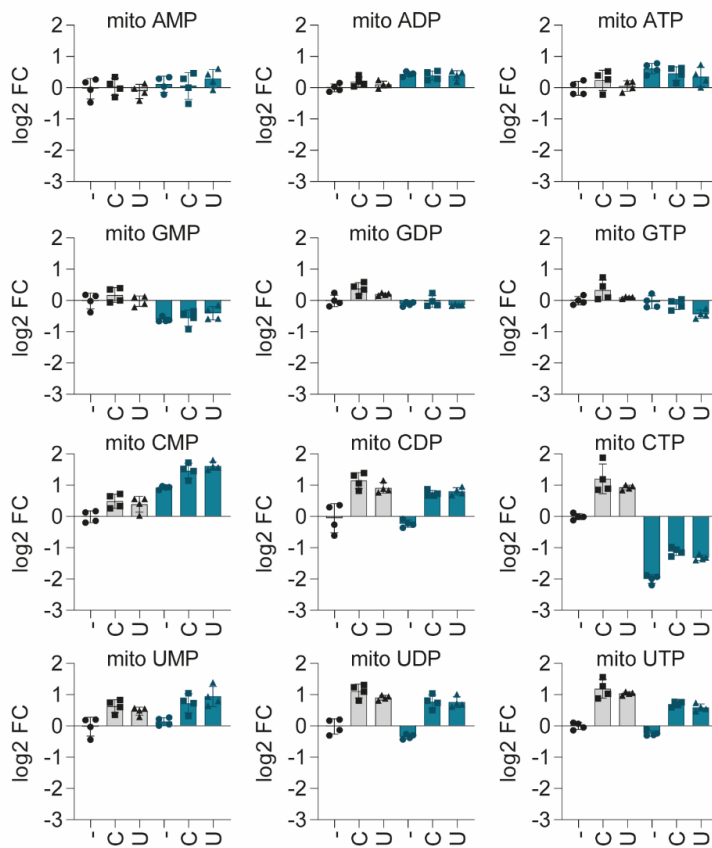
A



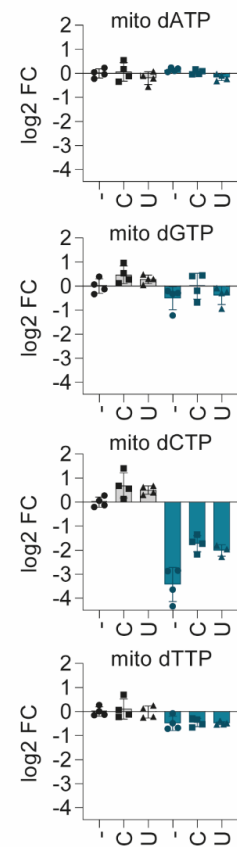
B



C



D



Appendix S1 – Pyrimidine nucleoside supplementation improves nucleotide scarcity in *NME6* KO HeLa cells

(A) Ribonucleotide levels of whole cell extracts of WT and *NME6* KO HeLa cells incubated with the indicated nucleoside species for 120 h as determined by quantitative mass spectrometry.

(B) Deoxyribonucleotide triphosphate levels of whole cell extracts of WT and *NME6* KO HeLa cells incubated with the indicated nucleoside species for 120 h as determined by quantitative mass spectrometry.

(C) Ribonucleotide levels of mitochondria enriched fractions of WT and *NME6* KO HeLa cells incubated with the indicated nucleoside species for 120 h as determined by quantitative mass spectrometry.

(D) Deoxyribonucleotide triphosphate levels of mitochondria enriched fractions of WT and *NME6* KO HeLa cells incubated with the indicated nucleoside species for 120 h as determined by quantitative mass spectrometry.

(log₂ fold change; n = 4 independent cultures)

2.7. Adenosine feeding exacerbates the nucleotide imbalance in *NME6* KO cells

During our nucleoside rescue experiments, we noticed that *NME6* knockout (KO) cells exhibited increased sensitivity towards adenosine supplementation. Mitochondrial transcripts and mitochondrial respiration were further reduced upon adenosine addition, which was not observed in HeLa WT control cells and was in contrast to the other nucleosides, which had either no effect (guanosine) or rescued (uridine, cytidine) the phenotype. Notably, adenosine supplementation did not cause these adverse effects, when given in combination with the other nucleosides. This suggests that adenosine supplementation individually causes a further imbalance in the nucleotide pools of *NME6* KO cells, which cannot be compensated for and therefore exacerbates the phenotype.

To address how and to what extent adenosine supplementation changes the nucleotide levels, we measured the steady state nucleotide levels of whole cell extracts and mitochondria enriched fractions of HeLa WT and *NME6* KO cells with and without adenosine addition.

Adenosine recycling is handled by the cytosolic purine salvage pathway, by which adenosine is converted into its nucleobase adenine by the enzyme purine nucleoside phosphorylase (PNP) and is then salvaged by APRT to produce AMP. Alternatively, adenosine is converted by adenosine deaminase (ADA) into inosine that also undergoes processing by PNP which leads to hypoxanthine. Hypoxanthine is then salvaged by HPRT, producing IMP, which is the precursor for AMP and GMP (**EV 9**)^{188–190,218}. Thus, adenosine supplementation will not only increase adenosine nucleotides but also guanosine nucleotides. Accordingly, we observed elevated levels of IMP, ATP and GTP in HeLa WT cells supplemented with adenosine (**Figure 2.12A**). Elevated levels of IMP were also detected in *NME6* KO cells, however ATP and GTP remained unchanged. Instead, the precursors AMP, ADP, GMP and GDP were significantly accumulated upon loss of *NME6*. Further, adenosine supplementation depleted the pyrimidine nucleotides CTP (>50%) and UTP (50%) in *NME6* KO cells, which was not observed in HeLa WT cells. Deoxyribonucleotide triphosphates, except for dGTP increased in WT cells, whereas all dNTPs were depleted (30-50%) in *NME6* KO cells upon adenosine supplementation (**Figure 2.12B**).

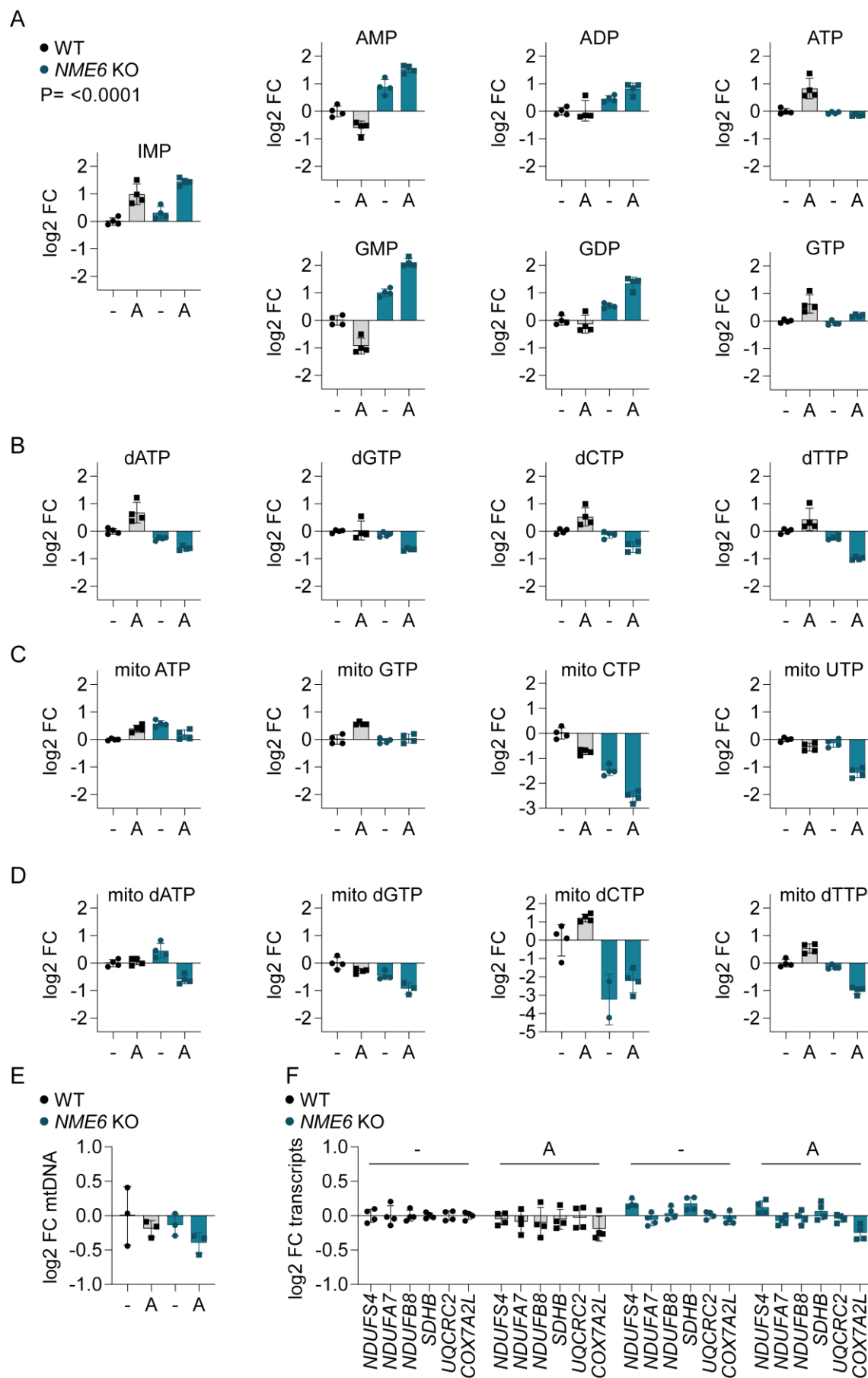


Figure 2.12 Adenosine feeding exacerbates the nucleotide imbalance in *NME6* KO cells

(A) Relative ribonucleotide levels of whole cell extracts from *NME6* KO cells compared to HeLa WT with or without adenosine (100 μ M, 120 h) as determined by quantitative mass spectrometry. P-value for A-D: two-way ANOVA; P-value (genotype) = <0.0001; P-value (metabolite) = <0.0001; P-value (interaction) = <0.0001. (log₂ fold change; n = 4 independent cultures).

(B) Relative deoxyribonucleotide levels of whole cell extracts from *NME6* KO cells compared to HeLa WT with or without adenosine (100 μ M, 120 h) as determined by quantitative mass spectrometry (log₂ fold change; n = 4 independent cultures).

(C) Relative ribonucleotide levels of mitochondria enriched fractions from *NME6* KO cells compared to HeLa WT with or without adenosine (100 μ M, 120 h) as determined by quantitative mass spectrometry (log₂ fold change; n = 4 independent cultures).

(D) Relative deoxyribonucleotide levels of mitochondria enriched fractions from *NME6* KO cells compared to HeLa WT with or without adenosine (100 μ M, 120 h) as determined by quantitative mass spectrometry (log₂ fold change; n = 4 independent cultures).

(E) Relative mtDNA levels of *NME6* KO and HeLa WT cells incubated with or without adenosine (100 μ M, 120 h) as determined by qPCR (log₂ fold change; n = 4 independent cultures).

(F) Relative nuclear-encoded transcript levels of *NME6* KO and HeLa WT cells incubated with or without adenosine (100 μ M, 120 h) as determined by qPCR (log₂ fold change; n = 4 independent cultures).

Adenosine induced changes of nucleotide pools of whole cell extracts were largely mirrored in the mitochondria enriched fraction in both HeLa WT and *NME6* KO cells.

Adenosine supplementation led to increased mitochondrial ATP and GTP levels in WT cells but to no accumulation in *NME6* KO cells. Already lower CTP levels decreased further in *NME6* KO cells (80%) and mitochondrial UTP pools were reduced by more than 50% (**Figure 2.12C**). Additionally, dATP, dGTP and dTTP levels decreased in *NME6* KO cells upon adenosine treatment (**Figure 2.12D**). We tested whether lower dNTP concentrations in mitochondria of *NME6* KO cells caused mtDNA depletion that could contribute to reduced mitochondrial transcript levels. QPCR-analysis revealed no significant changes in steady state mtDNA levels in WT and *NME6* KO cells upon adenosine addition, supporting the notion that the further depletion of mitochondrial transcripts is the underlying cause for the exacerbation of the OCR- and ECAR-phenotype observed in *NME6* KO cells (**Figure 2.12E**).

We also excluded the possibility that cytosolic transcription of OXPHOS subunits is impaired by adenosine addition. Transcript levels of several complex I as well as complex II, III and IV subunits remained unchanged in WT and *NME6* KO cells upon adenosine supplementation (**Figure 2.12F**).

Collectively these results show that adenosine supplementation exacerbates the preexisting nucleotide imbalance in *NME6* KO cells. We ascribe the further reduction in respiration to the exacerbated mitochondrial pyrimidine depletion that prevents the successful transcription of mitochondrial encoded OXPHOS

subunits. In contrast to pyrimidine nucleoside addition that increases UTP and CTP levels, adenosine treatment does not lead to accumulation of the respective purine NTPs in *NME6* KO cells. Accumulation of the mono- and diphosphate purine nucleosides suggests insufficient NDPK activity in *NME6* KO cells. Since this accumulation was only observed in whole cell extracts but not in the mitochondrial enriched fraction of *NME6* KO cells, the observed changes likely originate from the cytosolic pools. Whether the additional changes in pyrimidine (d)NTPs are a secondary effect due to the incomplete adenosine salvage cannot be concluded from these results. Mostly overlapping changes measured in whole cell extracts and mitochondria enriched fractions is supporting evidence for the intimate communication of the two nucleotide pools. However, differences observed in only one fraction, such as the accumulation of purine mono- and diphosphates also indicates that the two pools are not coupled perfectly.

Collectively our data highlight the difference between nucleotide depletion and nucleotide imbalance. Specifically, nucleotide imbalance here refers to the depletion of the pyrimidine ribonucleotide CTP, whereas nucleotide depletion describes a reduction of all non-adenine nucleotides. We conclude that mitochondrial transcription responds poorly to nucleotide imbalance caused by loss of *NME6*, whereas a general nucleotide depletion caused by loss of *SLC25A33* and *SLC25A36* is tolerated. Shifting the balance in either direction can either aggravate or alleviate the mitochondrial transcription defect.

3. Discussion

Mitochondrial gene expression is required to maintain mitochondrial function. The successful expression of mitochondrial genes critically relies on the sufficient supply of nucleotide building blocks. Here we have characterized different aspects of mitochondrial nucleotide metabolism and its impact on mitochondrial gene expression.

Surprisingly we found that inhibited mitochondrial pyrimidine uptake, by combined depletion of SLC25A33 and SLC25A36, does not majorly affect mitochondrial gene expression. We provide evidence that the mitochondrial genome is maintained by the synergistic effects of mitochondrial nucleotide uptake and salvage.

We further identified mitochondrial ribonucleotide metabolism as a so far understudied metabolic pathway, which is essential for functional mitochondrial gene expression. Specifically, we discovered that the mitochondrial NDPK NME6 sits at the convergence point of ribo- and deoxyribonucleotide metabolism and mitochondrial gene expression.

Our data suggests that mitochondrial transcription is particularly sensitive towards ribonucleotide imbalance but tolerates a general reduction of ribonucleotides. Nucleoside supplementation could either offset the imbalance or further exacerbate it which had alleviating or aggravating effects on mitochondrial gene expression, respectively.

In summary, our findings advance the current understanding of mitochondrial nucleotide metabolism and its effects on mitochondrial gene expression. We particularly emphasize the essential role of ribonucleotide metabolism on mitochondrial gene expression and the important differences between nucleotide imbalance and nucleotide depletion.

3.1. The role of SLC25A33 and SLC25A36 in nucleotide metabolism and mitochondrial gene expression

Mitochondria, which cannot *de novo* synthesize nucleotides, possess two different ways to maintain adequate nucleotide levels for genome maintenance and gene expression. The uptake of nucleotides from the cytosol is a major supply route for mitochondria, which is complemented by the uptake of nucleosides that are recycled within the mitochondrial matrix¹⁰⁴. The contribution of each supply route might vary depending on the nucleotide availability in the cytosol, which is tightly coupled to the cell cycle^{139,146,147}.

In this study we severed the NTP-exchange route between mitochondria and the cytosol by removing the two known pyrimidine nucleotide carriers SLC25A33 and SLC25A36. This is a novel approach as previous studies have characterized the individual loss of either carrier^{151,153}. Due to the overlapping substrate affinities of SLC25A33 and SLC25A36 it is likely that loss of only one carrier is insufficient to fully block mitochondrial NTP uptake. Indeed, we observed a reduction of all non-adenine nucleotides in *SLC25A33/SLC25A36* DKO HeLa cells, a nucleotide profile that can be explained by the combined loss of both carriers but differs from the profiles reported for the single knockout of either carrier^{151,153,206}. SLC25A33 and SLC25A36 are also referred to as PNCs or PNTs (pyrimidine nucleotide carriers/transporters) as they exhibit increased transport affinity towards pyrimidine nucleotides¹⁵¹. Notably our data showed an equally strong depletion of mitochondrial guanosine nucleotides in *SLC25A33/SLC25A36* DKO HeLa cells, indicating that despite the reported reduced *in vitro* transport activity, these carriers regulate guanosine nucleotide levels as well¹⁵¹. The observed depletion could be a result of the combined loss of both carriers, but could also be caused by regulatory factors that determine nucleotide affinities which are absent in *in vitro* systems^{159,219}. Additionally, physiological transport activities might differ from reported *in vitro* results if the nucleotide carriers are exposed to a complex nucleotide profile as present in cultured cells.

Despite the reduction of mitochondrial ribonucleoside triphosphates by 50-75% in *SLC25A33/SLC25A36* DKO HeLa cells, mitochondria were still able to match or surpass transcript levels observed in mitochondria of WT cells. This suggests that the mitochondrial rNTP pool size exceeds the nucleotide demand of mitochondrial transcription in proliferating HeLa cells in basal conditions. High

rNTP levels could serve as a buffer to be consumed in order to maintain transcript levels if cytosolic rNTP supply is limited. High mitochondrial rNTP levels might also support a fast metabolic adaptation to conditions that demand increased OXPHOS capacity. It would be intriguing to test whether *SLC25A33/SLC25A36* DKO HeLa cells can maintain mitochondrial transcript levels if cultured in low glucose or galactose containing medium. Absolute quantification of mitochondrial rNTP levels as well as a precise determination of the mitochondrial transcriptome size would enable the calculation of rNTP supply and demand and should be addressed in future experiments to support or challenge the previously made statements.

Conversely to mtRNA levels, mtDNA levels were decreased in *SLC25A33/SLC25A36* DKO HeLa cells and are in accordance with reduced dNTP levels in these cells. The reduction of mtDNA copy number was moderate however, despite a severe depletion of most dNTPs such as dCTP which was reduced by 90% compared to WT levels. Cytidine nucleotides can be transported by both carriers which could have additive effects and might explain the more severe depletion compared to other reported values obtained from single knockout cells^{151,153}. In light of the strong dCTP reduction also observed in *NME6* KO cells, it is also conceivable that the dCTP pool is intrinsically more sensitive to perturbation of the mitochondrial nucleotide homeostasis. It was previously reported that the mitochondrial dCTP levels are lower than the other dNTPs, which could serve as an explanation to why the dCTP pool drops so strongly, however others have not reported such discrepancy in mitochondrial dNTP pool sizes^{100,220}. Alternatively, dCTP could be further depleted by other nucleotide consuming processes. Cytidine nucleotides also play an important role in lipid metabolism²²¹. The synthesis of CDP-diacylglycerol (DAG), a precursor for several lipids such as cardiolipin, could be an additional strain on mitochondrial CTP-pools and further exacerbate a preexisting nucleotide scarcity²²¹. The observations that dCDP-DAG can be used for the synthesis of phosphatidylserine in yeast, and that human- and murine immune cells actively salvage dCDP-DAG from dC, make it intriguing to speculate that dCTP might act as a substitute in mitochondrial lipid metabolism if CTP levels are depleted^{222,223}.

The ratio between the amount of freely available mitochondrial dNTPs and the nucleotides required for mtDNA replication indicate that the free dNTPs will not

suffice for mtDNA replication if reduced by 90%. Yet, the entire mtDNA content is not replicated in one event as the nuclear genome, thus the nucleotide demand will likely not peak in a short period of time but rather be constant. In accordance, it was recently reported that HeLa cells contain distinct nucleoid populations that are either relaxed and replication active or compacted by increased TFAM-association and replication inactive²⁵. The latter was calculated to represent at least 50% of the whole nucleotide population²⁵. This further suggests that the mitochondrial nucleotide demand is spatially different and might be regulated accordingly. At sites of active nucleoid replication, the flux through the mitochondrial salvage pathway could be increased to boost local dNTP concentrations. Immediate dNTP incorporation into mtDNA might also bypass accumulation of these dNTPs in the free pools and thus prevent their detection by MS-based steady state approaches. The potential formation of a mitochondrial nucleotide metabolon at sites of mitochondrial replication could be investigated in future experiments to test this hypothesis.

Taking these considerations into account it is conceivable that low dNTP levels do not directly manifest in equally low mtDNA levels as observed in *SLC25A33/SLC25A36* DKO HeLa cells.

Loss of *SLC25A33* and *SLC25A36* also led to a reduction of total cellular nucleotide levels, which was not as pronounced as the reduction within mitochondria but nonetheless significant and ranged from 25-50% compared to HeLa WT cells. This reduction cannot be explained solely by the contribution of the diminished mitochondrial nucleotide pools that were part of the whole cell fractions. Given the previously reported volumes of the mitochondrial network of HeLa cells and their cytosol (ratio ~1:10), mitochondrial nucleotide concentrations would need to be five-fold higher compared to cytosolic concentrations to explain the reduction observed in the whole cell fractions¹⁰⁰. This is not in line with previous findings that calculated 50% lower nucleotide (dNTP) concentrations for mitochondria¹⁰⁰. Therefore, the loss of *SLC25A33* and *SLC25A36* likely affect cytosolic nucleotide homeostasis besides the distribution of nucleotides. The proteomic profiling of *SLC25A33/SLC25A36* DKO cells did not reveal differential regulation of cytosolic nucleotide metabolizing enzymes that could indicate reduced *de novo* synthesis rates or increased nucleotide catabolism. Reduced nucleotide demand due to the inhibited nucleotide sequestering into mitochondria

might be sensed in the cytosol, which could lead to a decelerated pathway flux without proteomic adaptations. The molecular mechanism how reduced mitochondrial nucleotide uptake could affect cytosolic nucleotide homeostasis remains to be explored in future studies.

Despite the inhibition of mitochondrial nucleotide uptake, mitochondrial nucleotide pools were not completely abolished but were still present at concentrations that allowed for largely functional gene expression. This suggests alternative supply route that provide dNTPs and rNTPs for mitochondrial genome replication and transcription.

We characterized the well-studied mitochondrial deoxyribonucleotide salvage pathway enzyme DGUOK and its impact on mitochondrial gene expression in the presence or absence of SLC25A33 and SLC25A36^{163,214}. Loss of DGUOK alone did not reduce mtDNA copy number, mitochondrial transcripts or OXPHOS capacity, confirming that the salvage of dNTPs is mostly dispensable under proliferating growth conditions when cytosolic *de novo* nucleotide synthesis is high²²⁴. The contribution of DGUOK to mitochondrial dNTP levels was revealed in *SLC25A33/SLC25A36/DGUOK* TKO cells that exhibited mtDNA depletion of 50% which was stronger than the depletion observed in *SLC25A33/SLC25A36* DKO cells. Thus DGUOK-mediated deoxy-purine recycling becomes increasingly important for mtDNA synthesis if nucleotide supply from the cytosol is inhibited. Yet, the further mtDNA depletion of 30% compared to the *SLC25A33/SLC25A36* DKO cells was likely not sufficiently strong to be detected by our arrayed CRISPR-screen approach. Notably, mitochondrial transcript levels of *SLC25A33/SLC25A36/DGUOK* TKO cells were still moderately elevated in accordance with steady state OXPHOS-subunit protein levels, confirming that cells can maintain their mitochondrial gene expression even in the absence of 50% of their mtDNA content²¹⁶. Stable transcript levels in *SLC25A33/SLC25A36/DGUOK* TKO cells suggest sufficient rNTP supply, even though we did not measure mitochondrial nucleotide levels in these cells directly. Future studies should determine more precisely the thresholds of nucleotide depletion that still suffice to maintain mitochondrial gene expression.

In summary, we confirm the important role of SLC25A33 and SLC25A36 in mitochondrial nucleotide metabolism, we define for the first time the mitochondrial nucleotide profile upon the loss of both carriers and observe a strong depletion

of all non-adenine ribo- and deoxyribonucleotides, that lead to a moderate reduction of mtDNA but not to a reduction of mitochondrial transcripts. SLC25A33 and SLC25A36 synergize with DGUOK to sustain mtDNA levels.

3.2. The role of NME6 in nucleotide metabolism and mitochondrial gene expression

In this study we ascribe a novel function to the mitochondrial NDPK NME6 in mitochondrial gene expression. We show that NME6 supplies ribo- and deoxyribonucleotides required for mitochondrial replication and transcription. Loss of NME6 leads to a significant reduction of mitochondrial cytidine nucleoside triphosphates that limit mitochondrial transcription and limit mitochondrial replication if cytosolic nucleotide uptake is impaired. We propose a model in which reduced mitochondrial CTP becomes rate-limiting for transcription, reduced transcript levels lead to a primary loss of mitochondrial encoded OXPHOS-subunits that is followed by the degradation of unassembled nuclear encoded subunits. We found that supplementation with pyrimidines but not with purines can fully restore mitochondrial transcript levels and OXPHOS deficiency observed in *NME6* KO cells.

Our data reinforces the notion that NME6 is a catalytically active mitochondrial NDPK and challenges a recent report that questioned this conclusion^{177,225}. The discrepancy between the two studies might be due to differences in the experimental setups that assayed the *in vitro* kinase activity of NME6. Kinase activity was observed when NME6 was provided with CDP as a substrate but not with dTDP, which is in accordance with our finding that shows a specific depletion of mitochondrial CTP but not dTTP^{177,225}. However, our results imply that NME6 possesses nucleotide substrate specificity which would be atypical for a NDPK¹⁸⁴. Our data would also fit to a model in which NME6 phosphorylates all nucleotide species but alternative supply routes for non-cytidine nucleotides exist that compensate for the reduced synthesis rates upon loss of NME6. ATP is regenerated mainly through the mitochondrial ETC-activity, it is the most abundant ribonucleotide by at least an order of magnitude and likely serves as the phosphate donor in most NDPK reactions, rather than as a phosphate receiver^{101,184}. Hence, it is unlikely that the mitochondrial ATP would be reduced upon the loss of NME6. Similarly, GTP can be synthesized by different means

and is continuously produced by the TCA cycle when succinyl-CoA is converted into succinate by succinyl-CoA synthetase which could dampen the effect of NME6 depletion on the mitochondrial GTP pool^{185,226}. Thus, NME6 substrate specificity, should unambiguously be verified by *in vitro* kinase activity assays performed with different nucleotide substrates.

Loss of NME6 also led to a reduction of mitochondrial dCTP by 90%, reminiscent of the dCTP levels observed in *SLC25A33/SLC25A36* DKO cells. In contrast to the reduced mtDNA levels of *SLC25A33/SLC25A36* DKO cells, loss of NME6 does not affect mtDNA copy number despite the striking reduction of dCTP. It remains speculative why the mitochondrial dCTP pool responds so dramatically to impaired mitochondrial nucleotide homeostasis and the putative explanations outlined in the previous chapter must be addressed in future experiments. Currently, it is also unclear, if the reduced dCTP levels damage the mitochondrial genome in ways that do not result in copy number reduction. Imbalanced nucleotide pools in mitochondria and the cytosol are considered mutagenic and might lead to increased mutation rates of the mitochondrial genome, which was not accessed experimentally in this study. Imbalances between ribo- and deoxyribonucleotides can lead to increased ribonucleotide incorporation into mtDNA, which reduces mtDNA stability²²⁷. Further, asymmetric mitochondrial nucleotide pools have been reported to cause mtDNA deletions, which have not yet been ruled out to be present in *NME6* KO- or *SLC25A33/SLC25A36* DKO cells¹⁷.

Cytosolic dNTP pools exceed mitochondrial pools by a factor of ~20 in proliferating HeLa cells and are a main source to replenish mitochondrial dNTPs^{100,104}. Cytosolic dCTP levels were completely unaffected in *NME6* KO cells, thus cytosolic dCTP is present in quantities that could fully restore the reduced mitochondrial dCTP levels with would deplete the cytosolic dCTP pool by less than 5%. This raises the question why *NME6* KO cells do not replenish mitochondrial dCTP levels at the cost of a minor reduction of cytosolic dCTP levels. Possible explanations are: 1. HeLa cells do not require higher mitochondrial dCTP levels; 2. low mitochondrial dCTP levels are not recognized by the cell; or 3. *NME6* KO cells are not able to replenish mitochondrial dCTP levels.

Since *NME6* KO cells contain WT-amounts of mtDNA without any apparent deficiencies, the first explanation is plausible but leads back to the question why the mitochondrial dCTP content is inflated in the first place.

Alternatively, mitochondria might not contain a “sensing mechanism” for nucleotide ratios and thus cannot relay a signal back to the cytosol to increase nucleotide sequestering towards mitochondria. Cytosolic dNTP ratios are controlled by RNR which contains an intricate allosteric regulatory module that determines RNR-nucleotide affinities and thereby controls dNTP ratios^{137,140}. RNR activity has been reported in mitochondria but other studies challenged this finding^{104,228–230}. Thus, mitochondria might lack the ability to control their dNTP ratios intrinsically and could therefore be more prone to nucleotide imbalances than the cytosol.

The third possibility is that *NME6* KO cells are incapable of diverting more dCTP into mitochondria due to their additional CTP depletion. The mitochondrial nucleotide carriers SLC25A33 and SLC25A36 are reported to mainly act as antiporters that import one nucleotide for the export of another nucleotide¹⁵¹. Which nucleotides are exchanged for which nucleotides has not been addressed and remains an open question^{148,219}. In case homo-exchange is favored by SLC25A33 and SLC25A36, reduced CTP levels in mitochondria of *NME6* KO cells might prevent the import of dCTP, because the corresponding exchange nucleotide for dCTP is not present in sufficient concentrations. Our pyrimidine supplementation experiments however do not support the later explanation, since uridine and cytidine addition led to elevated mitochondrial CTP and dCTP levels, suggesting functional nucleotide exchange in these cells. Cytosolic pyrimidines might be sequestered to mitochondria if they become overabundant after nucleoside supplementation. Uridine supplementation led to a partial rescue of mitochondrial CTP levels but also caused accumulation of cytosolic and mitochondrial UTP in *NME6* KO cells (data not shown). This suggests that cytosolic pyrimidines are imported into mitochondria irrespective of the mitochondrial pyrimidine levels and that the transport rates are governed by the cytosolic availabilities rather than by the mitochondrial demand.

Interestingly, *NME6*-dependent rNTP salvage is still sufficient to sustain mitochondrial gene expression if pyrimidine nucleotide uptake is impaired. This suggests an alternative source to SLC25A33 and SLC25A36 which must provide

NME6 with rNDP substrates. Mitochondrial rNDPs could be supplied by a yet unknown solute carrier with rNMP- or rNDP-transport capacity. Alternatively, a *bona fide* ribonucleotide salvage pathway could operate in mitochondria which would, together with the deoxyribonucleotide salvage pathway, equip mitochondria with complete nucleotide salvage capacity. Mitochondrial deoxyribonucleotide salvage enzymes AK4, CMPK2 and potentially GMPK might also participate in the salvage of rNTPs due to their reported dual affinities towards ribo- and deoxyribonucleoside monophosphates^{168,171,174}. Thus, the “missing-link” for a mitochondrial ribonucleotide salvage pathway is the primary phosphorylation reaction that is carried out by nucleoside kinases. Future studies should aim to verify the existence of an additional nucleotide carrier or mitochondrial ribonucleoside kinases.

In conclusion, we identify NME6 as a novel regulator of mitochondrial nucleotide metabolism that is required for functional mitochondrial gene expression. Loss of NME6 specifically depletes mitochondrial CTP and dCTP, and thus affect ribo- as well as deoxyribonucleotide homeostasis. This is the first study that describes the important role of mitochondrial ribonucleotide salvage for mitochondrial gene expression.

3.3. Nucleotide depletion vs nucleotide imbalance

Interestingly our data indicates, that the depletion of mitochondrial CTP, observed in *NME6* KO cells, has more adverse effects on mitochondrial transcription than the depletion of all non-adenine ribonucleotides, observed in *SLC25A33/SLC25A36* DKO cells. This relates back to the previously stated open question whether mitochondria are incapable of sensing their nucleotide content. Reduction of CTP might not be recognized by the transcription machinery which would continue to initiate transcription. CTP scarcity could then lead to POLRMT stalling and premature transcription termination, which could explain the more severe depletion of promotor-distant transcripts observed in *NME6* KO cells. It would be intriguing to test by northern blot analysis, whether *NME6* KO cells accumulate mitochondrial transcription intermediates which would support a premature transcription termination hypothesis.

Conversely to *NME6* KO cells, the depletion of all non-adenine nucleotides in *SLC25A33/SLC25A36* DKO cells did not cause mitochondrial transcript reduction

despite the equally strong depletion of CTP. Thus, mitochondrial transcription potentially requires balanced rNTP ratios rather than high rNTP concentrations. This hypothesis should be addressed by individual nucleoside supplementation in *SLC25A33/SLC25A36* DKO cells.

Strikingly, adenosine supplementation in *NME6* KO cells led to a further reduction of mitochondrial CTP and also depleted UTP whereas purine levels remained unchanged. This increased nucleotide imbalance was concomitantly observed with exacerbated mitochondrial transcript levels and OXPHOS activity. It remains currently unclear why loss of *NME6* leads to increased sensitivity towards adenosine treatment. Notably, purine mono- and diphosphates accumulated in whole cell fractions of *NME6* KO cells, suggesting defective NDPK activity in these cells. Even though it remains elusive for now why adenosine supplementation did not lead to increased ATP and GTP levels as observed for WT cells, the elevated AMP and ADP levels might lead to secondary knock-on effects that could affect nucleotide synthesis. An increased AMP/ATP ratio leads to the activation of AMP-activated protein kinase (AMPK) which is a known regulator of nucleotide metabolism^{231,232}. Interestingly, AMPK was shown to directly phosphorylate and thereby inhibit *NME1* *in vitro* and *in vivo*, which limits energy expensive nucleotide synthesis under ATP-scarce conditions²³³. The regulatory serine residue is conserved from yeast to humans and present in all human kinase-active NDPKs. A potential activation of AMPK due to the accumulated AMP levels in adenosine supplemented *NME6* KO cells might further inactivate cytosolic NDPKs and thus explain the reduction of dNTPs and pyrimidine rNTPs.

It should be noted that adenosine addition had no adverse effects on mitochondrial gene expression of *NME6* KO cells when given in combination with other nucleosides. This supports the notion that nucleotide balance is a key requirement for cellular homeostasis. In accordance with this, the detrimental effects of nucleotide imbalance were recently exemplified in a study that showed decoupled, aberrant cell growth and increased replication stress signaling upon excessive nucleoside supplementation²³⁴. Perturbances in the nucleotide ratios were not adequately recognized by the nutrient sensing hub mTOR and led to increased cell growth but inhibited cell proliferation. Cell cycle arrest could be overcome by additional purine or pyrimidine nucleoside supplementation that led

to a rebalancing of the cellular nucleotide pools²³⁴. Nucleoside supplementation in form of pyrimidines was also sufficient to blunt an mtDNA-dependent innate immune response upon the loss of the mitochondrial protease YME1L¹⁰⁶. Thus, nucleotide imbalance is an ambiguous term which can be used to refer to differences between purines and pyrimidines, between ribo- and deoxyribonucleotides or between cytosolic and mitochondrial nucleotides. Different imbalances will lead to distinct phenotypes such as aberrant growth, induction of an innate immune response, increased DNA damage or impaired mitochondrial gene expression^{105,106,205,227,234}. Defining what kind of imbalance is observed, will help to delineate how nucleotide metabolism affects cellular function and should help to devise strategies to rebalance nucleotide homeostasis.

Here we provide first evidence that nucleotide imbalance in form of mitochondrial CTP depletion causes deficient mitochondrial gene expression which can be rescued by uridine or cytidine supplementation but not by adenosine or dNTP supplementation.

3.4. NME6 beyond nucleotide metabolism

Our metabolomic and nucleoside supplementation experiments are strong indicators that deficient mitochondrial CTP levels are the underlying cause for reduced mitochondrial transcript levels in *NME6* KO cells.

Interestingly, our MS-based proteomic profiling of *NME6* KO cells revealed a second mechanism by which NME6 could potentially affect mitochondrial gene expression.

Loss of NME6 led to the reduction of the MRG-proteins ALKBH1, ERAL1, DHX30 and RCC1L, which are involved in tRNA-maturation and the assembly of the small and large ribosomal subunit, respectively^{64,70,71,235}. Moreover, RCC1L (also known as WBSCR16) is the only known interaction partner, identified by us and others. RCC1L is required for mitochondrial ribosome maturation and is a constituent of proteins complex termed pseudouridylation module, which was shown to modify the 16S rRNA^{72,73}. RCC1L and NME6 mutually affect their protein stability and might act as a functional unit in which NME6 increases GTP availability in proximity to RCC1L, which interacts with the GTPases that are required for ribosome assembly²³⁵. If GTP delivery to RCC1L was rate-limiting

for mitochondrial gene expression in *NME6* KO cells, guanosine supplementation could potentially bypass the loss of NME6. However, guanosine addition did not affect mitochondrial transcript levels and downstream respiration rates of *NME6* KO cells. Additionally, mitochondrial ribosomal proteins were not significantly reduced upon loss of NME6. Uridine and cytidine supplementation fully restored OXPHOS function, which further suggest functional mitochondrial ribosome biogenesis and protein translation in *NME6* KO cells.

Thus, the role of NME6-RCC1L interaction and its putative function in ribosome maturation and pseudouridylation awaits further inquiry

3.5. The physiologic role of NME6

NME6 was recently identified in a number of unbiased CRISPR- screens as an essential gene for intra-organelle buffering, cell growth and acidic pH adaptation ^{206–208}. The molecular characterization of NME6, performed in this study, provides for the first-time potential explanations to why NME6 is required in these processes.

A recent CRISPR-screen that employed small-molecule mitochondrial inhibitors identified NME6 as the top hit to be synthetic sick/lethal to complex V (CV) inhibitor Oligomycin A but not to other ETC inhibitors ²³⁶. Increased sensitivity towards CV inhibition upon loss of NME6 can be explained by the here demonstrated preexisting OXPHOS dysfunction of *NME6* KO cells. CV couples the predominantly matrix-directed proton flow to ATP regeneration but can also hydrolyze ATP and revert proton flow back into the IMS, which can stabilize the mitochondrial membrane potential. Oligomycin A blocks both CV-functions and thus does not reveal which of the two CV-functions *NME6* KO cells rely on. The recently described CV-mediated ATP-hydrolysis inhibitor Epicatechin could be used to address whether *NME6* KO cells depend on ATP synthesis or proton pumping by CV ²³⁹.

NME6 was also recently reported to be essential in cells cultured in physiological growth medium ²⁴⁰. The human plasma like medium (HPLM) used in that study was specifically designed to mimic the nutrient composition and concentrations of the human plasma, to improve the study of metabolic phenotypes in cell culture ²⁴¹. Here we provide evidence that the low glucose concentration of HPLM is a contributing factor to the reduced growth rates and eventual cell death of *NME6*

KO cells. The ECAR observed in *NME6* KO cells, which indicates increased glycolysis likely increases the dependency on high glucose concentrations to meet the cellular ATP demand that cannot be fully satisfied by the impaired OXPHOS function of *NME6* KO cells. This finding is in accordance with reduced growth rates of *NME6* KO cells in galactose containing medium that we reported here. High uric acid concentrations of HPLM, which were shown to limit pyrimidine *de novo* synthesis should further reduce pyrimidine levels in *NME6* KO cells and thus exacerbate the OXPHOS dysfunction, fueling the reliance on glycolysis²⁴¹.

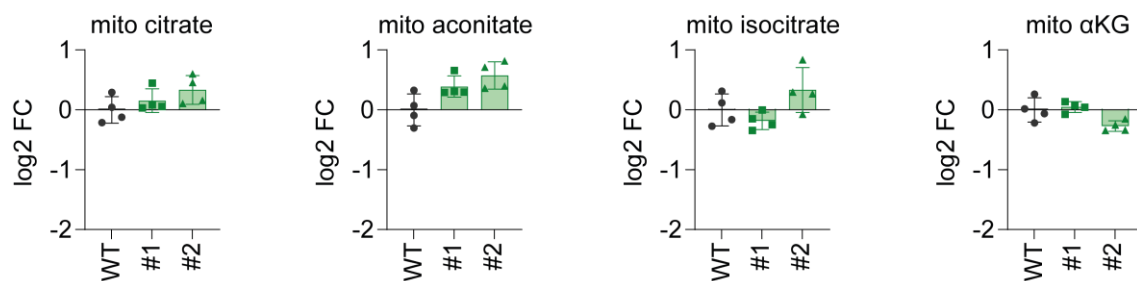
The increased dependency on glycolysis is also the probable explanation to why *NME6* was found as an essential gene in acidic growth conditions²³⁸. Low pH and the accumulation of acidic metabolites has been reported to limit glycolysis and induce a metabolic shift towards increased glutaminolysis and fatty acid oxidation^{242,243}. Due to the limited OXPHOS capacity of *NME6* KO cells, the metabolic shift away from glycolysis dependent ATP production likely cannot occur to the extent that is required at low pH conditions and thus makes *NME6* essential in acidic growth conditions.

Our work provides new insights which help to understand previous results regarding the important role of *NME6* in different cellular processes. We identify *NME6* as a novel regulator of nucleotide metabolism and mitochondrial gene expression, two processes that are intimately linked to cellular and organismal health. The poor prognosis of hepatocellular carcinoma patients with high *NME6* expression, further underscores the importance of *NME6* in the context of disease. Dysregulated nucleotide metabolism and altered mitochondrial gene expression have been associated with cancer development and are putative therapeutic targets to prevent disease progression^{244,245}. Our data places *NME6* at the intersection of nucleotide metabolism and mitochondrial gene expression and opens up new avenues for a better understanding of mitochondrial function in health and disease.

4. Appendix

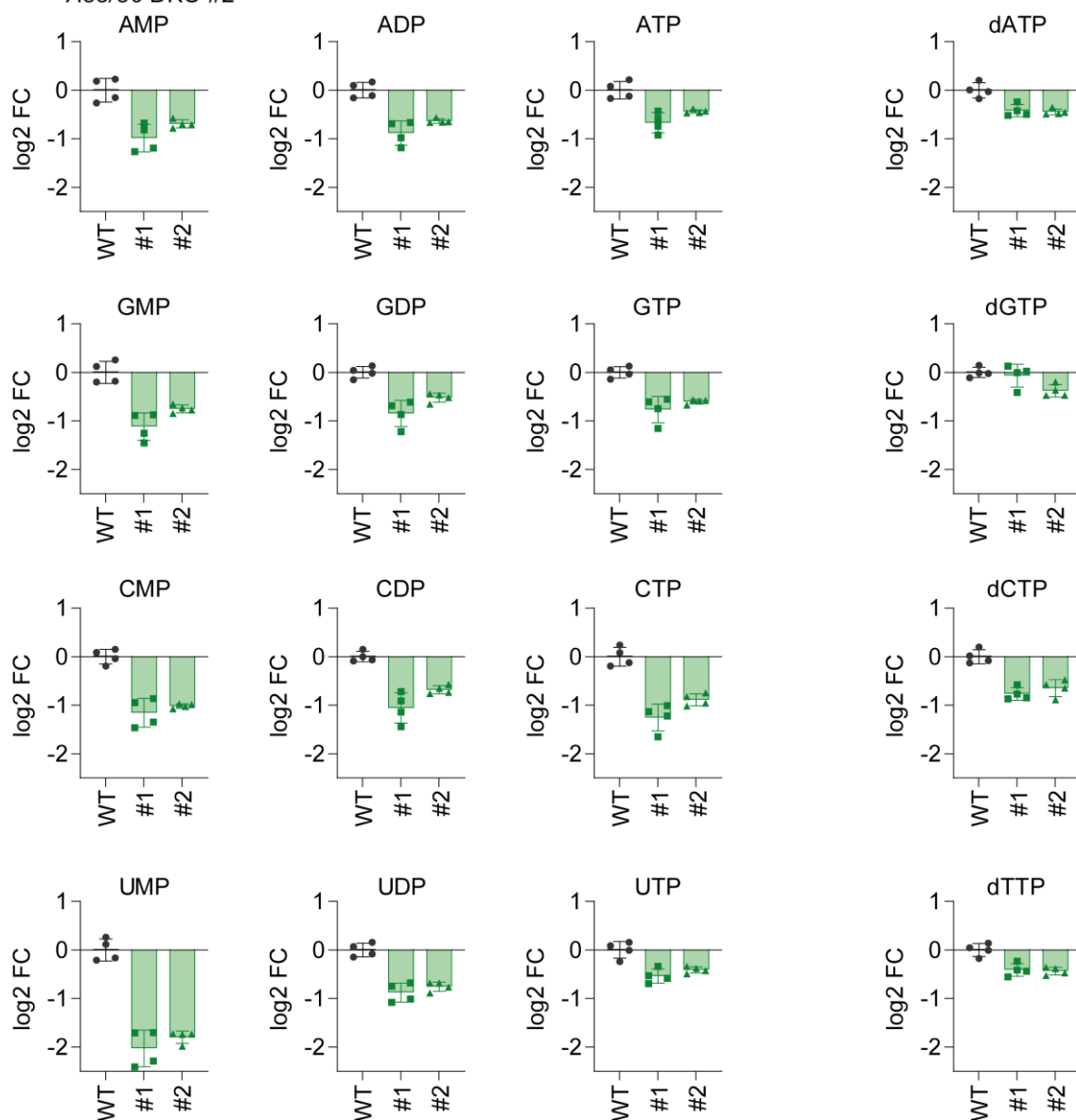
A

- WT
- A33/36 DKO #1
- ▲ A33/36 DKO #2



B

- WT
- A33/36 DKO #1
- ▲ A33/36 DKO #2



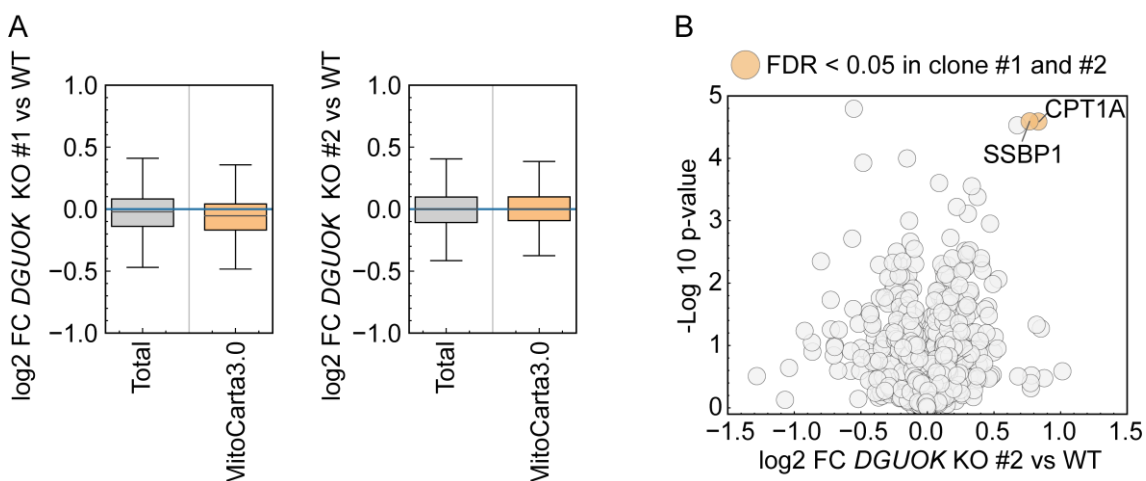
C

EV 7 Loss of SLC25A33 and SLC25A36 causes mitochondrial nucleotide depletion

(A) Relative levels of TCA-cycle intermediates of mitochondria enriched fractions of HeLa WT and *SLC25A33/SLC25A36* DKO cells (clone #1 and #2) as determined by quantitative mass-spectrometry (log₂ fold change; n = 4 independent cultures).

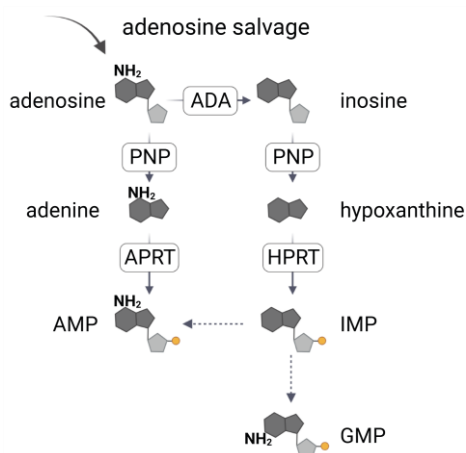
(B) Relative ribonucleotide levels of whole cell extracts of HeLa WT and *SLC25A33/SLC25A36* DKO cells (clone #1 and #2) as determined by quantitative mass-spectrometry (log₂ fold change; n = 4 independent cultures).

(C) Relative deoxyribonucleotide levels of whole cell extracts of HeLa WT and *SLC25A33/SLC25A36* DKO cells (clone #1 and #2) as determined by quantitative mass-spectrometry (log₂ fold change; n = 4 independent cultures).

**EV 8 Loss of DGUOK is not rate-limiting for mitochondrial gene expression**

(A) Box plot analysis of log₂ fold changes in protein intensities in *DGUOK* KO cells (clone #1 left and clone #2 right) compared to WT HeLa cells. Distribution of the complete set of quantified protein groups Total and MitoCarta 3.0 positive (Box limits denote 25- and 75% quartile, line denotes the median, whiskers denote 1.5 x interquartile range deviation from the median), (P-value: Welch's t-test; log₂ fold change; n = 3 independent cultures).

(B) Volcano plot representation of log₂ fold change in mitochondrial protein abundance of *DGUOK* KO cells (clone #2) compared to HeLa WT cells. FDR-significant (<0.05) protein changes in both clones in orange, with selected annotation (log₂ fold change, false discovery rate, n = 3 independent cultures).

**EV 9 Schematic representation of the cytosolic adenosine salvage pathway**

5. Material and Methods

5.1. Materials

Reagents and tools that were used in this thesis are listed in the Materials and Methods section of *Grotehans et al. 2023*²¹⁰. Additional resources that were exclusively used in this thesis are listed below.

Table 1 Reagents and tools

Reagent	Source	Identifier
Antibodies		
Human Vinculin	Cell Signaling	4650
Human DGUOK	Santa Cruz	sc-398093
Plasmid oligonucleotides		
pSpCas9(BB)-2A-Puro (PX459) V2.0	Addgene	62988
<i>DGUOK</i> gRNA	This study	CACCGACTTAGAAAGAGGCG GCCCCG

5.2. Methods

Methods that were used in this thesis are listed below and performed as described in the Materials and Methods section of *Grotehans et al. 2023*²¹⁰ if not stated otherwise.

Cell biology:

1. Generation of cell lines
2. Cell proliferation assays
3. Oxygen consumption and extracellular acidification measurements

Molecular biology:

4. DNA extraction, RNA extraction and cDNA synthesis
5. Quantitative PCR

Biochemistry:

6. Cell lysis and SDS-PAGE
7. Mitochondrial isolation
8. Extraction of polar metabolites
9. Anion-exchange chromatography mass spectrometry for the analysis of nucleotides
10. Sample preparation for mass spectrometry-based proteomics
11. *Liquid chromatography and mass spectrometry
12. Whole proteome analysis
13. Proteomics data analysis

11* Liquid chromatography and mass spectrometry settings were adjusted as follows:

LC-MS/MS instrumentation consisted of an Easy-LC 1200 (Thermo Fisher Scientific) coupled via a nano-electrospray ionization source to an Exploris 480 mass spectrometer (Thermo Fisher Scientific, Bremen, Germany). An Aurora Frontier column (60cm length, 1.7 μm particle diameter, 75 μm inner diameter, Ionopticks). A binary buffer system (A: 0.1% formic acid and B: 0.1% formic acid in 80% acetonitrile) based gradient was utilized as follows at a flow rate of 185 nL/min; a linear increase of buffer B from 4% to 28% within 100 min, followed by a linear increase to 40% within 10 min. The buffer B content was further ramped to 50% within 4 minutes and then to 65% within 3 minutes. 95% buffer B was kept

for a further 3 min to wash the column. The RF Lens amplitude was set to 45%, the capillary temperature was 275°C and the polarity was set to positive. MS1 profile spectra were acquired using a resolution of 30,000 (at 200 m/z) at a mass range of 450-850 m/z and an AGC target of 1×10^6 .

For MS/MS independent spectra acquisition, 34 equally spaced windows were acquired at an isolation m/z range of 7 Th, and the isolation windows overlapped by 1 Th. The fixed first mass was 200 m/z. The isolation center range covered a mass range of 500–740 m/z. Fragmentation spectra were acquired at a resolution of 30,000 at 200 m/z using a maximal injection time setting of 'auto' and stepped normalized collision energies (NCE) of 24, 28, and 30. The default charge state was set to 3. The AGC target was set to 3e6 (900% - Exploris 480). MS2 spectra were acquired in centroid mode. FAIMS was enabled using an inner electrode temperature of 100°C and an outer electrode temperature of 90°C. The compensation voltage was set to -45V.

6. List of abbreviations

Abbreviation	Full name
μM	micromolar
ABAT	4-aminobutyrate aminotransferase, mitochondrial
ADA	adenosine deaminase
ADP	adenosine diphosphate
ADSL	adenylosuccinate lyase
ADSS	adenylosuccinate synthetase
AK	adenylate kinase
ALKBH1	Nucleic acid dioxygenase ALKBH1
AMP	adenosine monophosphate
AMPK	AMP activated protein kinase
ANT	adenine nucleotide transporter
APRT	adenosine phosphoribosyl transferase
ATP	adenosine triphosphate
ATP8/6	ATP synthase protein 8/6
bp	base pair
CAD	carbamoyl-phosphate synthetase 2 - aspartate transcarbamylase - dihydroorotase
CBS	conserved sequence block
CDP	cytidine diphosphate
CI	NADH dehydrogenase
CII	succinate dehydrogenase
CIII	ubiquinol-cytochrome c reductase
CIV	cytochrome c oxidase
CMP	cytidine monophosphate
CMPK	cytidine uridine kinase
CO ₂	carbon dioxide
CoA	coenzyme A
COX1/3/4	cytochrome c oxidase subunit 1/3/4
CP	carbamoyl phosphate
CRISPR	clustered regularly interspaced short palindromic repeats
CTP	cytidine triphosphate
CTPS	CTP synthase
CV	ATP synthase
CYTB	cytochrome b
dA	deoxyadenosine
dADP	deoxy adenosine diphosphate
DAG	diacylglycerol
dAMP	deoxy adenosine monophosphate
dATP	deoxyadenosine triphosphate

dC	deoxycytidine
dCDP	deoxy cytidine diphosphate
dCMP	deoxy cytidine monophosphate
DCTD	deoxycytidylate deaminase
dCTP	deoxy cytidine triphosphate
dG	deoxyguanosine
dGDP	deoxy guanosine diphosphate
dGMP	deoxy guanosine monophosphate
dGTP	deoxy guanosine triphosphate
DGUOK	deoxyguanosine kinase
DHODH	dihydroorotate dehydrogenase
DHX30	ATP-dependent RNA helicase DHX30
DKO	double knockout
D-loop	displacement loop
DNA	deoxyribonucleic acid
dNDP	deoxyribonucleoside diphosphate
dNMP	deoxyribonucleoside monophosphate
dNTP	deoxyribonucleoside triphosphates
dT	deoxythymidine
dTDP	deoxy thymidine diphosphate
dTMP	deoxy thymidine monophosphate
dTTP	deoxy thymidine triphosphate
DTYMK	thymidine monophosphate kinase
dUDP	deoxy uridine diphosphate
dUMP	deoxy uridine monophosphate
ECAR	extracellular acidification rate
ENT	equilibrative nucleoside transporter
ERAL1	GTPase Era, mitochondrial
ETC	electron transport chain
FASTKD	FAST kinase domain-containing protein
FDR	false discovery rate
GDP	guanosine diphosphate
GMP	guanosine monophosphate
GMPK	guanosine monophosphate kinase
GTP	guanosine triphosphate
h	hour
HEK	human embryonic kidney cells
HeLa	human cervical cancer cells
HI/HA	hyperinsulinism/ hyperammonemia
HPLM	human plasma like medium
HPRT	hypoxanthine guanine phosphoribosyl transferase
HSP	heavy strand promotor
H-strand	heavy strand
IMM	inner mitochondrial membrane

IMP	inosine monophosphate
IMS	mitochondrial intermembrane space
KO	knockout
LC-MS	liquid chromatography-mass spectrometry
LPS	lipopolysaccharide
LRPPRC	leucine-rich pentatricopeptide repeat containing
LSP	light strand promotor
L-strand	light strand
MDa	mega Dalton
MDMD	mitochondrial DNA maintenance defect
MDS	mitochondrial DNA depletion syndrome
MGME1	mitochondrial genome maintenance exonuclease 1
mM	millimolar
MPV17L	Mpv17-like protein
MRG	mitochondrial RNA granule
mtDNA	mitochondrial DNA
mtEFG1	elongation factor G, mitochondrial 1
mtEFTu	elongation factor Tu, mitochondrial
MTFER1	mitochondrial transcription termination factor 1
mtIF2	mitochondrial translation initiation factor 2
mtLSU	mitochondrial large ribosomal subunit
mTOR	mechanistic target of rapamycin kinase
mtRNA	messenger RNA
mtSSBP1	mitochondrial single strand binding protein
mtSSU	mitochondrial small ribosomal subunit
NCR	noncoding region
ND5	NADH-ubiquinone oxidoreductase chain 5
ND6	NADH-ubiquinone oxidoreductase chain 6
NDP	nucleoside diphosphate
NDPK	nucleoside diphosphate kinase
NLRP3	NACHT, LRR and PYD domains-containing protein 3
nm	nanometer
NME6	nucleoside diphosphate kinase 6
NMP	nucleoside monophosphate
NRF	nuclear respiratory factor
NTP	nucleoside triphosphate
OCR	oxygen consumption rate
O _H	origin of replication of the heavy strand
O _L	origin of replication of the light strand
OMM	outer mitochondrial membrane
OXA1	oxidase (Cytochrome C) assembly 1-like
OXPHOS	oxidative phosphorylation
PCA	principal component analysis
PEO	progressive external ophthalmoplegia

PGC1 α	peroxisome proliferator-activated receptor gamma coactivator 1 α
P _i	inorganic phosphate
PNP	Purine nucleoside phosphorylase
PNT	pyrimidine nucleotide transporter
POLRMT	mitochondrial DNA-directed RNA polymerase
PPP	pentose phosphate pathway
PRPP	pentose-sugar phosphoribosyl pyrophosphate
qPCR	real-time quantitative polymerase chain reaction
RCC1L	RCC1-like G exchanging factor-like protein
RNA	ribonucleic acid
RNase H1	ribonuclease H1
rNDP	ribonucleoside diphosphate
rNMP	ribonucleoside monophosphate
RNR	ribonucleotide reductase
rNTP	ribonucleoside triphosphate
RPUSD	mRNA pseudouridine synthase RPUSD
RRM1	RNR subunit 1
RRM2	RNR subunit 2
RRM2B	RNR subunit 2B
rRNA	ribosomal RNA
SLC	solute carrier
TACO1	mitochondrial translation activator of COX1
TAS	termination associated sequence
TCA	tricarboxylic acid cycle
TEFM	mitochondrial transcription elongation factor
TFAM	transcription factor A mitochondrial
TFB2M	mitochondrial dimethyl adenosine transferase 2
TK2	thymidine kinase 2
TKO	triple knockout
TMPK	thymidylate monophosphate kinase
TRAF6	TNF receptor-associated factor 6
t-RNA	transfer RNA
TRUB2	TruB pseudouridine synthase family member 2
TWINKLE	T7 helicase-related protein with intramitochondrial nucleoid localization
TYMS	thymidylate synthase
UCK	uridine-cytidine kinase
UDP	uridine diphosphate
UMP	uridine monophosphate
UMPS	uridine monophosphate synthase
UTP	uridine triphosphate
VDAC	voltage dependent anion channel 3
YME1L	yeast mitochondrial DNA escape 1 like

7. References

1. Nicholls, D. G. & Ferguson, S. J. Quantitative Bioenergetics. in *Bioenergetics* 27–51 (2013).
2. Fontecilla-Camps, J. C. Primordial bioenergy sources: The two facets of adenosine triphosphate. *J. Inorg. Biochem.* 216, 111347 (2021).
3. Karnkowska, A. *et al.* A Eukaryote without a Mitochondrial Organelle. *Curr. Biol.* 26, 1274–1284 (2016).
4. Chandel, N. S. Mitochondria. *Cold Spring Harb. Perspect. Biol.* 13, 1–23 (2021).
5. Roger, A. J., Muñoz-Gómez, S. A. & Kamikawa, R. The Origin and Diversification of Mitochondria. *Curr. Biol.* 27, R1177–R1192 (2017).
6. Nicholls, D. G. & Ferguson, S. J. The Cell Biology of the Mitochondrion. *Bioenergetics* 303–325 (2013).
7. Anderson, S. *et al.* Sequence and organization of the human mitochondrial genome. *Nature* 290, 457–465 (1981).
8. Vercellino, I. & Sazanov, L. A. The assembly, regulation and function of the mitochondrial respiratory chain. *Nat. Rev. Mol. Cell Biol.* 23, 141–161 (2022).
9. Mitchell, P. Chemiosmotic coupling in oxidative and photosynthetic phosphorylation. *Biochim. Biophys. Acta - Bioenerg.* 1807, 1507–1538 (2011).
10. Ernster, L. & Schatz, G. Mitochondria: A historical review. *J. Cell Biol.* 91, (1981).
11. Zorova, L. D. *et al.* Mitochondrial membrane potential. *Anal. Biochem.* 552, 50–59 (2018).
12. MacVicar, T. & Langer, T. OPA1 processing in cell death and disease – the long and short of it. *J. Cell Sci.* 129, 2297–2306 (2016).
13. Wiedemann, N. & Pfanner, N. Mitochondrial machineries for protein import and assembly. *Annu. Rev. Biochem.* 86, 685–714 (2017).
14. Veatch, J. R., McMurray, M. A., Nelson, Z. W. & Gottschling, D. E. Mitochondrial Dysfunction Leads to Nuclear Genome Instability via an Iron-Sulfur Cluster Defect. *Cell* 137, 1247–1258 (2009).
15. Koshiba, T., Yasukawa, K., Yanagi, Y. & Kawabata, S. I. Mitochondrial membrane potential is required for MAVS-mediated antiviral signaling. *Sci. Signal.* 4, (2011).
16. Kopinski, P. K., Singh, L. N., Zhang, S., Lott, M. T. & Wallace, D. C. Mitochondrial DNA variation and cancer. *Nat. Rev. Cancer* 21, 431–445 (2021).
17. El-Hattab, A. W., Craigen, W. J. & Scaglia, F. Mitochondrial DNA maintenance defects. *Biochim. Biophys. Acta - Mol. Basis Dis.* 1863, 1539–1555 (2017).
18. Chinnery, P. F. & Hudson, G. Mitochondrial genetics. *Br. Med. Bull.* 106, 135–159 (2013).

19. Miller, F. J., Rosenfeldt, F. L., Zhang, C., Linnane, A. W. & Nagley, P. Precise determination of mitochondrial DNA copy number in human skeletal and cardiac muscle by a PCR-based assay: lack of change of copy number with age. *Nucleic Acids Res.* 31, (2003).
20. Nurk, S. *et al.* The complete sequence of a human genome. *Science* (80-.). 53, 74–80 (2022).
21. Bibb, M. J., Van Etten, R. A., Wright, C. T., Walberg, M. W. & Clayton, D. A. Sequence and gene organization of mouse mitochondrial DNA. *Cell* 26, 167–180 (1981).
22. Kukat, C. *et al.* Super-resolution microscopy reveals that mammalian mitochondrial nucleoids have a uniform size and frequently contain a single copy of mtDNA. *Proc. Natl. Acad. Sci. U. S. A.* 108, 13534–13539 (2011).
23. Kukat, C. & Larsson, N. G. mtDNA makes a U-turn for the mitochondrial nucleoid. *Trends Cell Biol.* 23, 457–463 (2013).
24. Kukat, C. *et al.* Cross-strand binding of TFAM to a single mtDNA molecule forms the mitochondrial nucleoid. *Proc. Natl. Acad. Sci. U. S. A.* 112, 11288–11293 (2015).
25. Brüser, C., Keller-Findeisen, J. & Jakobs, S. The TFAM-to-mtDNA ratio defines inner-cellular nucleoid populations with distinct activity levels. *Cell Rep.* 37, (2021).
26. Bonekamp, N. A. *et al.* High levels of TFAM repress mammalian mitochondrial DNA transcription in vivo. *Life Sci. alliance* 4, 1–17 (2021).
27. Miranda, M., Bonekamp, N. A. & Köhl, I. Starting the engine of the powerhouse: mitochondrial transcription and beyond. *Biol. Chem.* 0859, 1–12 (2022).
28. Falkenberg, M. Mitochondrial DNA replication in mammalian cells: Overview of the pathway. *Essays Biochem.* 62, 287–296 (2018).
29. Alexeyev, M. F. Mitochondrial DNA: the common confusions. *Mitochondrial DNA Part A* 45–47 (2020).
30. Berk, A. J. & Clayton, D. A. Mechanism of mitochondrial DNA replication in mouse L-cells: Asynchronous replication of strands, segregation of circular daughter molecules, aspects of topology and turnover of an initiation sequence. *J. Mol. Biol.* 86, 801–824 (1974).
31. Wanrooij, S. *et al.* Human mitochondrial RNA polymerase primes lagging-strand DNA synthesis in vitro. *Proc. Natl. Acad. Sci. U. S. A.* 105, 11122–11127 (2008).
32. Xuan, H. P. *et al.* Conserved Sequence Box II Directs Transcription Termination and Primer Formation in Mitochondria. *J. Biol. Chem.* 281, 24647–24652 (2006).
33. Nicholls, T. J. & Minczuk, M. In D-loop: 40 years of mitochondrial 7S DNA. *Exp. Gerontol.* 56, 175–181 (2014).
34. Tan, B. G. *et al.* The human mitochondrial genome contains a second light strand

- promoter. *Mol. Cell* 82, 3646–3660.e9 (2022).
35. Brown, T. A., Cecconi, C., Tkachuk, A. N., Bustamante, C. & Clayton, D. A. Replication of mitochondrial DNA occurs by strand displacement with alternative light-strand origins, not via a strand-coupled mechanism. *Genes Dev.* 19, 2466 (2005).
 36. Falkenberg, M. *et al.* Mitochondrial transcription factors B1 and B2 activate transcription of human mtDNA. *Nat. Genet.* 31, 289–294 (2002).
 37. Ramachandran, A., Basu, U., Sultana, S., Nandakumar, D. & Patel, S. S. Human mitochondrial transcription factors TFAM and TFB2M work synergistically in promoter melting during transcription initiation. *Nucleic Acids Res.* 45, 861 (2017).
 38. Inatomi, T. *et al.* TFB2M and POLRMT are essential for mammalian mitochondrial DNA replication. *Biochim. Biophys. Acta - Mol. Cell Res.* 1869, 119167 (2022).
 39. Fisher, R. P. & Clayton, D. A. Purification and characterization of human mitochondrial transcription factor 1. *Mol. Cell. Biol.* 8, 3496 (1988).
 40. Posse, V. *et al.* RNase H1 directs origin-specific initiation of DNA replication in human mitochondria. *PLOS Genet.* 15, (2019).
 41. Litonin, D. *et al.* Human mitochondrial transcription revisited: Only TFAM and TFB2M are required for transcription of the mitochondrial genes in vitro. *J. Biol. Chem.* 285, 18129–18133 (2010).
 42. Jiang, S. *et al.* TEFM regulates both transcription elongation and RNA processing in mitochondria. *EMBO Rep.* 20, 1–18 (2019).
 43. Agaronyan, K., Morozov, Y. I., Anikin, M. & Temiakov, D. Replication-transcription switch in human mitochondria. *Science (80-.).* 347, 548–551 (2015).
 44. Korhonen, J. A., Pham, X. H., Pellegrini, M. & Falkenberg, M. Reconstitution of a minimal mtDNA replisome in vitro. *EMBO J.* 23, 2423–2429 (2004).
 45. Miralles Fusté, J. *et al.* In Vivo Occupancy of Mitochondrial Single-Stranded DNA Binding Protein Supports the Strand Displacement Mode of DNA Replication. *PLOS Genet.* 10, e1004832 (2014).
 46. Mignotte, B., Barat, M. & Mounolou, J. C. Characterization of a mitochondrial protein binding to single-stranded DNA. *Nucleic Acids Res.* 13, 1703–1716 (1985).
 47. Korhonen, J. A., Gaspari, M. & Falkenberg, M. TWINKLE Has 5' → 3' DNA Helicase Activity and Is Specifically Stimulated by Mitochondrial Single-stranded DNA-binding Protein. *J. Biol. Chem.* 278, 48627–48632 (2003).
 48. Brown, G. G., Gadaleta, G., Pepe, G., Saccone, C. & Sbisà, E. Structural conservation and variation in the D-loop-containing region of vertebrate mitochondrial DNA. *J. Mol. Biol.* 192, 503–511 (1986).
 49. Wanrooij, S. *et al.* In vivo mutagenesis reveals that OriL is essential for mitochondrial DNA replication. *EMBO Rep.* 13, 1130–1137 (2012).

50. Fusté, J. M. *et al.* Mitochondrial RNA Polymerase Is Needed for Activation of the Origin of Light-Strand DNA Replication. *Mol. Cell* 37, 67–78 (2010).
51. Kornblum, C. *et al.* Loss-of-function mutations in MGME1 impair mtDNA replication and cause multisystemic mitochondrial disease. *Nat. Genet.* 45, 214–219 (2013).
52. Nicholls, T. J. *et al.* Linear mtDNA fragments and unusual mtDNA rearrangements associated with pathological deficiency of MGME1 exonuclease. *Hum. Mol. Genet.* 23, 6147–6162 (2014).
53. Lima, W. F. *et al.* Viable RNaseH1 knockout mice show RNaseH1 is essential for R loop processing, mitochondrial and liver function. *Nucleic Acids Res.* 44, 5299–5312 (2016).
54. Cerritelli, S. M. *et al.* Failure to Produce Mitochondrial DNA Results in Embryonic Lethality in Rnaseh1 Null Mice. *Mol. Cell* 11, 807–815 (2003).
55. Lakshmiathy, U. & Campbell, C. The Human DNA Ligase III Gene Encodes Nuclear and Mitochondrial Proteins. *Mol. Cell. Biol.* 19, 3869–3876 (1999).
56. Nicholls, T. J. *et al.* Topoisomerase 3 α Is Required for Decatenation and Segregation of Human mtDNA. *Mol. Cell* 69, 9-23.e6 (2018).
57. Zhu, X. *et al.* Non-coding 7S RNA inhibits transcription via mitochondrial RNA polymerase dimerization. *Cell* 185, 2309–2323 (2022).
58. Minczuk, M. *et al.* TEFM (c17orf42) is necessary for transcription of human mtDNA. *Nucleic Acids Res.* 39, 4284–4299 (2011).
59. Hillen, H. S., Temiakov, D. & Cramer, P. Structural basis of mitochondrial transcription. *Nat. Struct. Mol. Biol.* 25, 754–765 (2018).
60. Alexeyev, M. Mitochondrial DNA: the common confusions. *Mitochondrial DNA. Part A, DNA mapping, Seq. Anal.* 31, 45 (2020).
61. Jemt, E. *et al.* Regulation of DNA replication at the end of the mitochondrial D-loop involves the helicase TWINKLE. *Nucleic Acids Res.* 43, 9262–9275 (2015).
62. Ruzzenente, B. *et al.* MTERF1 Binds mtDNA to Prevent Transcriptional Interference at the Light-Strand Promoter but Is Dispensable for rRNA Gene Transcription Regulation. *Cell Metab.* 618–626 (2013).
63. Mercer, T. R. *et al.* The Human Mitochondrial Transcriptome. *Cell* 146, 645–658 (2011).
64. Xavier, V. J. & Martinou, J. C. Rna granules in the mitochondria and their organization under mitochondrial stresses. *Int. J. Mol. Sci.* 22, 1–3 (2021).
65. Antonicka, H., Sasarman, F., Nishimura, T., Paupe, V. & Shoubridge, E. A. The Mitochondrial RNA-Binding Protein GRSF1 Localizes to RNA Granules and Is Required for Posttranscriptional Mitochondrial Gene Expression. *Cell Metab.* 17, 386–398 (2013).
66. Jourdain, A. A. *et al.* GRSF1 Regulates RNA Processing in Mitochondrial RNA

- Granules. *Cell Metab.* 17, 399–410 (2013).
67. Ojala, D., Montoya, J. & Attardi, G. tRNA punctuation model of RNA processing in human mitochondria. *Nature* 290, 470–474 (1981).
 68. Holzmann, J. *et al.* RNase P without RNA: Identification and Functional Reconstitution of the Human Mitochondrial tRNA Processing Enzyme. *Cell* 135, 462–474 (2008).
 69. Siira, S. J. *et al.* Concerted regulation of mitochondrial and nuclear non-coding RNAs by a dual-targeted RNase Z. *EMBO Rep.* 19, 1–18 (2018).
 70. Antonicka, H. & Shoubridge, E. A. Mitochondrial RNA Granules Are Centers for Posttranscriptional RNA Processing and Ribosome Biogenesis. *Cell Rep.* 10, 920–932 (2015).
 71. Antonicka, H. *et al.* A pseudouridine synthase module is essential for mitochondrial protein synthesis and cell viability. *EMBO Rep.* 18, 28–38 (2017).
 72. Arroyo, J. D. *et al.* A Genome-wide CRISPR Death Screen Identifies Genes Essential for Oxidative Phosphorylation. *Cell Metab.* 24, 875–885 (2016).
 73. Antonicka, H. *et al.* A High-Density Human Mitochondrial Proximity Interaction Network. *Cell Metab.* 32, 479–497.e9 (2020).
 74. Kummer, E. & Ban, N. Mechanisms and regulation of protein synthesis in mitochondria. *Nat. Rev. Mol. Cell Biol.* 22, 307–325 (2021).
 75. Bogenhagen, D. F., Ostermeyer-Fay, A. G., Haley, J. D. & Garcia-Diaz, M. Kinetics and Mechanism of Mammalian Mitochondrial Ribosome Assembly. *Cell Rep.* 22, 1935–1944 (2018).
 76. Brown, A. *et al.* Structures of the human mitochondrial ribosome in native states of assembly. *Nat. Struct. Mol. Biol.* 24, 866–869 (2017).
 77. Jaskolowski, M. *et al.* Structural Insights into the Mechanism of Mitoribosomal Large Subunit Biogenesis. *Mol. Cell* 79, 629–644.e4 (2020).
 78. Gaur, R. *et al.* A Single Mammalian Mitochondrial Translation Initiation Factor Functionally Replaces Two Bacterial Factors. *Mol. Cell* 29, 180 (2008).
 79. Spencer, A. C. & Spremulli, L. L. Interaction of mitochondrial initiation factor 2 with mitochondrial fMet-tRNA. *Nucleic Acids Res.* 32, 5464–5470 (2004).
 80. Hammarsund, M. *et al.* Identification and characterization of two novel human mitochondrial elongation factor genes, hEFG2 and hEFG1, phylogenetically conserved through evolution. *Hum. Genet.* 109, 542–550 (2001).
 81. Schwartzbach, C. J. & Spremulli, L. L. Bovine mitochondrial protein synthesis elongation factors: Identification and initial characterization of an elongation factor Tu-elongation factor Ts complex. *J. Biol. Chem.* 264, 19125–19131 (1989).
 82. Chacinska, A., Koehler, C. M., Milenkovic, D., Lithgow, T. & Pfanner, N. Importing Mitochondrial Proteins: Machineries and Mechanisms. *Cell* 138, 628–644 (2009).

83. Haque, M. E. *et al.* Properties of the C-terminal Tail of Human Mitochondrial Inner Membrane Protein Oxa1L and Its Interactions with Mammalian Mitochondrial Ribosomes. *J. Biol. Chem.* 285, 28353 (2010).
84. Soleimanpour-Lichaei, H. R. *et al.* mtRF1a Is a Human Mitochondrial Translation Release Factor Decoding the Major Termination Codons UAA and UAG. *Mol. Cell* 27, 745–757 (2007).
85. Nozaki, Y., Matsunaga, N., Ishizawa, T., Ueda, T. & Takeuchi, N. HMRF1L is a human mitochondrial translation release factor involved in the decoding of the termination codons UAA and UAG. *Genes Cells* 13, 429–438 (2008).
86. Cobb, M. 60 years ago, Francis Crick changed the logic of biology. *PLoS Biol.* 15, (2017).
87. Tang, J. X., Thompson, K., Taylor, R. W. & Oláhová, M. Mitochondrial OXPHOS Biogenesis: Co-Regulation of Protein Synthesis, Import, and Assembly Pathways. *Int. J. Mol. Sci.* 21, 3820 (2020).
88. Virbasius, J. V. & Scarpulla, R. C. Activation of the human mitochondrial transcription factor A gene by nuclear respiratory factors: a potential regulatory link between nuclear and mitochondrial gene expression in organelle biogenesis. *Proc. Natl. Acad. Sci.* 91, 1309–1313 (1994).
89. Bruni, F., Polosa, P. L., Gadaleta, M. N., Cantatore, P. & Roberti, M. Nuclear Respiratory Factor 2 Induces the Expression of Many but Not All Human Proteins Acting in Mitochondrial DNA Transcription and Replication. *J. Biol. Chem.* 285, 3939–3948 (2010).
90. Mootha, V. K. *et al.* PGC-1 α -responsive genes involved in oxidative phosphorylation are coordinately downregulated in human diabetes. *Nat. Genet.* 34, 267–273 (2003).
91. Scarpulla, R. C., Vega, R. B. & Kelly, D. P. Transcriptional integration of mitochondrial biogenesis. *Trends Endocrinol. Metab.* 23, 459–466 (2012).
92. Puigserver, P. *et al.* A Cold-Inducible Coactivator of Nuclear Receptors Linked to Adaptive Thermogenesis. *Cell* 92, 829–839 (1998).
93. Chujo, T. *et al.* LRPPRC/SLIRP suppresses PNPase-mediated mRNA decay and promotes polyadenylation in human mitochondria. *Nucleic Acids Res.* 40, 8033–8047 (2012).
94. Ruzzenente, B. *et al.* LRPPRC is necessary for polyadenylation and coordination of translation of mitochondrial mRNAs. *EMBO J.* 31, 443–456 (2012).
95. Soto, I. *et al.* Balanced mitochondrial and cytosolic translomes underlie the biogenesis of human respiratory complexes. *Genome Biol.* 2021.05.31.446345 (2022).
96. Weraarpachai, W. *et al.* Mutation in TACO1, encoding a translational activator of COX I, results in cytochrome c oxidase deficiency and late-onset Leigh syndrome. *Nat. Genet.* 41, 833–837 (2009).

97. Richman, T. R. *et al.* Loss of the RNA-binding protein TACO1 causes late-onset mitochondrial dysfunction in mice. *Nat. Commun.* 7, 1–14 (2016).
98. Richter-Dennerlein, R. *et al.* Mitochondrial Protein Synthesis Adapts to Influx of Nuclear-Encoded Protein. *Cell* 167, 471–483.e10 (2016).
99. Lane, A. N. & Fan, T. W. M. Regulation of mammalian nucleotide metabolism and biosynthesis. *Nucleic Acids Res.* 43, 2466–2485 (2015).
100. Gandhi, V. V. & Samuels, D. C. A review comparing deoxyribonucleoside triphosphate (dNTP) concentrations in the mitochondrial and cytoplasmic compartments of normal and transformed cells. *Nucleosides, Nucleotides and Nucleic Acids* 30, 317–339 (2011).
101. Traut, T. W. Physiological concentrations of purines and pyrimidines. *Mol. Cell. Biochem.* 140, 1–22 (1994).
102. Adam, S. A. The nuclear pore complex. *Genome Biol.* 2, 1–6 (2001).
103. Kabachinski, G. & Schwartz, T. U. The nuclear pore complex – structure and function at a glance. *J. Cell Sci.* 128, 423–429 (2015).
104. Wang, L. Mitochondrial purine and pyrimidine metabolism and beyond. *Nucleosides, Nucleotides and Nucleic Acids* 35, 578–594 (2016).
105. Hämäläinen, R. H. *et al.* Defects in mtDNA replication challenge nuclear genome stability through nucleotide depletion and provide a unifying mechanism for mouse progerias. *Nat. Metab.* 1, 958–965 (2019).
106. Sprenger, H. G. *et al.* Cellular pyrimidine imbalance triggers mitochondrial DNA–dependent innate immunity. *Nat. Metab.* 3, 636–650 (2021).
107. Wai, T. *et al.* The role of mitochondrial DNA copy number in mammalian fertility. *Biol. Reprod.* 83, 52–62 (2010).
108. D’Erchia, A. M. *et al.* Tissue-specific mtDNA abundance from exome data and its correlation with mitochondrial transcription, mass and respiratory activity. *Mitochondrion* 20, 13–21 (2015).
109. Reznik, E. *et al.* Mitochondrial DNA copy number variation across human cancers. *Elife* 5, 1–20 (2016).
110. Pedley, A. M. & Benkovic, S. J. A New View into the Regulation of Purine Metabolism: The Purinosome. *Trends Biochem. Sci.* 42, 141–154 (2017).
111. Warner, D. F., Evans, J. C. & Mizrahi, V. Nucleotide Metabolism and DNA Replication. *Microbiol. Spectr.* 2, 1–20 (2014).
112. Okesli, A., Khosla, C. & Bassik, M. C. Human pyrimidine nucleotide biosynthesis as a target for antiviral chemotherapy. *Curr. Opin. Biotechnol.* 48, 127–134 (2017).
113. An, S., Kumar, R., Sheets, E. D. & Benkovic, S. J. Reversible compartmentalization of de novo purine biosynthetic complexes in living cells. *Science (80-.)*. 320, 103–105 (2008).

114. French, J. B., Fang, Y. & Benkovic, S. J. The purinosome, a multi-protein complex involved in the de novo biosynthesis of purines in humans. *Chem. Commun.* 49, 4444–4452 (2013).
115. Pareek, V., Tian, H., Winograd, N. & Benkovic, S. J. Metabolomics and mass spectrometry imaging reveal channeled de novo purine synthesis in cells. *Science (80-.)*. 368, 283–290 (2020).
116. Oliver, J. C., Linger, R. S., Chittur, S. V. & Davisson, V. J. Substrate activation and conformational dynamics of guanosine 5'-monophosphate synthetase. *Biochemistry* 52, 5225–5235 (2013).
117. Hedstrom, L. IMP dehydrogenase: Structure, mechanism, and inhibition. *Chem. Rev.* 109, 2903–2928 (2009).
118. Li, X. *et al.* Comparative molecular characterization of ADSS1 and ADSS2 genes in pig (*Sus scrofa*). *Comp. Biochem. Physiol. Part B Biochem. Mol. Biol.* 147, 271–277 (2007).
119. Kmoch, S. *et al.* Human adenylosuccinate lyase (ADSL), cloning and characterization of full-length cDNA and its isoform, gene structure and molecular basis for ADSL deficiency in six patients. *Hum. Mol. Genet.* 9, 1501–1513 (2000).
120. Sun, H. *et al.* Molecular cloning and characterization of a novel muscle adenylosuccinate synthetase, AdSSL1, from human bone marrow stromal cells. *Mol. Cell. Biochem.* 269, 85–94 (2005).
121. Lowenstein, J. M. Ammonia production in muscle and other tissues: the purine nucleotide cycle. *Physiol. Rev.* 52, 382–414 (1972).
122. Fitzgibbon, J. *et al.* Human guanylate kinase (GUK1): cDNA sequence, expression and chromosomal localisation. *FEBS Lett.* 385, 185–188 (1996).
123. Khan, N. *et al.* Solution structure and functional investigation of human guanylate kinase reveals allosteric networking and a crucial role for the enzyme in cancer. *J. Biol. Chem.* 294, 11920–11933 (2019).
124. Wilson, D. E., Povey, S. & Harris, H. Adenylate kinases in man: evidence for a third locus. *Ann. Hum. Genet.* 39, 305–313 (1976).
125. Panayiotou, C., Solaroli, N. & Karlsson, A. The many isoforms of human adenylate kinases. *Int. J. Biochem. Cell Biol.* 49, 75–83 (2014).
126. Parks, R. E. & Agarwal, R. P. Nucleoside Diphosphokinases. in *Enzymes* 307–331 (1973).
127. Lacombe, M. L. L., Munier, A., Mehus, J. G. & Lambeth, D. O. The human Nm23/Nucleoside diphosphate kinases. *J. Bioenerg. Biomembr.* 32, 247–258 (2000).
128. del Caño-Ochoa, F., Moreno-Morcillo, M. & Ramón-Maiques, S. *CAD, A Multienzymatic Protein at the Head of de Novo Pyrimidine Biosynthesis. Macromolecular Protein Complexes II: Structure and Function. Subcellular Biochemistry* 93, (Springer, 2019).

129. Huang, M. & Graves, L. M. De novo synthesis of pyrimidine nucleotides; emerging interfaces with signal transduction pathways. *Cell. Mol. Life Sci.* 60, 321–336 (2003).
130. Li, G., Li, D. & Wang, T. Pyrimidine Biosynthetic Enzyme CAD : Its Function , Regulation , and Diagnostic Potential. (2021).
131. Brown, G. K. & O’Sullivan, W. J. Subunit Structure of the Orotate Phosphoribosyltransferase- Orotidylate Decarboxylase Complex from Human Erythrocytes. *Biochemistry* 16, 3942 (1977).
132. Jones, M. E. Pyrimidine Nucleotide Biosynthesis in Animals: Genes, Enzymes, and Regulation of UMP Biosynthesis. *Ann. Rev. Biochem.* 49, 253–79 (1980).
133. Yang, R. *et al.* De novo pyrimidine biosynthetic complexes support cancer cell proliferation and ferroptosis defence. *Nat. Cell Biol.* 25, 836–847 (2023).
134. Van Rompay, A. R., Johansson, M. & Karlsson, A. Phosphorylation of deoxycytidine analog monophosphates by UMP-CMP kinase: Molecular characterization of the human enzyme. *Mol. Pharmacol.* 56, 562–569 (1999).
135. Minet, N. *et al.* Differential roles of CTP synthetases CTPS1 and CTPS2 in cell proliferation. *Life Sci. Alliance* 6, (2023).
136. Aye, Y., Li, M., Long, M. J. C. & Weiss, R. S. Ribonucleotide reductase and cancer: Biological mechanisms and targeted therapies. *Oncogene* 34, 2011–2021 (2014).
137. Long, M. J. C., Van Hall-Beauvais, A. & Aye, Y. The more the merrier: how homo-oligomerization alters the interactome and function of ribonucleotide reductase. *Curr. Opin. Chem. Biol.* 54, 10–18 (2020).
138. Cho, E. C. & Yen, Y. Novel regulators and molecular mechanisms of p53R2 and its disease relevance. *Biochimie* 123, 81–84 (2016).
139. Björklund, S., Skog, S., Tribukait, B. & Thelander, L. S-Phase-Specific Expression of Mammalian Ribonucleotide Reductase R1 and R2. *Biochemistry* 29, 5452–5458 (1990).
140. Long, M. J. C., Ly, P. & Aye, Y. Still no Rest for the Reductases: Ribonucleotide Reductase (RNR) Structure and Function: An Update. in *Subcellular Biochemistry* 99, 155–197 (Springer Science and Business Media B.V., 2022).
141. Ellims, P. H., Kao, A. Y. & Chabner, B. A. Deoxycytidylate deaminase. Purification and some properties of the enzyme isolated from human spleen. *J. Biol. Chem.* 256, 6335–6340 (1981).
142. Fox, J. T. & Stover, P. J. Chapter 1 Folate-Mediated One-Carbon Metabolism. *Vitam. Horm.* 79, 1–44 (2008).
143. Carreras, C. W. & Santi, D. V. The Catalytic Mechanism and Structure of Thymidylate Synthase. *Annu. Rev. Biochem.* 64, 721–762 (1995).
144. Frisk, J. H., Eriksson, S., Pejler, G. & Wang, L. Identification of a novel thymidylate kinase activity. *Nucleosides, Nucleotides and Nucleic Acids* 39, 1359–1368 (2020).

145. Hu Frisk, J., Pejler, G., Eriksson, S. & Wang, L. Structural and functional analysis of human thymidylate kinase isoforms. *Nucleosides, Nucleotides and Nucleic Acids* 41, 321–332 (2022).
146. Navalgund, L. G., Rossana, C., Muench, A. J. & Johnson, L. F. Cell cycle regulation of thymidylate synthetase gene expression in cultured mouse fibroblasts. *J. Biol. Chem.* 255, 7386–7390 (1980).
147. Hu, C. M. & Chang, Z. F. Mitotic control of dTTP pool: A necessity or coincidence? *J. Biomed. Sci.* 14, 491–497 (2007).
148. Kunji, E., King, M., Ruprecht, J. & Thangaratnarajah, C. The SLC25 carrier family: important transport proteins in mitochondrial physiology and pathology. *Physiology* 302–327 (2020). doi:10.1152/physiol.00009.2020
149. Palmieri, F. Mitochondrial transporters of the SLC25 family and associated diseases: A review. *J. Inherit. Metab. Dis.* 37, 565–575 (2014).
150. Cl  men  on, B., Babot, M. & Tr  z  guet, V. The mitochondrial ADP/ATP carrier (SLC25 family): Pathological implications of its dysfunction. *Mol. Aspects Med.* 34, 485–493 (2013).
151. Di Noia, M. A. *et al.* The human SLC25A33 and SLC25A36 genes of solute carrier family 25 encode two mitochondrial pyrimidine nucleotide transporters. *J. Biol. Chem.* 289, 33137–33148 (2014).
152. Franzolin, E. *et al.* The pyrimidine nucleotide carrier PNC1 and mitochondrial trafficking of thymidine phosphates in cultured human cells. *Exp. Cell Res.* 318, 2226–2236 (2012).
153. Shahroor, M. A. *et al.* PNC2 (SLC25A36) Deficiency Associated With the Hyperinsulinism / Hyperammonemia Syndrome. *J. Clin. Endocrinol. Metab.* 2, 1346–1356 (2022).
154. Pastor-Anglada, M. & P  rez-Torras, S. Emerging roles of nucleoside transporters. *Front. Pharmacol.* 9, 1–8 (2018).
155. Young, J. D. The SLC28 (CNT) and SLC29 (ENT) nucleoside transporter families: A 30-year collaborative odyssey. *Biochem. Soc. Trans.* 44, 869–876 (2016).
156. Ho, H. T. B. & Wang, J. *Drug Transporters: Molecular Characterization and Role in Drug Disposition.* (2014).
157. Govindarajan, R. *et al.* Facilitated mitochondrial import of antiviral and anticancer nucleoside drugs by human equilibrative nucleoside transporter-3. *Am. J. Physiol. - Gastrointest. Liver Physiol.* 296, 910–922 (2009).
158. Lai, Y., Tse, C. M. & Unadkat, J. D. Mitochondrial Expression of the Human Equilibrative Nucleoside Transporter 1 (hENT1) Results in Enhanced Mitochondrial Toxicity of Antiviral Drugs. *J. Biol. Chem.* 279, 4490–4497 (2004).
159. Harborne, S. P. D., King, M. S., Crichton, P. G. & Kunji, E. R. S. Calcium regulation of the human mitochondrial ATP-Mg/Pi carrier SLC25A24 uses a locking pin mechanism. *Sci. Rep.* 7, 1–13 (2017).

160. Traba, J., Del Arco, A., Duchon, M. R., Szabadkai, G. & Satrústegui, J. SCaMC-1 promotes cancer cell survival by desensitizing mitochondrial permeability transition via ATP/ADP-mediated matrix Ca²⁺ buffering. *Cell Death Differ.* 19, 650–660 (2012).
161. Fiermonte, G., Paradies, E., Todisco, S., Marobbio, C. M. T. & Palmieri, F. A Novel Member of Solute Carrier Family 25 (SLC25A42) Is a Transporter of Coenzyme A and Adenosine 3',5'-Diphosphate in Human Mitochondria. *J. Biol. Chem.* 284, 18152–18159 (2009).
162. Alonzo, J. R., Venkataraman, C., Field, M. S. & Stover, P. J. The mitochondrial inner membrane protein MPV17 prevents uracil accumulation in mitochondrial DNA. *J. Biol. Chem.* 293, 20285–20294 (2018).
163. Wang, L., Karlsson, A., Arner, E. S. J. & Eriksson, S. Substrate specificity of mitochondrial 2'-deoxyguanosine kinase. Efficient phosphorylation of 2-chlorodeoxyadenosine. *J. Biol. Chem.* 268, 22847–22852 (1993).
164. Sjöberg, A. H., Wang, L. & Eriksson, S. Substrate specificity of human recombinant mitochondrial deoxyguanosine kinase with cytostatic and antiviral purine and pyrimidine analogs. *Mol. Pharmacol.* 53, 270–273 (1998).
165. Munch-Petersen, B., Cloos, L., Tyrsted, G. & Eriksson, S. Diverging substrate specificity of pure human thymidine kinases 1 and 2 against antiviral dideoxynucleosides. *J. Biol. Chem.* 266, 9032–9038 (1991).
166. Eriksson, S., Kierdaszuk, B., Munch-Petersen, B., Obergt, B. & Gunnar Johansson, N. Comparison of the Substrate Specificities of Human Thymidine Kinase 1 and 2 and Deoxycytidine Kinase Toward Antiviral and Cytostatic Nucleoside Analogs. *Biochem. Biophys. Res. Commun.* 176, 586–592 (1991).
167. Wang, L., Saada, A. & Eriksson, S. Kinetic properties of mutant human thymidine kinase 2 suggest a mechanism for mitochondrial DNA depletion myopathy. *J. Biol. Chem.* 278, 6963–6968 (2003).
168. Xu, Y., Johansson, M. & Karlsson, A. Human UMP-CMP kinase 2, a novel nucleoside monophosphate kinase localized in mitochondria. *J. Biol. Chem.* 283, 1563–1571 (2008).
169. Noma, T. *et al.* Structure and expression of human mitochondrial adenylate kinase targeted to the mitochondrial matrix. *Biochem. J.* 358, 225–232 (2001).
170. Panayiotou, C., Solaroli, N., Johansson, M. & Karlsson, A. Evidence of an intact N-terminal translocation sequence of human mitochondrial adenylate kinase 4. *Int. J. Biochem. Cell Biol.* 42, 62–69 (2010).
171. Amiri, M., Conserva, F., Panayiotou, C., Karlsson, A. & Solaroli, N. The human adenylate kinase 9 is a nucleoside mono- and diphosphate kinase. *Int. J. Biochem. Cell Biol.* 45, 925–931 (2013).
172. Zhong, Z. *et al.* New mitochondrial DNA synthesis enables NLRP3 inflammasome activation. *Nature* 560, 198–203 (2018).

173. Rath, S. *et al.* MitoCarta3.0: An updated mitochondrial proteome now with sub-organelle localization and pathway annotations. *Nucleic Acids Res.* 49, D1541–D1547 (2021).
174. Agarwal, K. C., Miech, R. P. & Parks, R. E. Guanylate Kinases from Human Erythrocytes, Hog Brain, and Rat Liver. *Methods Enzymol.* 51, 483–490 (1978).
175. Su, J. yuan & Sclafani, R. A. Molecular cloning and expression of the human deoxythymidylate kinase gene in yeast. *Nucleic Acids Res.* 19, 823–827 (1991).
176. Lam, C. wan, Yeung, W. L., Ling, T. ki, Wong, K. chung & Law, C. yiu. Deoxythymidylate kinase, DTYMK, is a novel gene for mitochondrial DNA depletion syndrome. *Clin. Chim. Acta* 496, 93–99 (2019).
177. Tsuiki, H. *et al.* A novel human nucleoside diphosphate (NDP) kinase, Nm23-H6, localizes in mitochondria and affects cytokinesis. *J. Cell. Biochem.* 76, 254–269 (2000).
178. Milon, L. *et al.* nm23-H4, a new member of the family of human nm23/nucleoside diphosphate kinase genes localised on chromosome 16p13. *Hum. Genet.* 99, 550–557 (1997).
179. Milon, L. *et al.* The human nm23-H4 gene product is a mitochondrial nucleoside diphosphate kinase. *J. Biol. Chem.* 275, 14264–14272 (2000).
180. Chen, C. W. *et al.* Two separate functions of NME3 critical for cell survival underlie a neurodegenerative disorder. *Proc. Natl. Acad. Sci. U. S. A.* 116, 566–574 (2019).
181. Tokarska-Schlattner, M. *et al.* The nucleoside diphosphate kinase D (NM23-H4) binds the inner mitochondrial membrane with high affinity to cardiolipin and couples nucleotide transfer with respiration. *J. Biol. Chem.* 283, 26198–26207 (2008).
182. Lacombe, M. L. *et al.* Interaction of NDPK-D with cardiolipin-containing membranes: Structural basis and implications for mitochondrial physiology. *Biochimie* 91, 779–783 (2009).
183. Boissan, M. *et al.* Nucleoside diphosphate kinases fuel dynamin superfamily proteins with GTP for membrane remodeling. *Science (80-.)*. 344, 1510–1515 (2014).
184. Gonin, P. *et al.* Catalytic mechanism of nucleoside diphosphate kinase investigated using nucleotide analogues, viscosity effects, and x-ray crystallography. *Biochemistry* 38, 7265–7272 (1999).
185. Besse, A. *et al.* The GABA transaminase, ABAT, is essential for mitochondrial nucleoside metabolism. *Cell Metab.* 21, 417–427 (2015).
186. Kowluru, A., Tannous, M. & Chen, H. Q. Localization and characterization of the mitochondrial isoform of the nucleoside diphosphate kinase in the pancreatic β cell: Evidence for its complexation with mitochondrial succinyl-CoA synthetase. *Arch. Biochem. Biophys.* 398, 160–169 (2002).
187. Ernst, O. *et al.* A genome-wide screen uncovers multiple roles for mitochondrial

- nucleoside diphosphate kinase D in inflammasome activation. *Sci. Signal.* (2021).
188. Kelley, W. N., Rosenbloom, F. M., Henderson, J. F. & Seegmiller, J. E. A specific enzyme defect in gout associated with overproduction of uric acid. *Proc. Natl. Acad. Sci. U. S. A.* 57, 1735–1739 (1967).
 189. Seegmiller, J. E., Rosenbloom, F. M. & Kelley, W. N. Enzyme Defect Associated with a Sex-Linked Human Neurological Disorder and Excessive Purine Synthesis. *Science* (80-.). 155, 7–10 (1967).
 190. Kelley, W. N., Levy, R. I., Rosenbloom, F. M., Henderson, J. F. & Seegmiller, J. E. Adenine phosphoribosyltransferase deficiency: a previously undescribed genetic defect in man. *J. Clin. Invest.* 47, 2281–2289 (1968).
 191. Van Rompay, A. R., Norda, A., Lindén, K., Johansson, M. & Karlsson, A. Phosphorylation of uridine and cytidine nucleoside analogs by two human uridine-cytidine kinases. *Mol. Pharmacol.* 59, 1181–1186 (2001).
 192. Gorman, G. S. *et al.* Mitochondrial diseases. *Nat. Rev. Dis. Prim.* 2, 1–22 (2016).
 193. Schapira, A. H. V. Mitochondrial diseases. *Lancet* 379, 1825–1834 (2012).
 194. Stefano, G. B., Bjenning, C., Wang, F., Wang, N. & Kream, R. M. Mitochondrial heteroplasmy. in *Mitochondrial Dynamics in Cardiovascular Medicine, Advances in Experimental Medicine and Biology* 982, 577–594 (Springer New York LLC, 2017).
 195. Chanprasert, S. *et al.* Molecular and clinical characterization of the myopathic form of mitochondrial DNA depletion syndrome caused by mutations in the thymidine kinase (TK2) gene. *Mol. Genet. Metab.* 110, 153–161 (2013).
 196. Zhou, X. *et al.* Severe mtDNA depletion and dependency on catabolic lipid metabolism in DGUOK knockout mice. *Hum. Mol. Genet.* 28, 2874–2884 (2019).
 197. Ronchi, D. *et al.* Next-generation sequencing reveals DGUOK mutations in adult patients with mitochondrial DNA multiple deletions. *Brain* 135, 3404–3415 (2012).
 198. Tynismaa, H. *et al.* Thymidine kinase 2 mutations in autosomal recessive progressive external ophthalmoplegia with multiple mitochondrial DNA deletions. *Hum. Mol. Genet.* 21, 66–75 (2012).
 199. Krishnan, S. *et al.* Transgene Expression of *Drosophila melanogaster* Nucleoside Kinase Reverses Mitochondrial Thymidine Kinase 2 Deficiency. *J. Biol. Chem.* 288, 5072 (2013).
 200. Fratter, C. *et al.* RRM2B mutations are frequent in familial PEO with multiple mtDNA deletions. *Neurology* 76, 2032–2034 (2011).
 201. Pitceathly, R. D. S. *et al.* Adults with RRM2B-related mitochondrial disease have distinct clinical and molecular characteristics. *Brain* 135, 3392–3403 (2012).
 202. Gandhi, V. V & Samuels, D. C. Enzyme Kinetics of the Mitochondrial Deoxyribonucleoside Salvage Pathway Are Not Sufficient to Support Rapid

- mtDNA Replication. *PLoS Comput Biol* 7, 1002078 (2011).
203. Palmieri, L. *et al.* Complete loss-of-function of the heart/muscle-specific adenine nucleotide translocator is associated with mitochondrial myopathy and cardiomyopathy. *Hum. Mol. Genet.* 14, 3079–3088 (2005).
 204. Blázquez-Bermejo, C. *et al.* Increased dNTP pools rescue mtDNA depletion in human POLG-deficient fibroblasts. *FASEB J.* 33, 7168–7179 (2019).
 205. Nikkanen, J. *et al.* Mitochondrial DNA Replication Defects Disturb Cellular dNTP Pools and Remodel One-Carbon Metabolism. *Cell Metab.* 23, 635–648 (2016).
 206. Floyd, S. *et al.* The Insulin-like Growth Factor-I – mTOR Signaling Pathway Induces the Mitochondrial Pyrimidine Nucleotide Carrier to Promote Cell Growth. *Mol. Biol. Cell* 18, 3545–3555 (2007).
 207. Song, S. *et al.* DNA precursor asymmetries in mammalian tissue mitochondria and possible contribution to mutagenesis through reduced replication fidelity. *Proc. Natl. Acad. Sci. U. S. A.* 102, 4990–4995 (2005).
 208. Ferraro, P., Nicolosi, L., Bernardi, P., Reichard, P. & Bianchi, V. Mitochondrial deoxynucleotide pool sizes in mouse liver and evidence for a transport mechanism for thymidine monophosphate. *Proc. Natl. Acad. Sci. U. S. A.* 103, 18586–18591 (2006).
 209. Rampazzo, C. *et al.* Mitochondrial Deoxyribonucleotides, Pool Sizes, Synthesis, and Regulation. *J. Biol. Chem.* 279, 17019–17026 (2004).
 210. Grotehans, N. *et al.* Ribonucleotide synthesis by NME6 fuels mitochondrial gene expression. *The EMBO Journal.* 42, 1–20 (2023).
 211. Favre, C., Zhdanov, A., Leahy, M., Papkovsky, D. & O’connor, R. Mitochondrial pyrimidine nucleotide carrier (PNC1) regulates mitochondrial biogenesis and the invasive phenotype of cancer cells. *Oncogene* 29, 3964–3976 (2010).
 212. Panayiotou, C., Solaroli, N., Xu, Y., Johansson, M. & Karlsson, A. The characterization of human adenylate kinases 7 and 8 demonstrates differences in kinetic parameters and structural organization among the family of adenylate kinase isoenzymes. 534, 527–534 (2011).
 213. Wang, L. & Eriksson, S. Cloning and characterization of full-length mouse thymidine kinase 2: the N-terminal sequence directs import of the precursor protein into mitochondria. *Biochem. J.* 469–476 (2000).
 214. Sjöberg, A. H., Wang, L. & Eriksson, S. Substrate specificity of human recombinant mitochondrial deoxyguanosine kinase with cytostatic and antiviral purine and pyrimidine analogs. *Mol. Pharmacol.* 53, 270–273 (1998).
 215. Cooper, S. Reappraisal of serum starvation, the restriction point, G0, and G1 phase arrest points. *FASEB J.* 17, 333–340 (2003).
 216. Larsson, N. G. *et al.* Mitochondrial transcription factor A is necessary for mtDNA maintenance and embryogenesis in mice. *Nat. Genet.* 18, 231–236 (1998).

217. West, A. P. *et al.* Mitochondrial DNA stress primes the antiviral innate immune response. *Nature* 520, (2015).
218. Van Acker, K. J., Simmonds, H. A., Potter, C. & Cameron, S. Complete Deficiency of Adenine phosphoribosyltransferase- Report of a family. *N. Engl. J. Med.* 2020 (1975).
219. Taylor, E. B. Functional Properties of the Mitochondrial Carrier System. *Trends Cell Biol.* 27, 633–644 (2017).
220. Song, S., Wheeler, L. J. & Mathews, C. K. Deoxyribonucleotide Pool Imbalance Stimulates Deletions in HeLa Cell Mitochondrial DNA. *J. Biol. Chem.* 278, 43893–43896 (2003).
221. Blunsom, N. J. & Cockcroft, S. CDP-Diacylglycerol Synthases (CDS): Gateway to Phosphatidylinositol and Cardiolipin Synthesis. *Front. Cell Dev. Biol.* 8, (2020).
222. Spasokukotskaja, T., Taljanidisz, J., Sasvari-Szekely, M. & Staub, M. Deoxycytidine is salvaged not only into DNA but also into phospholipid precursors. dCDP-diacylglycerol formation in tonsillar lymphocytes. *Biochem. Biophys. Res. Commun.* 174, 680–687 (1991).
223. Hrabak, A., Spasokukotskaja, T., Temesi, A. & Staub, M. The salvage of deoxycytidine into dCDP-diacylglycerol by macrophages and lymphocytes. *Biochem. Biophys. Res. Commun.* 193, 212–219 (1993).
224. Franco, M., Johansson, M. & Karlsson, A. Depletion of mitochondrial DNA by down-regulation of deoxyguanosine kinase expression in non-proliferating HeLa cells. *Exp. Cell Res.* 313, 2687–2694 (2007).
225. Proust, B. *et al.* NME6 is a phosphotransfer-inactive, monomeric NME/NDPK family member and functions in complexes at the interface of mitochondrial inner membrane and matrix. *Cell Biosci.* 11, 1–23 (2021).
226. Kowluru, A., Tannous, M. & Chen, H. Q. Localization and Characterization of the Mitochondrial Isoform of the Nucleoside Diphosphate Kinase in the Pancreatic β Cell: Evidence for Its Complexation with Mitochondrial Succinyl-CoA Synthetase. *Arch. Biochem. Biophys.* 398, 160–169 (2002).
227. Wanrooij, P. H. & Chabes, A. Ribonucleotides in mitochondrial DNA. *FEBS Lett.* 593, 1554–1565 (2019).
228. Young, P., Leeds, J. M., Slabaugh, M. B. & Mathews, C. K. Ribonucleotide Reductase: Evidence for Specific Association with HeLa-Cell Mitochondria. *Biochem. Biophys. Res. Commun.* 203, 46–52 (1994).
229. Chimpoy, K., Song, S., Wheeler, L. J. & Mathews, C. K. Ribonucleotide Reductase Association with Mammalian Liver Mitochondria. *J. Biol. Chem.* 288, 13145–13155 (2013).
230. Morris, G. W., Iams, T. A., Slepchenko, K. G. & McKee, E. E. Origin of pyrimidine deoxyribonucleotide pools in perfused rat heart: Implications for 3'-azido-3'-deoxythymidine-dependent cardiotoxicity. *Biochem. J.* 422, 513–520 (2009).

231. Qian, X. *et al.* Conversion of prps hexamer to monomer by AMPK-mediated phosphorylation inhibits nucleotide synthesis in response to energy stress. *Cancer Discov.* 8, 94–107 (2018).
232. Ben-Sahra, I., Howell, J. J., Asara, J. M. & Manning, B. D. Stimulation of de novo pyrimidine synthesis by growth signaling through mTOR and S6K1. *Science* (80-.). 339, 1323–1328 (2013).
233. Onyenwoke, R. U. *et al.* AMPK directly inhibits NDPK through a phosphoserine switch to maintain cellular homeostasis. *Mol. Biol. Cell* 23, 381–389 (2012).
234. Diehl, F. F. *et al.* Nucleotide imbalance decouples cell growth from cell proliferation. *Nat. Cell Biol.* 24, 1252–1264 (2022).
235. Reyes, A., Favia, P., Vidoni, S., Petruzzella, V. & Zeviani, M. RCC1L (WBSCR16) isoforms coordinate mitochondrial ribosome assembly through their interaction with GTPases. *PLoS Genet.* 16, 1–26 (2020).
236. To, T. *et al.* A Compendium of Genetic Modifiers of Mitochondrial Dysfunction Reveals Intra-organelle Buffering. *Cell* 179, 1222–1238 (2019).
237. Rossiter, N. J. *et al.* CRISPR screens in physiologic medium reveal conditionally essential genes in human cells. *Cell Metab.* 33, 1248–1263 (2021).
238. Michl, J. *et al.* CRISPR-Cas9 screen identifies oxidative phosphorylation as essential for cancer cell survival at low extracellular pH. *CellReports* 38, 110493 (2022).
239. Acin-Perez, R. *et al.* Inhibition of ATP synthase reverse activity restores energy homeostasis in mitochondrial pathologies . *The EMBO Journal* 42, (2023).
240. Rossiter, N. J. *et al.* CRISPR screens in physiologic medium reveal conditionally essential genes in human cells. *Cell Metab.* 33, 1248-1263.e9 (2021).
241. Cantor, J. R. *et al.* Physiologic Medium Rewires Cellular Metabolism and Reveals Uric Acid as an Endogenous Inhibitor of UMP Synthase. *Cell* 169, 258-272.e17 (2017).
242. LaMonte, G. *et al.* Acidosis induces reprogramming of cellular metabolism to mitigate oxidative stress. *Cancer Metab.* 2013 11 1, 1–19 (2013).
243. Corbet, C. *et al.* The SIRT1/HIF2 α axis drives reductive glutamine metabolism under chronic acidosis and alters tumor response to therapy. *Cancer Res.* 74, 5507–5519 (2014).
244. Bonekamp, N. A. *et al.* Small-molecule inhibitors of human mitochondrial DNA transcription. *Nature* 588, 712–716 (2020).
245. Mullen, N. J. & Singh, P. K. Nucleotide metabolism: a pan-cancer metabolic dependency. *Nat. Rev. Cancer* 23, 275–294 (2023).

8. Summary

Nucleotide metabolism delivers the essential building blocks to maintain the genome and to sustain gene expression. This also holds true for the few but essential mitochondrial genes, which encode core components of the electron transport chain. Mitochondria take up cytosolic nucleotides or recycle precursor nucleosides that are used to fuel mitochondrial gene expression. Mutations in nucleotide metabolizing genes have been linked to multiple mitochondrial diseases highlighting the intimate connection between nucleotide metabolism and mitochondrial- as well as organismal health. Nucleotide metabolism is a complex biological process which involves the uptake, synthesis, distribution and recycling of different nucleotide species across multiple cellular compartments and thus requires a detailed understanding of its various effects on cellular function.

Here, we explored the role of cellular nucleotide metabolism in regulating mitochondrial gene expression.

In this study we highlight for the first time that ribonucleotide metabolism is essential for functional mitochondrial gene expression. Furthermore, we identified nucleoside diphosphate kinase 6 (NME6) as a key regulator of mitochondrial nucleotide balance, which is required for sustaining mitochondrial transcription. We further showed that nucleoside supplementation could either alleviate or aggravate a preexisting nucleotide imbalance and thereby either rescue or worsen mitochondrial gene expression. Surprisingly we found that inhibition of mitochondrial pyrimidine uptake did not severely affect mitochondrial gene expression despite a significant reduction of mitochondrial nucleotide levels. Our findings suggest that mitochondrial gene expression is vulnerable to nucleotide imbalance but prevails upon a general depletion of nucleotides (**Figure 8.1**).

Exploring whether our findings are broadly applicable to other systems of impaired nucleotide homeostasis and investigating the potential involvement of other proteins in regulating mitochondrial ribonucleotide metabolism present exciting directions for future research.

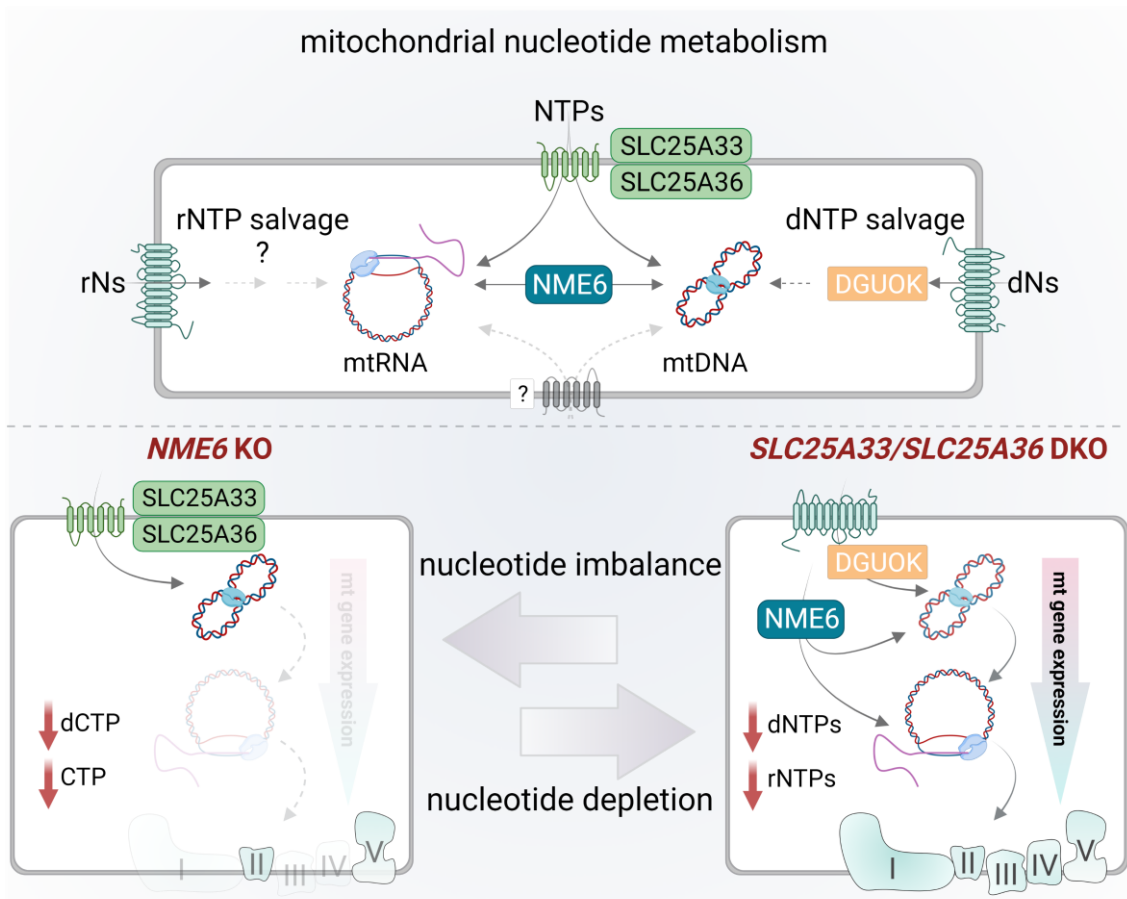


Figure 8.1 Nucleotide metabolism and the control of mitochondrial gene expression

(Top) Schematic representation of the mitochondrial nucleotide supply routes for dNTPs and rNTPs, including a putative rNTP salvage pathway and a putative unknown nucleotide carrier.

(Bottom) Consequences of nucleotide imbalance (*NME6* KO; left) and nucleotide depletion (*SLC25A33/SLC25A36* DKO; right) on mitochondrial gene expression.

(rNs: ribonucleosides; dNs: deoxyribonucleosides; NTPs: (d/r) nucleoside triphosphates, nucleoside transporters in teal: ENT1 and ENT3).

9. Acknowledgements

First and foremost, I would like to thank you Thomas for putting the trust in me during all the ups and downs of my PhD! I have learned many things in your lab which I am grateful for and hope that I can put them to good use in the future.

Thank you, Jan for being such a helpful and supportive TAC-member I appreciate all the efforts you have made to help me with my PhD.

Thank you, Marcus for the continuous support from the Master till the PhD. If it wasn't for your suggestion I might not have applied to Thomas's lab.

Tom, you are not part of my TAC but I have gotten so much support from you and I am very grateful that we worked on this project together. Thank you.

I would also like to thank all current and former lab-members. You guys have made my time here so enjoyable! I hope the lab maintains the good spirit for the years to come. Special thanks to Yohsuke, who taught me all the basics when I joined the lab. Thank you, Hendrik, for being such a patient helper and a long-time companion, I have also learned many things from you. Thank you Dr. Sri Master General for all the teasing in the lab, the support, the calmness and the fresh perspectives. Thanks to Pablo, Jun, Amir, Dusanka and Sadig for support, advice, mocking and lots of fun in and outside the lab.

Huge thanks to the two people I spent the most time with, Álvaro and Soni. I would need to write another thesis about the many things you did for me. I hope you know how grateful I am. I am happy that we have met.

Zuletzt möchte ich mich bei meiner Familie bedanken. Danke, dass ihr mich bei allem begleitet und ich mich immer auf euch verlassen kann. Ihr seid die Besten!

10. Eidesstattliche Erklärung

Erklärung zur Dissertation

gemäß der Promotionsordnung vom 12. März 2020

Hiermit versichere ich an Eides statt, dass ich die vorliegende Dissertation selbstständig und ohne die Benutzung anderer als der angegebenen Hilfsmittel und Literatur angefertigt habe. Alle Stellen, die wörtlich oder sinngemäß aus veröffentlichten und nicht veröffentlichten Werken dem Wortlaut oder dem Sinn nach entnommen wurden, sind als solche kenntlich gemacht. Ich versichere an Eides statt, dass diese Dissertation noch keiner anderen Fakultät oder Universität zur Prüfung vorgelegen hat; dass sie - abgesehen von unten angegebenen Teilpublikationen und eingebundenen Artikeln und Manuskripten - noch nicht veröffentlicht worden ist sowie, dass ich eine Veröffentlichung der Dissertation vor Abschluss der Promotion nicht ohne Genehmigung des Promotionsausschusses vornehmen werde. Die Bestimmungen dieser Ordnung sind mir bekannt. Darüber hinaus erkläre ich hiermit, dass ich die Ordnung zur Sicherung guter wissenschaftlicher Praxis und zum Umgang mit wissenschaftlichem Fehlverhalten der Universität zu Köln gelesen und sie bei der Durchführung der Dissertation zugrundeliegenden Arbeiten und der schriftlich verfassten Dissertation beachtet habe und verpflichte mich hiermit, die dort genannten Vorgaben bei allen wissenschaftlichen Tätigkeiten zu beachten und umzusetzen. Ich versichere, dass die eingereichte elektronische Fassung der eingereichten Druckfassung vollständig entspricht."

Teilpublikationen:

„Ribonucleotide synthesis by NME6 fuels mitochondrial gene expression“

Grotehans et al. 2023 The EMBO Journal

Köln, 11.08.2023

Ort, Datum



Nils Grotehans

11. Curriculum Vitae

Nils Grotehans

Max Planck Institute for Biology of Ageing

Joseph-Stelzmann Str. 9b

50931 Cologne, Germany

ngrotehans@age.mpg.de

Education

Max Planck Institute for Biology of Ageing, PhD 2018-2023
Department of Genetics

University of Cologne, Germany, MSc 2016-2018
Masters in Biological Sciences

University of Cologne, Germany, BSc 2012-2015
Bachelor in Biology

Research Experience

Postdoctoral researcher 2023-present
Max-Planck Institute for Biology of Ageing, Cologne, Germany
Department of Mitochondrial Proteostasis
Prof. Thomas Langer

Doctoral degree 2018-2023
Max-Planck Institute for Biology of Ageing, Cologne, Germany
Prof. Thomas Langer
Nucleotide Metabolism and the Control of Mitochondrial Gene Expression

Master thesis 2018
Cologne Excellence Cluster on Cellular Stress responses in Ageing-Associated Diseases, Germany
Department of Proteomics
Prof. Marcus Krüger
Deciphering Global Phosphorylation Dynamics in Myostatin-dependent Signaling Pathways by Quantitative Mass Spectrometry

Bachelor thesis 2015
 University of Cologne
 Department of Biochemistry
 Prof. Günter Schwarz
Functional Characterization of Potentially Human Pathogenic MOCS1-mutations

Research Internship 2015
 Life and Brain Center, University of Bonn
 Department of Neurochemistry
 Prof. Wolfram Kunz
Mitochondrial Gene Expression in Human Embryonic Kidney Cells

Publication

Ribonucleotide synthesis by NME6 fuels mitochondrial gene expression.
Grotehans N, McGarry L, Nolte N, Kroker M, Narbona-Perez A, Deshwal S, Giavalisco P, Langer T, MacVicar T. *The EMBO Journal* 2023

Recognition and Fellowship

EMBO travel grand to present at the EMBO workshop *Molecular Biology of Mitochondrial Gene Maintenance and Expression*, Bro, Sweden 2022

PhD fellowship Cologne Graduate School of Ageing Research 2018-2022
 International Max Planck Research School (IMPRS)

Talks and Conferences

MitoChats webinar series 2023
 (selected for talk)

Cologne Spring Meeting *Cell death and Mitochondrial signaling in health and disease* 2023
 Cologne, Germany (poster presentation)

EMBO workshop *Molecular Biology of Mitochondrial Gene Maintenance and Expression* 2022
 Bro, Sweden (selected for short talk)

10th CGA Graduate Symposium 2022

Cologne, Germany (talk)
MitoChats *Symposium on Mitochondrial Biology* 2019
Cologne, Germany

7th International Symposium Crossroads in Biology 2019
Cologne, Germany

Workshops and Training

Statistics and Data Visualization in PRISM 2023
Omics Data Analysis and Visualization in Instant Clue 2021
Adobe Illustrator 2021
Academic Writing 2020
Statistical Literacy 2019
Scientific Presentation 2019
Good Scientific Practice 2019

Languages

Native in German
Fluent in English

References

Prof. Dr. Thomas Langer (PhD supervisor)
Max-Planck-Institute for Biology of Ageing
Department of Mitochondrial Proteostasis
Joseph-Stelzmann-Str. 9b
50931 Cologne, Germany
Tlanger@age.mpg.de

Dr. Thomas MacVicar (PhD second mentor)
The CRUK Institute
Switchback Road
Bearsden Glasgow G61 1BD
Thomas.macvicar@glasgow.ac.uk